Entry Guidance for Abort Scenarios

by

2Lt Jeffrey D. Barchers

B.S. Astronautical Engineering
United States Air Force Academy, 1995

SUBMITTED TO THE DEPARTMENT OF AERONAUTICS AND ASTRONAUTICS IN PARTIAL FULFILLMENT OF THE REQUIREMENTS FOR THE DEGREE OF

MASTER OF SCIENCE IN AERONAUTICS AND ASTRONAUTICS
AT THE
MASSACHUSETTS INSTITUTE OF TECHNOLOGY

JUNE 1997

Signature of Author.....
Department of Aeronautics and Astronautics
June 1997

Approved by.....
Owen Deutsch
Charles Stark Draper Laboratory, Inc.
Technical Supervisor

Certified by.....
Wallace E. Vander Velde
Professor of Aeronautics and Astronautics
Thesis Supervisor

Accepted by.....
Jaime Peraire
Professor of Aeronautics and Astronautics
Chair, Graduate Office

Entry Guidance for Abort Scenarios

by

Jeffrey D. Barchers

Submitted to the Department of Aeronautics and Astronautics
on May 23, 1997 in Partial Fulfillment of the
Requirements for the Degree of Master of Science in
Aeronautics and Astronautics

ABSTRACT

Current and future developments in reusable launch vehicle technology demand on-board, real time autonomous abort handling. If an engine failure occurs, the guidance system must quickly determine a footprint of reachable landing sites and select a robust site. A robust site is one which maximizes the vehicle's ability to reach that site in the presence of multiple uncertainties. After selecting a robust landing site, the guidance system must successfully bring the vehicle to a safe landing.

A versatile approach for abort guidance is presented here. The guidance problem is posed as a nonlinear model matching problem. Reference profiles are replaced by a reference dynamic model defined by the nominal vehicle dynamics and a nominal guidance algorithm. The guidance system is built around this reference model. Vehicle capability is examined in the model based framework. A footprint definition and trajectory design algorithm using the nominal bank angle for range control evolves naturally from the reference model. A tracking algorithm uses bank angle and angle of attack perturbations to ensure that vehicle states track the reference model states. Large disturbances and initial condition errors are rejected by a trajectory redesign algorithm. The trajectory redesign algorithm operates continuously in flight to control vehicle range by adjusting the nominal bank angle. The use of a reference model leads to a simple method for analytic evaluation of landing site robustness as a function of control saturation. The algorithm is developed and verified for the X-34, a reusable launch vehicle currently being designed and built by Orbital Sciences Corporation. The system is verified in a three degree of freedom simulation environment. Multiple test cases, including a variety of abort scenarios and parametric uncertainties, verify system performance.

Thesis Supervisor: Professor Wallace E. Vander Velde
Title: Professor, Department of Aeronautics and Astronautics

Technical Supervisor: Owen Deutsch
Title: Principal Member Technical Staff, C. S. Draper Laboratory, Inc.

Acknowledgments

I want to sincerely thank everyone who has helped bring this thesis to completion. Great thanks goes to my advisors, Owen Deutsch and Dr. Wallace Vander Velde. Owen's guidance and support was instrumental in the development of this thesis. I thank Dr. Vander Velde for his numerous ideas and suggestions and his insight in the field of control and optimization. Thanks must also go out to Tom Fill for sharing his wealth of experience in guidance system design. Tony Bogner and Chris Stoll provided invaluable technical support. Brent Appleby's and Chris D'Souza's incredible insight into the field of control systems was crucial in helping me through several stumbling blocks. Thank you to the other members of Draper Lab's X-34 guidance design team, Gregg Barton, Andy Staugler, and Christina Chomel for endless support, enthusiasm, and helpful ideas.

A special thanks goes out to my roommates, Naresh Shah and Varun Puri. Thanks for being great friends and for all the help and support along the way. Thanks to Varun for patiently enduring hour upon hour of "conceptual discussion" about one problem after another. Even more, thanks for answering countless Framemaker questions. Also thanks to all my other friends and co-workers who made the endless hours in the computer lab fun.

Thanks to all my climbing partners. You kept my sanity intact and my motivation going for two years. The "Gravy Gang" - Bruno, Isabelle, Kozo, Johan, Coucou and Paul. Especially Bruno for reminding me that there's more to climbing and life than the number. The bold Scotsman Alastair for running it out, and Andrea for keeping us from always talking about climbing. Adam and Jack - truly embody The Program. The Rhody Loadies Whitie and Ryan. The list goes on and on. Thank you all for your friendship and belays.

To my family, Mom, Dad, and Josh. Thanks so much for your untiring love and support throughout the years. Thanks for always listening. Thanks for being there and inspiring me to always do my best.

This thesis was prepared at the Charles Stark Draper Laboratory, Inc., under Orbital Sciences Corporation / Draper contract XC-9609-103.

Publication of this thesis does not constitute approval by the Draper Laboratory or the sponsoring agency of the findings or conclusions contained herein. It is published for the exchange and stimulation of ideas.

_____

Jeffrey D. Barchers

Table of Contents

1 Introduction 21

1.1 Problem Definition: Robust Abort Guidance 21

1.2 Background 22

1.3 Algorithm Summary 23

1.4 Thesis Overview 25

2 Vehicle Description 27

2.1 Physical Configuration 27

2.2 Aerodynamic and Mass Properties 28

2.3 Coordinate Frames 33

2.4 Equations of Motion 35

2.4.1 Trajectory Design and Tracking Equations of Motion 35

2.4.2 Vehicle Constraints 36

2.5 Uncertainty Sources 37

2.5.1 Atmospheric 37

2.5.2 Aerodynamic 37

2.6 Simulation Environments 38

3 Nominal Trajectory / Reference Dynamic Model Definition 39

3.1 Introduction to Reference Dynamic Model Based Guidance 39

3.1.1 Reference Profile Based Approach 40

3.1.2 Predictor-Corrector Guidance Approach 42

3.1.3 Reference Dynamic Model Based Approach 43

3.2 Space Shuttle Glide Return to Launch Site Guidance 47

3.2.1 Alpha Recovery 47

3.2.2 Nz Hold 48

3.2.3 Alpha Transition 48

3.3 X-34 Nominal Entry Guidance 48
3.3.1 Alpha Recovery 49
3.3.2 Closed Loop Alpha Transition (CLAT) 50
3.4 X-34 Reference Dynamic Model Definition 54
3.4.1 Alpha Recovery Reference Dynamic Model 54
3.4.2 Closed Loop Alpha Transition Reference Dynamic Model 55
3.4.3 Summary of Guidance and Reference Dynamic Model Free Parameters 56

4 Vehicle Capability Analysis 59
4.1 Effects of Modifying the Nominal Trajectory 59
4.1.1 Alpha Recovery 61
4.1.2 Closed Loop Alpha Transition 65
4.2 Guidance-Limited Footprint Definition 72
4.3 Implications for Trajectory Design 74

5 Trajectory Design 75
5.1 Design Algorithm: General Approach 75
5.2 Footprint Definition and Range Prediction: Reference Profile Based Approaches 78
5.2.1 Analytic Approach: Drag-Velocity or Drag-Energy Approximation 78
5.2.2 Exact Solution of Families of Drag-Velocity Profiles for Footprint Definition 80
5.3 Footprint Definition and Range Prediction for a Reference Model 80
5.3.1 Reference Dynamic Model Parameter Optimization Problem 81
5.3.2 Minimum and Maximum Range Prediction - Baseline Footprint . . 82
5.3.3 Site Weighting 83
5.3.4 Range Prediction Fine Tuning and Initial Reference Bank Angle Command 88

5.3.5 Final Altitude Control Using Bank Angle. 89
5.4 Initial Trajectory Design Algorithm 92
5.5 Closed Loop Reference Model Redesign Using Basis Energy vs. Range-to-Go Trajectories 94
5.5.1 Robustness of Drag-Velocity Based Range Prediction. 94
5.5.2 Energy-Range Space Variations due to Parametric Uncertainties . . 99
5.5.3 Implication for Closed-Loop Trajectory Design. 102
5.5.4 Closed Loop Redesign: Energy-Range Feedback. 103
5.6 Trajectory Design Algorithm Summary 104

6 Trajectory Tracking 107
6.1 Traditional SISO Entry Guidance Approaches. 108
6.1.1 Glide Return to Launch Site Open Loop Alpha Transition. 108
6.1.2 Entry Guidance Drag-Velocity or Altitude-Velocity Tracking 108
6.1.3 Robustness of Traditional Approaches 113
6.2 Multivariable Approach - Drag and Altitude Tracking. 114
6.3 Multivariable Reference Dynamic Model Based Entry Guidance 116
6.3.1 Overview and Block Diagram Representation 116
6.3.2 Advantages of Reference Dynamic Model. 118
6.4 Control Laws. 118
6.4.1 Introductory Control Problem Definition 119
6.4.2 Output Feedback Approach. 122
6.4.3 LQR Approach 128
6.5 Tracking Performance Robustness Comparisons 130
6.5.1 Linearized Comparison. 131
6.5.2 Nonlinear Simulation Results 133
6.5.3 Tracking Algorithm Performance Summary. 138

7 Performance Robustness Analysis. 139
7.1 Nominal Performance Results. 139

7.1.1 High Crossrange Example. 139
7.1.2 Zero Crossrange Example. 141
7.2 Control Saturation and Performance Robustness 143
7.2.1 Robust Footprint Definition: Analytic Approximations for Site Robustness as a Function of Control Saturation 143
7.2.2 Comparison between High and Zero Crossrange Examples. 148
7.3 Robust Performance Results. 156

8 Conclusion 167

List of Figures

1.1 X-34 Reference Dynamic Model Based Guidance 24

2.1 Baseline X-34 Design 27

2.2 Baseline Aerodynamic Coefficients 29

2.3 Lift/Drag Ratio 30

2.4 Maximum speedbrake deflection aerocoefficient effects ('-' mach 10.0, '--' mach 5.0, '-.' mach 3.5, ':' mach 2.5) 30

2.5 Maximum elevon deflection aerocoefficient effects ('-' mach 9.96, '--' mach 4.96, '-.' mach 2.74) 31

2.6 Maximum body flap deflection aerocoefficient effects ('-' mach 9.96, '--' mach 4.96, '-.' mach 2.74) 32

2.7 Body Frame & local level frame 34

2.8 Body Frame and Velocity Direction Frame 35

3.1 Reference Profile Based Guidance 40

3.2 Reference Profile Based Guidance with Redesign Capability 41

3.3 Predictor-Corrector Based Guidance 42

3.4 Reference Dynamic Model Based Guidance 45

3.5 Alpha Recovery Guidance - "Perfect" Angle of Attack Control Law 50

3.6 CLAT Angle of Attack Nominal Guidance Law 51

3.7 Bank Angle Azimuth Guidance Law 52

3.8 Nominal Vertical Profile with 0 bank('-') and 30 bank ('--') 53

3.9 Alpha Recovery Reference Dynamic Model 54

3.10 Closed Loop Alpha Transition Reference Dynamic Model 56

4.1 Downrange and Dynamic Pressure wrt Nominal Angle of Attack in AR 62

4.2 Ground range and maximum dynamic pressure wrt alpha recovery bank angle . . . 64

4.3 Ground range and altitude errors due to CLAT bank angle 66

4.4 Downrange and crossrange CLAT banking effects 67

4.5 Downrange and altitude errors, and trajectory quality index wrt constant pitch command 69

4.6 Downrange, Altitude vs. Alpha Bias 71

4.7 AR + CLAT footprints 73
5.1 Ground range effects due to CLAT bank angle 77
5.2 Footprint approximation using minimum and maximum range trajectories. 83
5.3 Minimum bank angle computation free body diagram. 84
5.4 Constant bank variations on X-34 D-V trajectories 90
5.5 Altitude "shaped" trajectories via bank command only.. 91
5.6 Final Altitude vs. with and without altitude shaping 91
5.7 Drag-Velocity Space Variations due to Parametric Uncertainties 96
5.8 Drag-Velocity Space Variations due to L/D Uncertainties. 98
5.9 Constant Bank Variations in Energy-Range Space. 99
5.10 Energy-Range Space Variations due to Parametric Uncertainties 101
5.11 Energy-Range Space Variations due to L/D Uncertainties. 102
5.12 Basis RGO Computation. 103
6.1 Multivariable Reference Dynamic Model Based Guidance 117
6.2 Open Loop Block Diagram. 120
6.3 Output Feedback Controller 120
6.4 Full State Feedback Controller 121
6.5 Full State Feedback Control (Drag, Angle of Attack States Included). 122
6.6 Output Feedback Controller with Integrated Angle of Attack Control. 122
6.7 Open loop frequency response with and without angle of attack integrator. 123
6.8 Transfer Function Relationships. 125
6.9 Output Feedback Loop Transfer Function Singular Values 125
6.10 Output Feedback Sensitivity Transfer Function Singular Values. 126
6.11 Output Feedback Complementary Sensitivity Transfer Function Singular Values . 127
6.12 Frequency Domain Comparison ('-' Output Feedback, '--' LQR). 132
6.13 State and control errors with no uncertainty. 134
6.14 State and control errors with +10% CD bias. 135
6.15 State and control errors with +10% CL bias. 136
6.16 State and control errors with +25% Density Bias. 138
7.1 High Cross Range Example. 140
7.2 Zero Cross Range Example. 142

7.3 Plant Uncertainty Representation 146
7.4 Zero Crossrange Trajectory with -10% CL bias 150
7.5 High Crossrange Trajectory with -10% CL bias. 151
7.6 Zero Crossrange Trajectory with -20% CL bias. Little saturation occurs. 154
7.7 High Crossrange Trajectory with -20% CL bias. Large control saturations. 155
7.8 Mach 6 Abort Trajectory. 158
7.9 Mach 7 Abort Trajectory. 159

List of Tables

1.1 Guidance System Functions 25
4.1 Nominal abort trajectory final states 60
5.1 Guidance System Functions 76
5.2 Actual vs. Estimated Bank Angles 86
5.3 Guidance System Functions 106
7.1 Site Robustness Assessment 149
7.2 Predicted Bank Angle Response for -10% CL bias 152
7.3 Guidance Performance Goals 160
7.4 Nominal Performance Results 161
7.5 Performance Results: CD Uncertainty 162
7.6 Performance Results CL Uncertainty 163
7.7 Performance Results: Density Uncertainty 164

List of Symbols

Symbol	Description
A	plant dynamics matrix
Az	azimuth
abs	absolute value
AR	alpha recovery
acos	arc cosine
atan	arc tangent
B	plant input matrix
C	plant output matrix
C_D	coefficient of drag
C_L	coefficient of lift
C_{LQ}	LQR performance variable output matrix
C_{20},C_{21},C_{22}	coefficient for computing bank angle command for Ishimoto's method [9]
CLAT	closed loop alpha transition
cos	cosine
D	drag
D	plant feedforward matrix
D_{LQ}	LQR performance variable feedforward matrix
dB	decibels
deg	degrees
E	energy
F	force
ft	feet
f_α	angle of attack gain for angle of attack modulation
g	gravitational acceleration
GRTLS	glide return to launch site
h	altitude

H	atmospheric scale height
H_2	control methodology to minimize mean squared error
H_∞	control methodology to minimize peak gain
I	identity matrix
J	cost function for range control
J_{LQ}	LQR cost function
K	control matrix
k_D , k_h , $k_{D\alpha}$, $k_{D\sigma}$, $k_{h\alpha}$, $k_{h\sigma}$, k_α , k_σ	coefficients for LQR output and feedforward performance matrices
K_p	proportional control term for linear bank angle control law
K_d	derivative control term for linear bank angle control law
$K_{\Delta D \to \Delta\alpha}$, $K_{\Delta D \to \Delta\sigma}$, $K_{\Delta h \to \Delta\alpha}$, $K_{\Delta h \to \Delta\sigma}$	elements of control matrix for reference model tracking
l_1 norm, $\| \ \|_1$	l_∞ to l_∞ induced norm, i.e. worst case peak to peak gain
l_∞ norm, $\| \ \|_\infty$	maximum magnitude of signal
L	lift
L_Δ	matrix representation from C_L bias to dynamics
L/D	lift to drag ratio
$(L/D)_v$	vertical component of lift to drag ratio
LQG	linear quadratic gaussian
LQR	linear quadratic regulator
lvlh	local vertical local horizontal
m	mass
MIMO	multiple input multiple output
min	minimum
midval(x,y,z)	middle value of variables x,y,z
nm	nautical miles
n, n_z	normal acceleration
q	dynamic pressure

r	radial position from the center of the earth
r_s	radius of the earth
R	ground range
R_{LQ}	LQR control weighting matrix
R_{cir}	radius of the circle for minimum bank angle computation
R_{GO}	range to go
R_X	vehicle downrange position
R_Y	vehicle crossrange position
RLV	reusable launch vehicle
S_a	vehicle surface area
sec	seconds
sgn	sign
sin	sine
SISO	single input single output
sup	supremum
t	time
T	integral term time constant for nonlinear PID bank angle control law
TAEM	terminal area of energy management
$T_C(s)$	complementary sensitivity transfer function matrix
$T_L(s)$	loop gain transfer function matrix
$T_S(s)$	sensitivity transfer function matrix
$T_{u\Delta}$	transfer function matrix from uncertainty to control signal
u_L	linear bank angle control law (Space Shuttle)
u_N	feedback linearized bank angle control law
$\dot{x}$	rate of x, i.e. time derivative of x
v	vehicle air relative velocity
v_h	vertical component of air relative velocity
wrt	with respect to
z	drag-velocity state space variable

Δz	LQR performance variable
3DOF	three degree of freedom
6DOF	six degree of freedom
1/s	Laplace transform represenation of an integrator
α	angle of attack
Δu_α	angle of attack control variable
β	sideslip angle
γ	flight path angle
Δ	error / difference / perturbation
ζ	damping ratio
θ	pitch angle
μ	integration temporary variable
ν	drag acceleration temporary variable to define tracking laws
ρ	air density
ρ_s	sea level air density
Σ	sum
σ	bank angle
σ_{CROSS}	minimum bank angle to meet cross-range requirements for a site
σ_{max}	maximum allowable bank angle
σ_{SITE}	bank angle to meet ground range requirements for a site
$\Delta\sigma_{INIT}$	bank angle perturbation due to initial condition uncertainty
$\Delta\sigma_L$	lower bank angle robustness bound
$\Delta\sigma_U$	upper bank angle robustness bound
$\Delta\sigma_{SS}$	steady state bank angle perturbation to reject C_L bias
$\Delta\sigma_{tr}$	maximum magnitude of transient bank angle perturbation to reject C_L bias
τ	current time in derivation of nonlinear PID bank angle control law
ϕ	roll angle
$\Phi(s)$	plant transfer function matrix
ψ	yaw / azimuth / heading angle
$\psi_{deadband}$	azimuth angle deadband magnitude

ω	frequency
∞	infinity

Subscripts

basis	basis trajectory
ShiftBasis	shifted basis trajectory
CMD	command
ERR	error
f,F	value at final time
i	"ith" value
LL	lower limit
MAX	maximum
PREV	previous
r	reference
REF,ref	reference
Temp	temporary variable
tot	total
TGT	target landing site
UL	upper limit
0	value at initial time

Superscripts

$\dot{}$	first time derivative
$\ddot{}$	second time derivative
$\bar{}$	mean value
$^{\circ}$	degree
^{T}	transpose
$^{+}$	positive perturbation
$^{-}$	negative perturbation

Chapter 1

Introduction

Recent interest in reusable launch vehicle (RLV) technology has rekindled an effort to improve entry guidance system technology. One of the goals of the RLV program is to increase vehicle autonomy. This goal highlights a need for simple, fast, and effective on-board robust abort guidance systems. This thesis presents a robust abort guidance system for Orbital Sciences Corporation's X-34, one of several RLVs under development. While developed specifically for the X-34, the robust abort guidance system has much wider application and provides a systematic approach to entry guidance. The focus is on defining an algorithm which maximizes robustness to parametric and initial condition uncertainties. This chapter introduces the problem, summarizes previous approaches to the problem, and outlines the proposed abort guidance algorithm.

1.1 Problem Definition: Robust Abort Guidance

Before addressing the specific problems of abort guidance, a brief description of the X-34 is necessary. The X-34 is a high lift to drag ratio reusable launch vehicle. The X-34 is launched from Orbital Sciences Corporation's L-1011 aircraft. After being dropped from the L-1011, the X-34's single engine ignites and accelerates the vehicle to some prescribed mach and altitude target. The engine is then shut off and the vehicle glides to a safe landing through application of angle of attack and bank angle controls.

A nominal guidance algorithm to safely land the vehicle is relatively simple to define. Through iteration and optimization, engineers can design control and state trajectories which guarantee a safe landing. This assumes that the engine fires successfully. This investigation focuses on scenarios in which only a partial engine firing occurs. An engine failure prior to reaching the prescribed mach and altitude target causes two main problems. First, the nominal state and control histories are specified for the nominal initial conditions. The perturbed initial conditions require a new control history to reach the desired landing site. The even greater problem is that

the nominal landing site may not even be achievable in an abort scenario.

The objective of this thesis is to define a robust abort guidance system capable of several key functions. A robust abort guidance algorithm must recognize when the nominal site is no longer achievable and beyond that it must select an achievable site. After selecting a landing site the abort guidance algorithm must design a state and control trajectory to reach the desired site. Most importantly, a robust abort guidance system must accomplish all of these functions in real time. This thesis primarily concerns itself with fast definition of a state and control trajectory to reach the target site. Footprint definition and site selection are addressed primarily as by-products of the trajectory design algorithm.

1.2 Background

Autonomous robust abort guidance is relatively undeveloped. A great number of references exist for the general problem of entry guidance. Because the abort guidance algorithm must design entry trajectories, examining the many approaches provides a logical starting point for analysis. The most thoroughly studied and tested entry guidance algorithm is the space shuttle entry guidance algorithm [8]. Shuttle entry guidance relies on analytical approximations relating predicted downrange to drag-velocity reference profiles. Perturbing the vehicle control variables to track the drag-velocity profile guarantees that the vehicle meets the desired range and altitude targets [8]. The tracking algorithm in the shuttle uses linearized assumptions. A number of papers propose nonlinear tracking algorithms for a drag-velocity based entry guidance algorithm [9, 10, 14]. The nonlinear tracking algorithms improve reference profile tracking performance.

Shuttle entry guidance does not account for many of the problems associated with an abort. Extending the shuttle entry guidance algorithm into an abort guidance algorithm is possible. Owen Deutsch designed an abort planning algorithm based on the shuttle entry guidance algorithm. Deutsch defines a family of possible reference profiles. The reference profiles define a vehicle footprint of achievable landing sites. An algorithm chooses the best site and generates a reference profile to fly to that site.

An entry guidance approach which avoids drag-velocity reference profiles is a numerical predictor-corrector entry guidance algorithm [4, 7]. The predictor-corrector approach numerically integrates the equations of motion using some predefined control history from the current state to the final state to predict the final range. Based on this prediction, the corrector modifies the control history to meet the range target [4].

More detail on the above methods is provided throughout this thesis as necessary for comparison and evaluation. The robust abort guidance algorithm presented in this thesis attempts to combine many of the strengths of the traditional approaches. Combining these strengths maximizes robustness while minimizing complexity.

1.3 Algorithm Summary

The abort guidance algorithm is summarized here to introduce the basic elements of the system. The easiest way to view the proposed algorithm is as a nonlinear model based compensator. This model based guidance approach is developed in detail in chapter 3. As an introduction, figure 1.1 captures the general idea. All guidance systems operate real time. Upon initiation of an abort, the trajectory design algorithm defines a footprint of achievable landing sites through a combination of numerical prediction (state integration from the initial conditions to a final velocity) and analytic approximations. The algorithm chooses the best landing site within the achievable footprint based on some set of performance criteria. Accept for the moment that associated with any achievable landing site is some magnitude of bank angle to reach the site. The trajectory design algorithm determines the bank angle to reach the desired site. The "model" in the model based compensator is the reference dynamic model. The reference model is defined by the nominal vehicle dynamics subject to a nominal guidance algorithm. The states and controls of the reference model are the commanded nominal states and controls. A tracking algorithm forces the actual vehicle states to track the reference model states through application of control perturbations. The control perturbations (to bank angle and angle of attack) are a function of the state errors (drag and altitude errors). Finally a trajectory redesign algorithm modifies the reference bank angle command to reject initial condition errors. The redesign algorithm controls the vehicle energy as a function of range to go to the target site. This discussion is very general.

The method becomes clear through analysis of the individual elements.

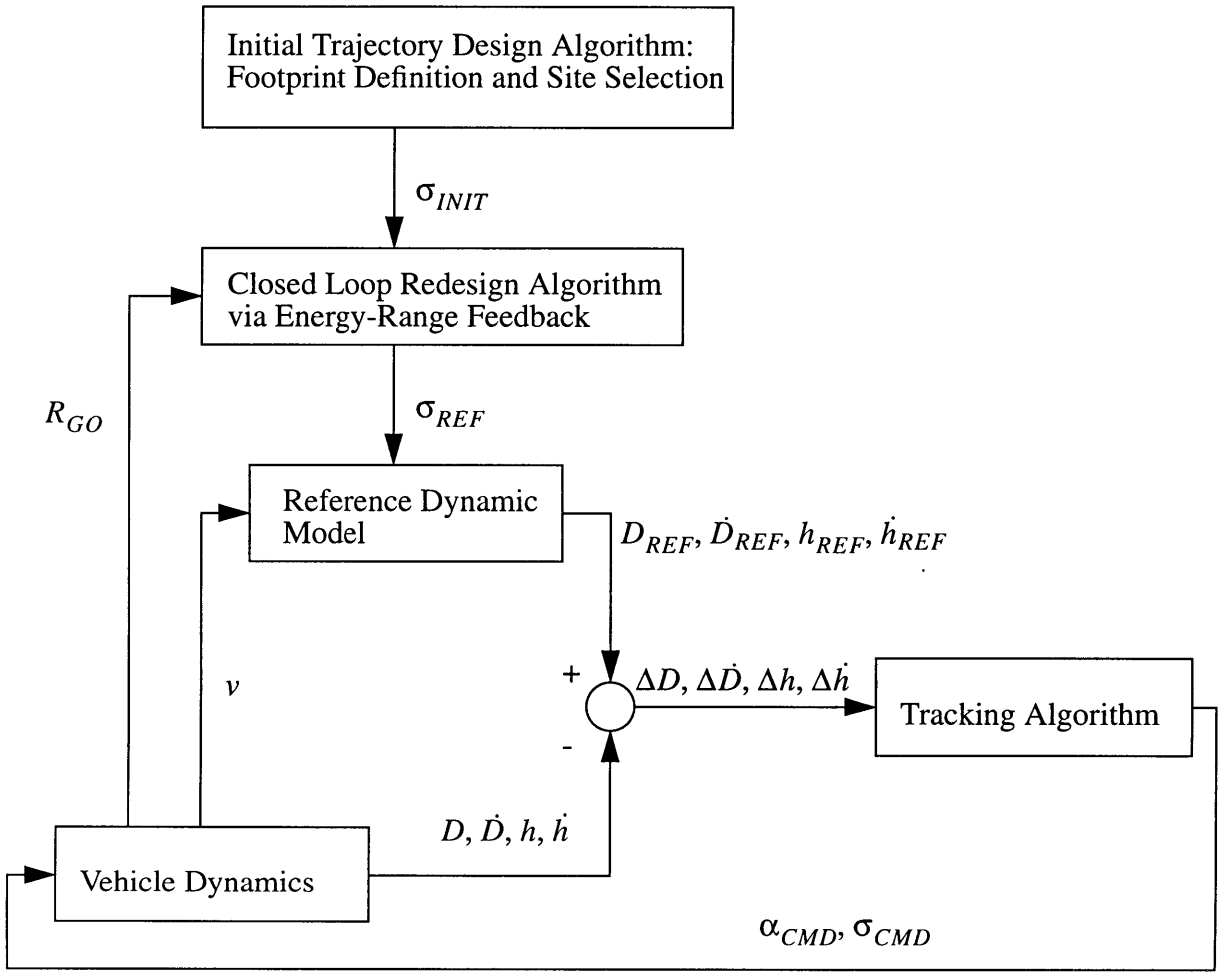

Figure 1.1 : X-34 Reference Dynamic Model Based Guidance

Table 1.1 summarizes the various guidance system functions. At this point, the table only includes general information. Throughout this thesis, updates to the table define important guidance system functions.

Table 1.1 : Guidance System Functions

	Trajectory Design Algorithm	Reference Dynamic Model	Trajectory Tracking
In-flight functions:	Defines parameters of Reference Model to meet range and constraint requirements	Propagates nominal vehicle dynamics - modified by the Trajectory Design Algorithm	Tracks Reference Dynamic Model

1.4 Thesis Overview

A great deal of information is presented to explain and verify the robust abort guidance system. Chapter 2 introduces the X-34 vehicle characteristics, applicable reference frames, and equations of motion. Chapter 3 is devoted to describing and defining the reference dynamic model. All of the other chapters build on the discussion of model based guidance presented in chapter 3. Chapter 4 analyzes vehicle capability and provides some insight into footprint definition and trajectory design. Chapter 5 presents the initial in-flight trajectory design and in-flight trajectory redesign algorithms. Chapter 6 discusses trajectory tracking and compares an output feedback classical approach to a state feedback linear quadratic regulator. Tracking algorithm robustness is addressed. Chapter 7 presents performance robustness results. In addition to performance results, chapter 7 also presents useful tools for defining performance robustness in terms of control saturation. These tools are specific to a model based guidance approach and useful for site selection. Finally, chapter 8 makes some concluding comments and suggestions for future work.

Chapter 2

Vehicle Description

Design of an abort guidance system begins with the nominal vehicle model. This chapter summarizes the X-34 vehicle parameters used for analysis. Other important elements of the design framework are presented, including reference frames, equations of motion, and uncertainty sources. The final section of this chapter discusses levels of computer simulation and their relative strengths and weaknesses.

2.1 Physical Configuration

The X-34 is a high *L/D* vehicle capable of flights up to speeds of mach 8. It has a wing span of 27.7 feet and length of 58.3 feet. A drawing of the X-34 is in figure 2.1 [16].

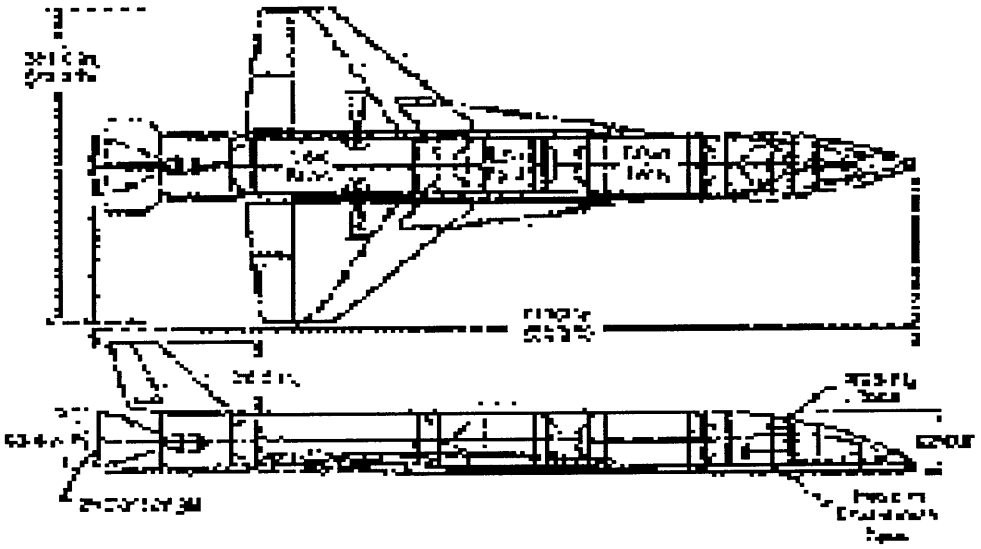

Figure 2.1 : Baseline X-34 Design

The X-34 has only a single engine. It is a liquid oxygen / kerosene engine capable of generating up to 60,000 pounds of thrust [16]. The typical X-34 flight begins with a drop from Orbital Sciences Corporation's L-1011 aircraft. The engine then starts and the vehicle accelerates up to the planned Mach number and altitude. Next a short coast phase is followed by re-entry and landing [16].

2.2 Aerodynamic and Mass Properties

Vehicle properties are provided by Orbital Sciences Corporation. For the purposes of analysis only the base lift and drag coefficients are used. Speedbrake, elevon, and body flap effects are all ignored to maintain simplicity. It is assumed that closed loop feedback can take care of unmodeled aerodynamic effects and this issue is addressed in the algorithm robustness analysis. In fact, the contributions of the various aerosurfaces are actually very small for the flight regimes that the analysis presented here focuses on.

This thesis assumes a simplified vehicle model with a point mass of 840 slugs. The value for vehicle surface area is 350 ft^2. The aerodynamic data used for X-34C analysis is derived from the X-34B actual aerodynamic data. The data is scaled to adjust for the size differences between the two vehicles. The baseline lift and drag coefficients vs. angle of attack and mach number are plotted in Figure 2.2.

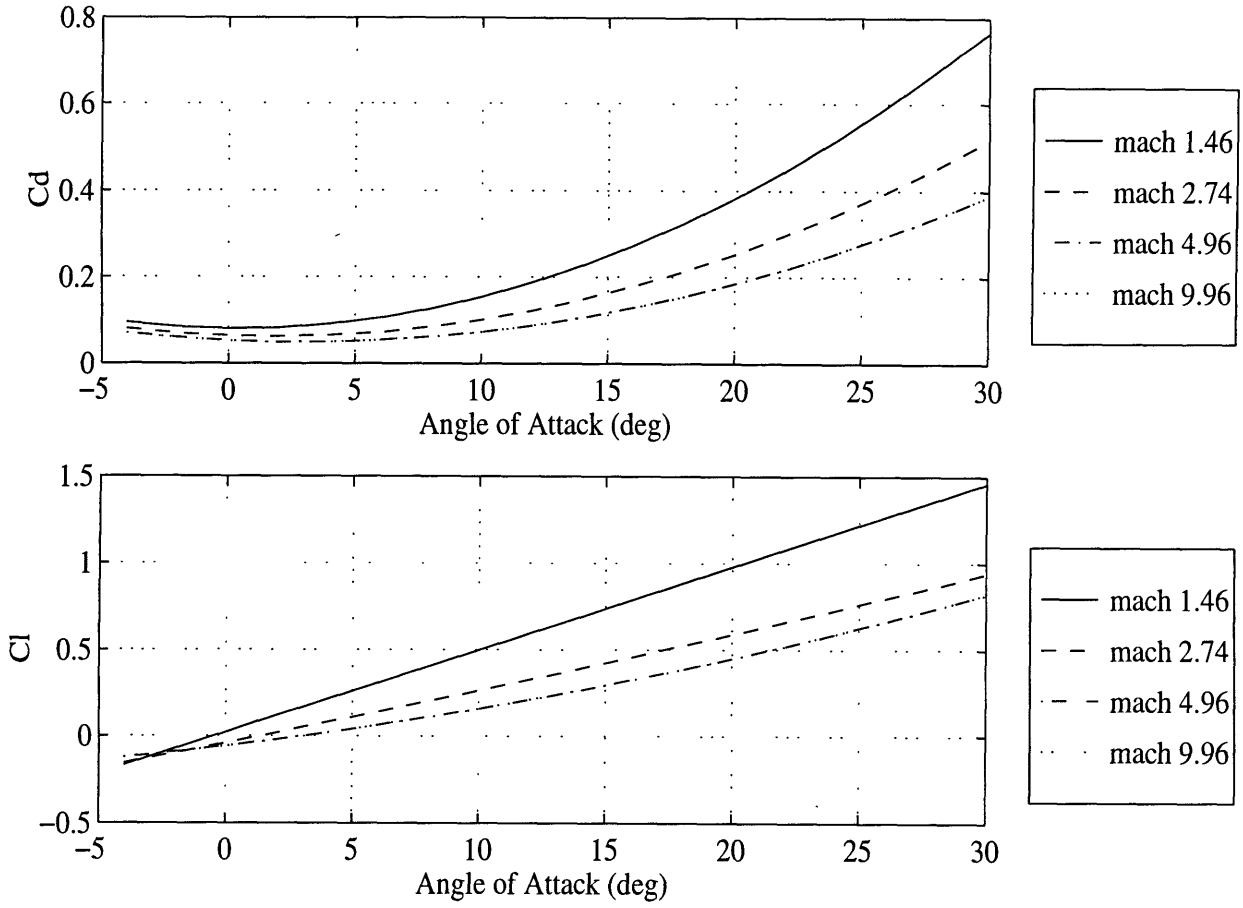

Figure 2.2 : Baseline Aerodynamic Coefficients

The vehicle lift to drag ratio (*L/D*) is an important property for controlling gliding range. *L/D* is plotted in Figure 2.3 below. Maximum range is achieved at maximum *L/D*. Controlling the vehicle *L/D* is very important for trajectory design and tracking.

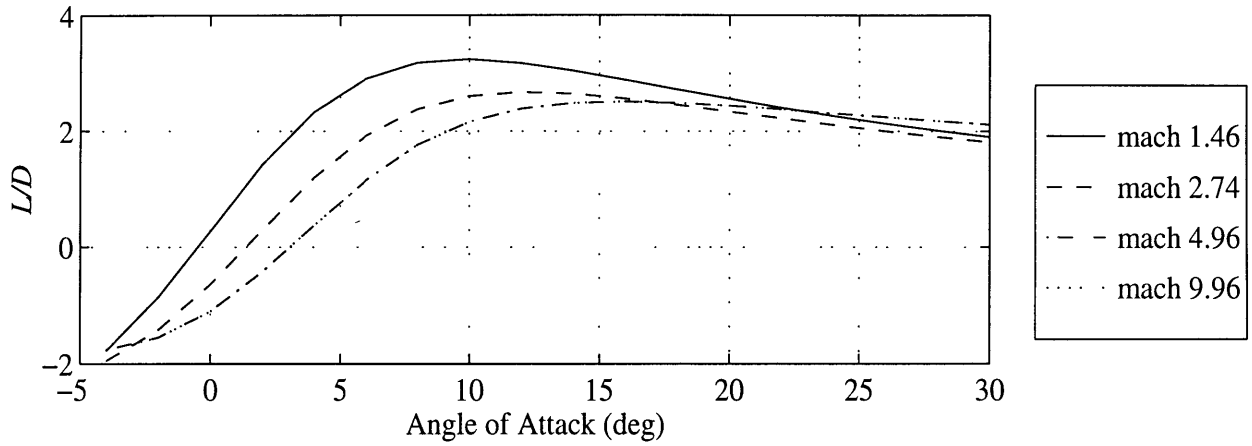

Figure 2.3 : Lift/Drag Ratio

The contributions of speedbrake, elevon, and body flap are plotted below in Figures 2.4 through 2.6. The plots present differences to the aerocoefficients due to maximum applications of the aerosurfaces. The maximum speedbrake deflection is 87.5 degrees. Maximum elevon deflections are +10 degrees and -20 degrees. Maximum body flap deflections are +/- 10 degrees. The figures below indicate that the contributions of the aerosurfaces are relatively small.

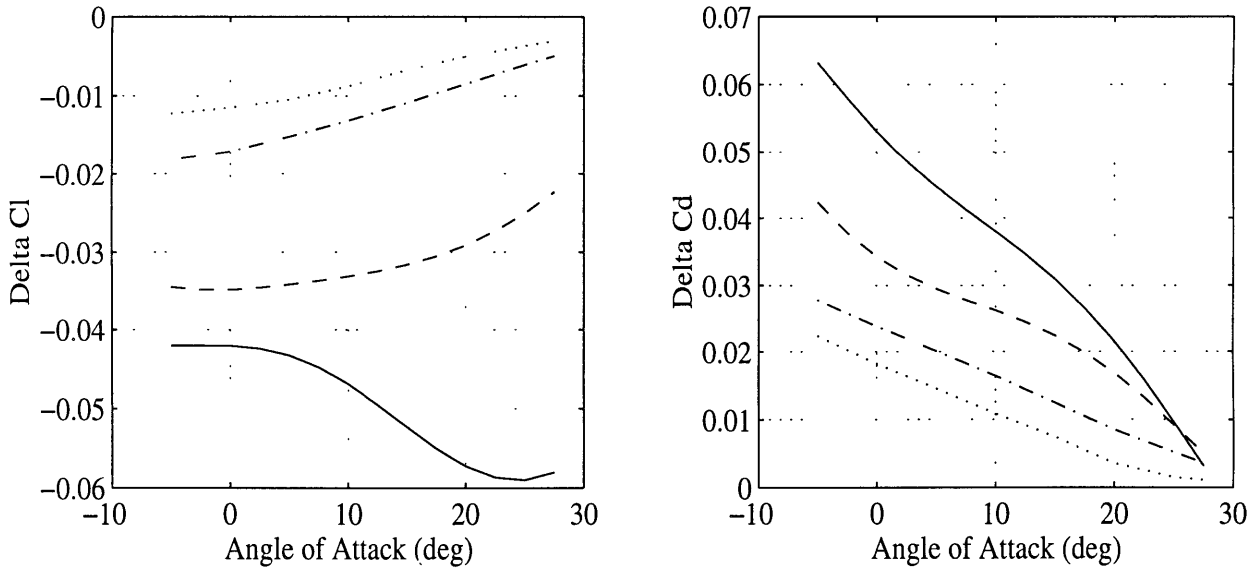

Figure 2.4 : Maximum speedbrake deflection aerocoefficient effects ('-' mach 10.0, '--' mach 5.0, '-.' mach 3.5, ':' mach 2.5)

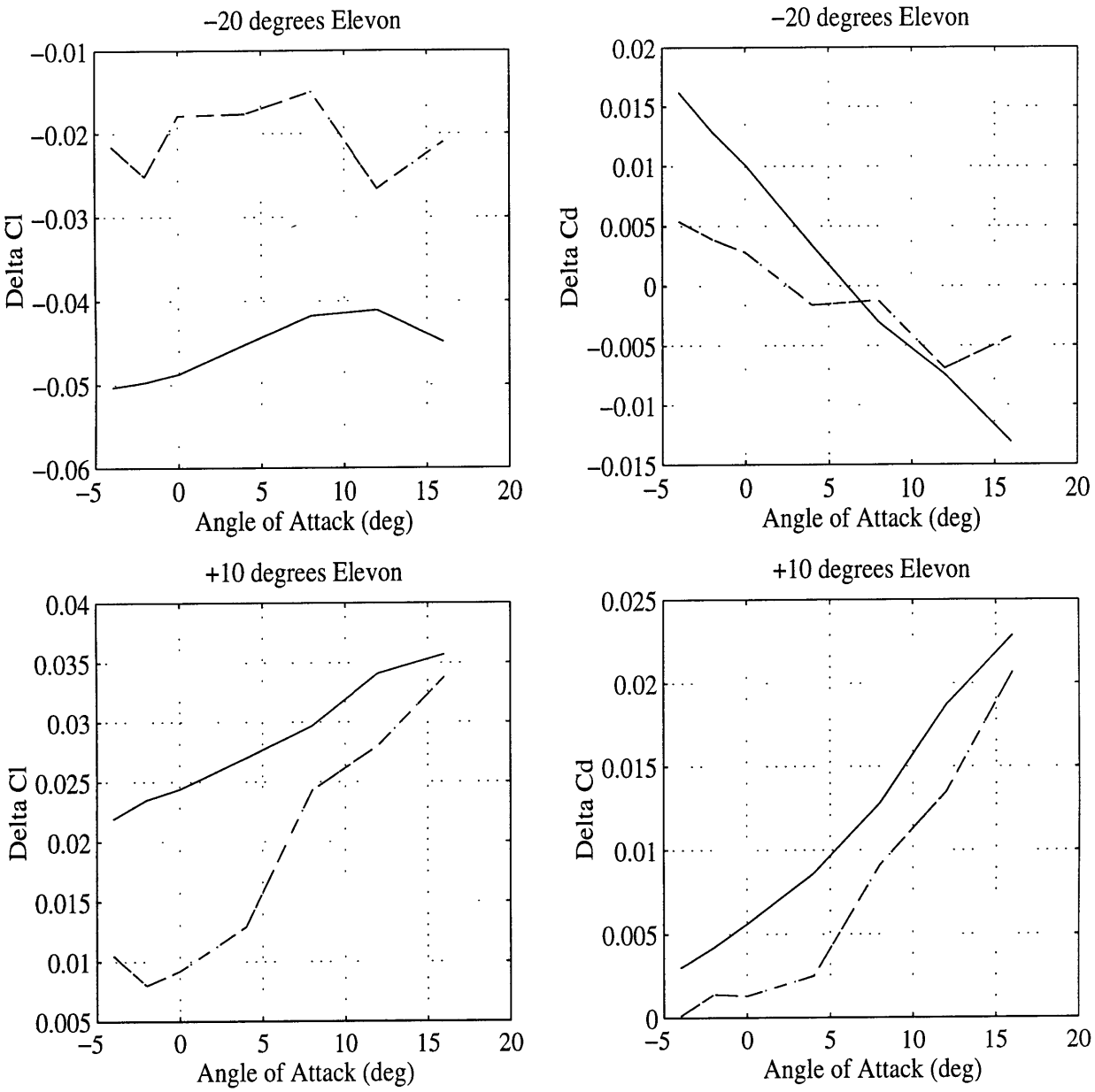

Figure 2.5 : Maximum elevon deflection aerocoefficient effects ('-' mach 9.96, '--' mach 4.96, '-.' mach 2.74)

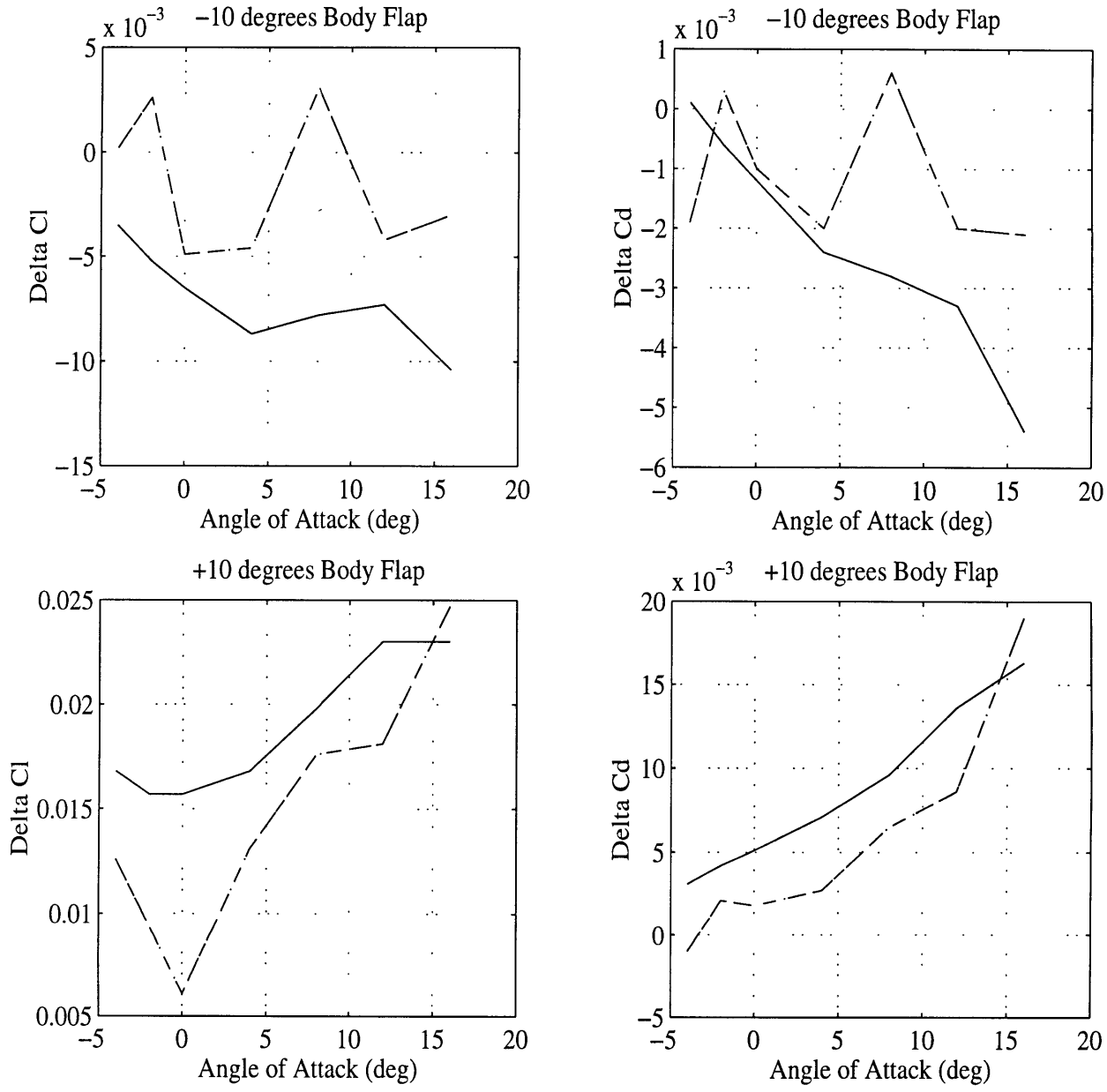

Figure 2.6 : Maximum body flap deflection aerocoefficient effects ('-' mach 9.96, '--' mach 4.96, '-.' mach 2.74)

Another important issue to consider is the necessity of trimming the vehicle to achieve the desired state. Again to maintain simplicity, the effects of trimming the vehicle using the aerosurfaces is ignored. Small variations in aerodynamic properties occur due to the effects of trimming the vehicle but again it is assumed that closed loop feedback can correct for these variations.

2.3 Coordinate Frames

Several different reference frames are used for design and analysis of entry guidance systems. The applicable frames are defined below.

Inertial Frame

The non-rotating earth centered frame is used as the inertial reference. The origin is the center of the earth. The **I** axis is defined through zero longitude at time zero. The **K** axis points through the North Pole. The **J** axis is defined perpendicular to the first two components to complete a right handed set.

Earth Centered Earth Fixed Frame

The earth centered earth fixed (ecef) frame rotates in the inertial frame at the earth's rotation rate. Again the origin is the earth's center and the **K'** axis is through the North Pole. The **I'** axis is defined through zero longitude at all times. **J'** completes the right handed set.

Local Level Frame

The local level frame is defined by north (**N**), east (**E**), and down (**D**) components relative to the vehicle's center of gravity (cg). The down component points to the center of the earth.

Body Frame

The body frame is fixed to the vehicle cg with the $\mathbf{u_{bx}}$ axis fixed through the nose, $\mathbf{u_{by}}$ axis fixed to the right wing, and the $\mathbf{u_{bz}}$ axis is defined by the right hand rule to be "down".

Velocity Direction Frame

The velocity direction frame is also fixed to the vehicle cg. The $\mathbf{u_{vx}}$ axis is defined along the vehicle's earth relative velocity vector. The $\mathbf{u_{vy}}$ axis is defined as the cross product of the gravity vector and $\mathbf{u_{vx}}$. The $\mathbf{u_{vz}}$ axis completes the right handed set.

Local Vertical Local Horizontal Frame

Finally, the most heavily used frame for trajectory design and tracking is the local vertical local horizontal (lvlh) frame. This frame's origin is again the vehicle cg. The $\mathbf{u}_{lvz}$ axis (local vertical) is pointed towards the earth's center. $\mathbf{u}_{lvy}$ is then defined by the cross product of $\mathbf{u}_{lvz}$ and the vehicle's earth relative velocity vector. Then the $\mathbf{u}_{lvx}$ axis (local horizontal) is defined by the cross product of the $\mathbf{u}_{lvy}$ and the $\mathbf{u}_{lvz}$ axes to complete the right hand set.

Relationships of Reference Frames

Figure 2.7 shows the relationships between the body frame and the local level frame. This coordinate transformation defines the vehicle body attitude (roll - ϕ, pitch - θ, yaw - ψ). Figure 2.8 illustrates the relationships between the body frame and the velocity direction frame. This coordinate transformation defines the vehicle angle of attack (α), bank angle (σ), and sideslip angle (β). These angles are important in defining the aerodynamic forces acting on the vehicle. In general for the analysis here, β will always be assumed to be zero or small.

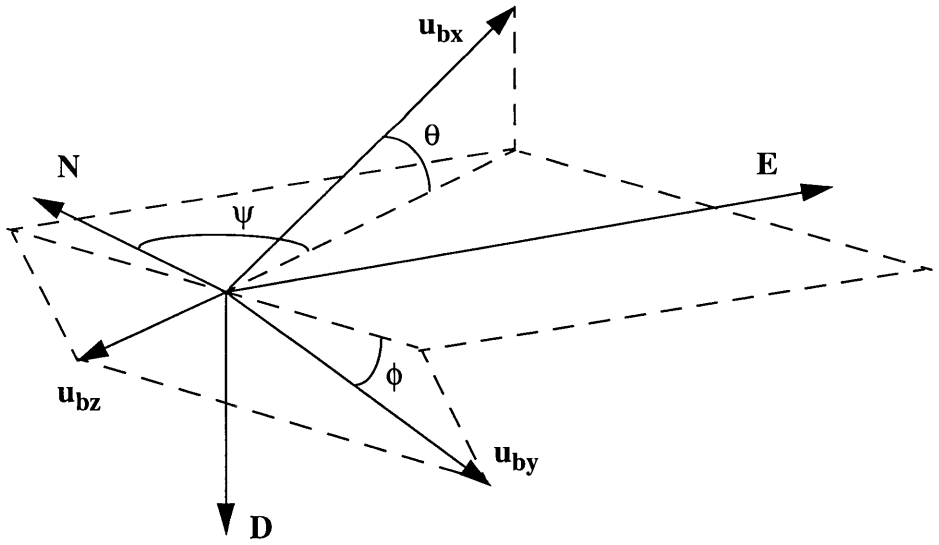

Figure 2.7 : Body Frame & local level frame

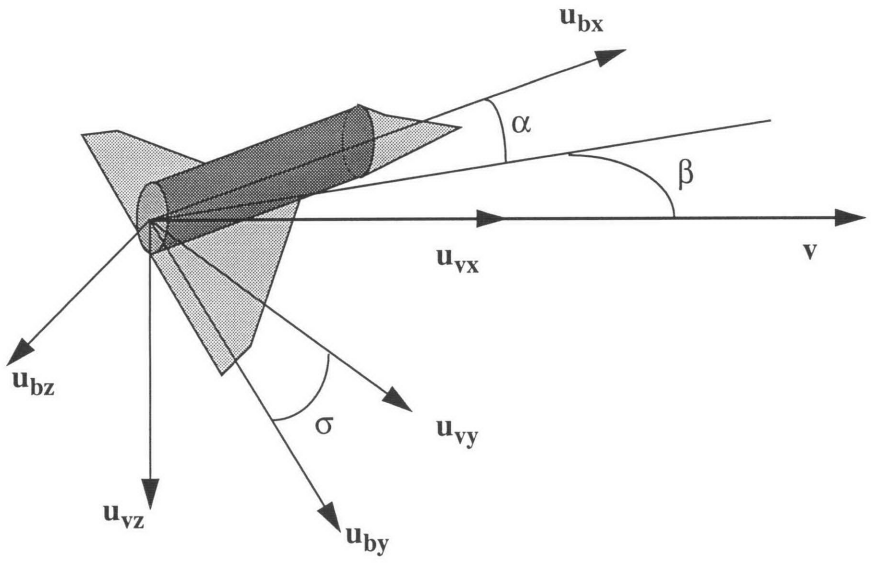

Figure 2.8 : Body Frame and Velocity Direction Frame

2.4 Equations of Motion

2.4.1 Trajectory Design and Tracking Equations of Motion

For trajectory design and tracking several assumptions are made to simplify the vehicle equations of motion. The lvlh frame is used as the reference and a point mass is assumed. Coriolis and transport terms are ignored for simplicity. The variables of interest are the downrange, crossrange, radial position (altitude), velocity, flight path angle, and heading angle. The following equations describe the vehicle dynamics of a point mass for a nonrotating, spherical earth (i.e. coriolis and transport terms neglected):

$$\rho = \rho_s e^{\left(-\frac{(r-r_s)}{H}\right)} \tag{2.1}$$

$$D = \frac{1}{2}\rho v^2 C_D \frac{S_a}{m} \tag{2.2}$$

$$\frac{dR_x}{dt} = v\cos\gamma\cos\psi \tag{2.3}$$

$$\frac{dR_y}{dt} = v\cos\gamma\sin\psi \tag{2.4}$$

$$\frac{dr}{dt} = v\sin\gamma \qquad \textbf{2.5}$$

$$\frac{d\gamma}{dt} = \left(\frac{1}{v}\right)\left(L\cos\sigma - \left(g - \frac{v^2}{r}\right)\cos\gamma\right) \qquad \textbf{2.7}$$

$$\frac{d\psi}{dt} = \left(\frac{1}{v}\right)\left(L\frac{\sin\sigma}{\cos\gamma} - \frac{v^2}{r}\cos\gamma\sin\psi\right) \qquad \textbf{2.8}$$

$$\frac{dv}{dt} = -D - g\sin\gamma \qquad \textbf{2.6}$$

These equations of motion are used in varying manners for trajectory design and tracking. In some cases state transformations will be applied for ease of analysis. These are explained as the case arises.

2.4.2 Vehicle Constraints

Perhaps the most difficult aspect in designing a guidance system is found in dealing with the vehicle constraints. The constraints on the X-34 include: maximum normal load, maximum dynamic pressure, and limited controllability of bank and angle of attack.

The normal load (in g's) generated by the vehicle is limited to 4.0 and is defined below. Note that angle of attack is capable of directly controlling the normal load.

$$n = \frac{L\cos\alpha + D\sin\alpha}{g} \qquad \textbf{2.9}$$

Maximum dynamic pressure is limited to 700 lbf/ft^2. Dynamic pressure is given by the following:

$$q = \frac{1}{2}\rho v^2 \qquad \textbf{2.10}$$

Vehicle controllability is especially important in the early phases of flight. While the vehicle is high in the atmosphere and before dynamic pressure is built up, the aerosurfaces can not act to control angle of attack and bank. This requires the use of the aerojet thrusters which can not be used to generate large sustained moments. Therefore, in the early phase of flight, guidance assumes that no closed loop control is possible. Another controllability issue is that during the flight, the aerosurfaces may not be able to generate the moment necessary to meet the guidance

commands on angle of attack and bank. This concern is only addressed to the degree that the nominal case is defined to be well within the achievable region and perturbations from this region are assumed to be within the capability of the vehicle.

2.5 Uncertainty Sources

Entry guidance problems face a wide variety of uncertainties. The types of uncertainty considered include atmospheric and aerodynamic uncertainties. Constant multiplicative biases and stochastic multiplicative uncertainties are applied to verify algorithm robustness.

2.5.1 Atmospheric

The primary source of atmospheric uncertainty is air density. A "thick" or "thin" atmosphere has different effects on vehicle performance and capability. A summary of possible air density variations for the earth is found in [5, 6]. Generally, three uncertainty models capture the worst case density variations. A +/- 25% constant multiplicative bias shows the steady state response. A shift from a "thick" +20% atmosphere to a "thin" -20% atmosphere in mid-trajectory or vice versa is the worst case scenario. Finally a stochastic density model is the most realistic. White noise is filtered to generate a slowly time-varying multiplicative density bias.

2.5.2 Aerodynamic

Aerodynamic uncertainty is also very important. Aerodynamic uncertainty results simply from using the aerosurfaces to trim the vehicle. Aerodynamic uncertainty also results from modeling errors. Modeling errors can appear in the form of constant multiplicative biases on the lift and/or drag coefficients. The C_L and C_D errors may or not be correlated with one another. Uncorrelated C_L and C_D biases result in an *L/D* bias. The biases may or not be correlated in time. Again, constant +/-10% biases are considered. The shifted bias also is important for assessing transient response characteristics. A filtered stochastic uncertainty model provides the final measure of guidance robustness.

2.6 Simulation Environments

Before proceeding, a description of simulation environments and their relative merits is necessary. A balance between accuracy and simplicity is sought for analysis of guidance systems. Three levels of simulation are considered, each adding complexity but also realism.

The most heavily used simulation is a three degree of freedom (3DOF) Matlab simulation environment. The state is propagated in the guidance frame and the guidance frame equations of motion are used for all computations. A point mass is assumed. The aerodynamic coefficients are approximated by polynomials as a function of angle of attack for different mach numbers. Linear interpolation between mach numbers is used. The vehicle is assumed to be trimmed and aerosurface contributions are ignored. Angle of attack and bank angle commands are rate limited to prevent unrealistic commands and body attitude oscillations. The atmosphere is assumed to be exponential.

The next level of simulation fidelity includes the effects of a rotating earth and the contributions of the aerosurfaces. This 3DOF simulation environment assumes a perfect attitude response. Guidance commands an angle of attack and bank angle which corresponds to a commanded body attitude. In the actual environment, the body attitude response is rate limited to prevent unrealistic responses. The contributions of speedbrake, elevon, and body flap are included. However, the vehicle is not trimmed through closed loop control. Instead a table lookup simulates vehicle trimming by choosing the appropriate aerosurface deflections for some L/D or normal acceleration command. A U.S. 1962 Standard Atmosphere is used. Due to time constraints, no analysis was performed using this type of simulation.

Finally, the most accurate level of simulation is the six degree of freedom (6DOF) environment. This environment includes the complete rigid body dynamics and the vehicle aerosurfaces are controlled to properly trim the vehicle. Again due to time constraints, no 6DOF analysis was performed.

Chapter 3

Nominal Trajectory / Reference Dynamic Model Definition

X-34 entry guidance is required to deal with very specific problems resulting from the wide variety of vehicle abort initial conditions. The powered phase of flight puts the vehicle on a ballistic trajectory. Recovering from a ballistic trajectory limits guidance system options and creates potential for wide variations in initial conditions. The proposed guidance framework maximizes robustness to both initial condition and parametric uncertainties by utilizing the strengths of other guidance approaches. In addition to the overall framework, the nominal X-34 trajectory is presented through its relations to the guidance system framework. X-34 trajectories are not unlike space shuttle abort trajectories and the guidance system used for shuttle aborts serves as a starting point for design of the X-34 abort guidance system. The primarily open loop nature of the shuttle guidance system is insufficient for dealing with X-34 aborts. Several modifications to the shuttle guidance algorithm are made to define the nominal X-34 guidance algorithm and nominal X-34 trajectory. The robust abort guidance system builds upon the nominal algorithm to handle the special requirements of abort guidance.

3.1 Introduction to Reference Dynamic Model Based Guidance

Before describing the X-34 nominal trajectory the overall framework of the proposed guidance system must be introduced. Examining the strengths and weaknesses of other guidance approaches and understanding how these strengths relate to the problem of abort guidance leads to a robust framework for abort guidance. Abort guidance must, in real time, handle wide variations in initial conditions and reject atmospheric and aerodynamic uncertainties. These are difficult requirements to meet and defining the guidance system framework to meet these requirements is even more important than the details of implementation.

3.1.1 Reference Profile Based Approach

Traditional atmospheric entry guidance approaches rely on the use of reference profiles which are generated before the vehicle even leaves the ground. The term "reference profile" is used to describe a state or control history defined with respect to some monotonic parameter (i.e. time, velocity, or energy). The reference profiles are designed by engineers through iteration and optimization to guarantee that the vehicle will reach the desired target state. All design is based on the best knowledge of the nominal vehicle aerodynamic properties and it is assumed that large initial condition uncertainties do not exist. The profiles are designed to give some robustness to initial condition and environment uncertainties but it is difficult to maximize robustness for some problems using only a reference profile. Figure 3.1 illustrates the basic reference profile based approach to entry guidance.

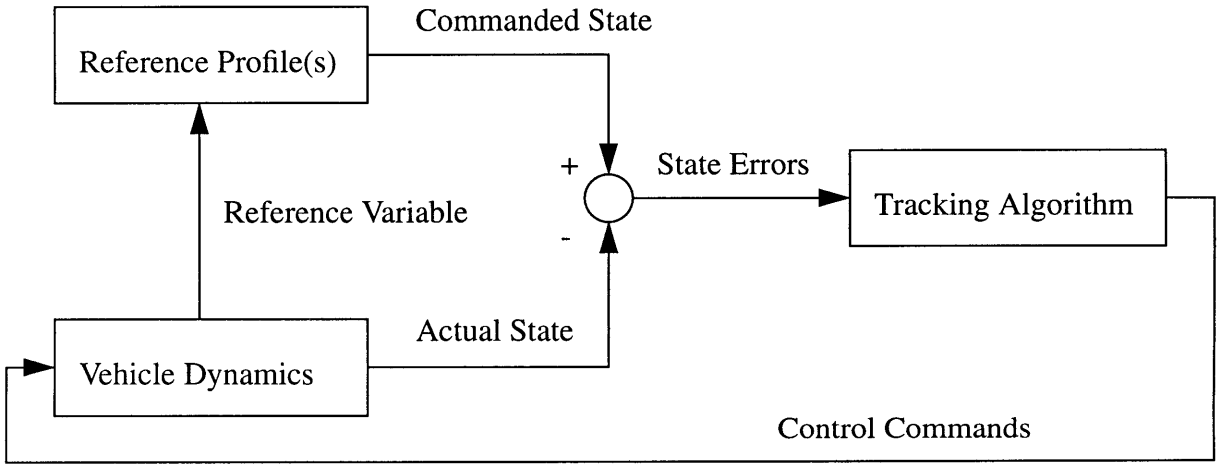

Figure 3.1 : Reference Profile Based Guidance

The most thoroughly tested example of an entry guidance algorithm is the space shuttle entry guidance algorithm [8]. A drag command profile is specified with respect to velocity prior to the mission and the tracking algorithm modulates the vehicle bank angle to track this profile. Tracking vehicle drag rejects parametric uncertainties and guarantees convergence to the desired range target (refer to chapter 5, Appendix A, or [8]). An additional feature of shuttle entry guidance is the capacity to modify the reference profile or some limited number of pieces of the profile during the flight [8]. The in-flight redesign capability is based on analytic approximations of how the drag vs. velocity profile affects the final range. Final range is a function of the entire

profile. A redesign function examines how the entire profile must be modified to meet final range requirements. Figure 3.2 below summarizes the guidance approach with redesign capability. Shuttle entry trajectories are reasonably benign and the variation in initial conditions is not large. Thus the in-flight redesign capability of the shuttle has not truly been tested beyond rejection of small perturbations.

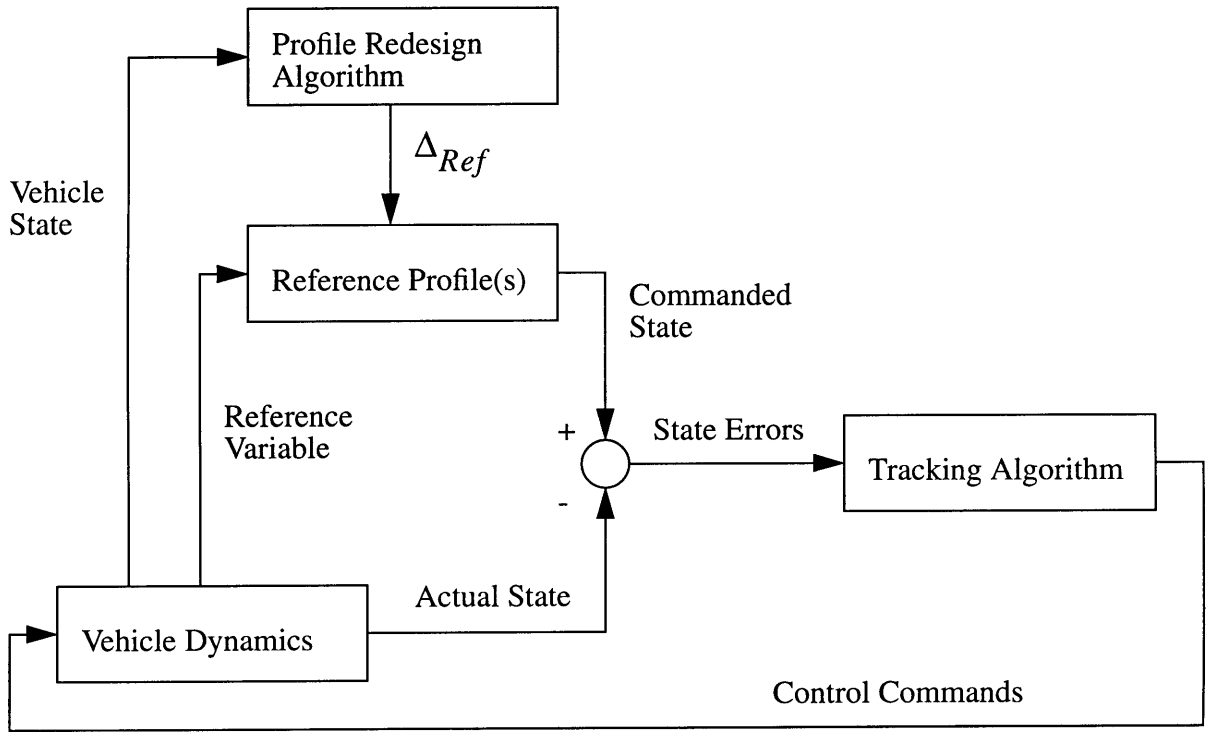

Figure 3.2 : Reference Profile Based Guidance with Redesign Capability

Another important distinction when using the term reference profile is that reference profiles are limited to some predefined form even if the profile is defined in flight. Although shuttle entry guidance allows in flight profile modification, the form of the profile is fixed prior to the mission to meet some array of expected vehicle initial conditions. To capture all of the possible abort conditions for X-34 trajectories, a huge number of reference profiles would have to be generated prior to the mission.

3.1.2 Predictor-Corrector Guidance Approach

A guidance methodology which eliminates many of the limitations of a profile based approach is the predictor-corrector entry guidance approach. An excellent summary of predictor-corrector guidance approaches as they have been applied to various problems is found in Entry Vehicle Performance Analysis and Atmospheric Guidance Algorithm for Precision Landing on Mars. This Master's thesis was written by Todd Dierlam for the Draper Laboratory. Dierlam and other designers recognized the inherent weaknesses of profile based approaches [4]. Recognizing these weaknesses led to refining a numerical predictor-corrector approach to entry guidance problems. The approach is summarized by two parts: the predictor and the corrector. Prediction is accomplished by numerical integration of the vehicle dynamics subject to a control history defined over time. The correction chooses the current control command based on the numerical prediction and the sensitivities of the final states to changes in the control profile. Included in the numerical prediction is an estimation of uncertain environment parameters such as air density and vehicle lift to drag ratio (*L/D*). The estimated parameter values are used in the numerical prediction and the correction term includes sensitivities to the estimated parameters. The value of the parameters used in the prediction is always the current estimated value. No attempt is made at estimation of the dynamics of the uncertainty. Predictor-corrector based guidance is summarized by the following block diagram:

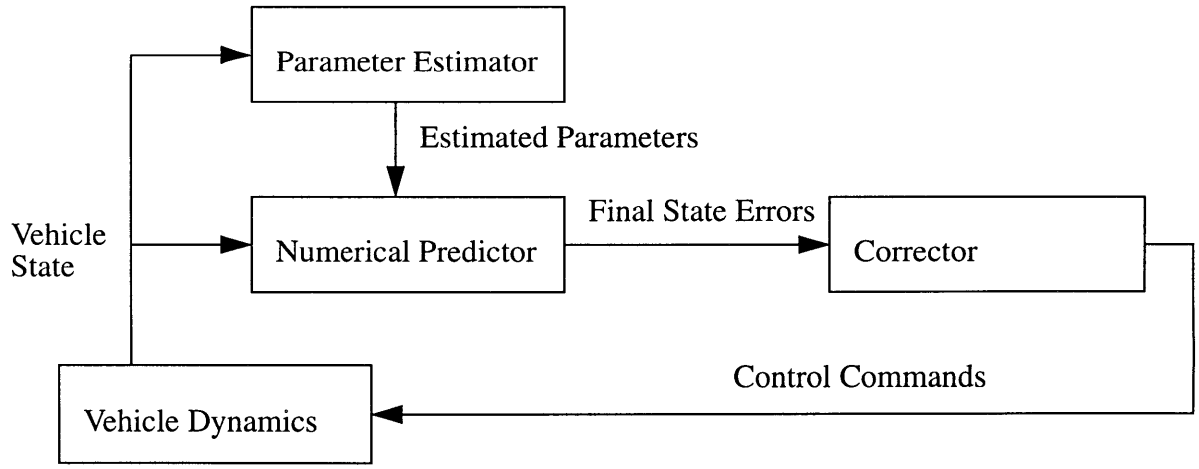

Figure 3.3 : Predictor-Corrector Based Guidance

Predictor-corrector routines do not have problems dealing with variations in initial conditions

because the numerical prediction is always initialized from the current vehicle state. This avoids the necessity of generating multiple reference profiles for handling multiple abort scenarios. A potential drawback of the predictor-corrector approach is that the control commands are completely dependent on the accuracy of the parameter estimation to reject the disturbances caused by the parametric uncertainty. Because the current range control command is chosen as a function of the estimated environment, it is possible that an incorrect control decision could be made early in the trajectory which makes it difficult for the vehicle to recover late in the trajectory. Such cases can arise for large shifts in the parametric uncertainty. Although reliance on environment estimation can cause problems, in some applications parametric uncertainty estimation may be desirable, if not absolutely necessary. A Mars atmospheric entry guidance problem is an excellent example. Knowledge of the Mars atmosphere is far from perfect. Thus a real time estimate of the air density may be very important. Predictor-corrector guidance has been studied extensively for use in Mars entry guidance and earth aerobraking applications [4, 7]. Aerobraking refers to the use of the earth's atmosphere to impart orbit changes. Both of these applications take place in low density applications generally with low to mid *L/D* vehicles. Overall trajectory control authority is very low and is much more dependent on the actual air density and *L/D*. Thus uncertainty estimation can be important if not critical to success.

3.1.3 Reference Dynamic Model Based Approach

Both of the approaches presented above have strengths and weaknesses. The profile based approach takes advantage of the use of closed loop control to reject uncertainty. However, profile based approaches may have difficulty in handling wide variations in initial conditions. The predictor-corrector approach deals effectively with wide variations in initial conditions but is dependent on an estimation of parameter uncertainties to reject these same uncertainties. An attempt to combine the strengths of both approaches is presented here.

The term "reference dynamic model" is defined as the nominal vehicle equations of motion subject to a nominal guidance algorithm. The nominal guidance algorithm is defined by a combination of open and closed loop controls. The reference model is really just a high fidelity form of a reference profile. The distinction between a "model" and a "profile" is that the model is only generated for the current guidance step. The model state is initialized to the vehicle state at

the start of closed loop tracking of the reference model. Like the predictor-corrector approach, this allows for wide variations in initial conditions. Once initialized, the model propagates in-flight at each guidance step to match the current vehicle velocity. The model states propagate according to the nominal vehicle equations of motion and nominal guidance algorithm. The model is only initialized once at the start of closed loop tracking so its behavior is slaved to the nominal dynamics. A numerical prediction is used to predict the effects of modifying the reference dynamic model's control commands on the final range. The numerical prediction is simplified and formulated as an integral feedback term because the prediction only considers nominal dynamics. Uncertainties are not included in the prediction. Parametric uncertainties are rejected by closed loop tracking of the reference model. Once closed loop tracking begins, at each guidance step the model propagates to match the current vehicle velocity. The states of the model are the reference commands. The controls of the model are the nominal control commands. The errors between the vehicle states and the model states are fed back to generate perturbations to the nominal control commands. Matching the vehicle state to the model state ensures that the vehicle meets final range and altitude target states. Rejection of parametric uncertainties is accomplished through closed loop tracking, rather than estimation.

A helpful parallel for understanding the distinction between a profile based approach and a model based approach is to recognize that model based guidance is simply a nonlinear model based compensator. All control problems are ultimately viewed as model matching problems. A control system designer chooses a reference model with some desirable properties and designs a compensator to force the plant to follow the model. The reference dynamic model based guidance system presented in this thesis builds on the same concepts. Readers unfamiliar with model based compensators can consult most standard controls texts [2, 12]. Figure 3.4 illustrates the basic features of model based guidance.

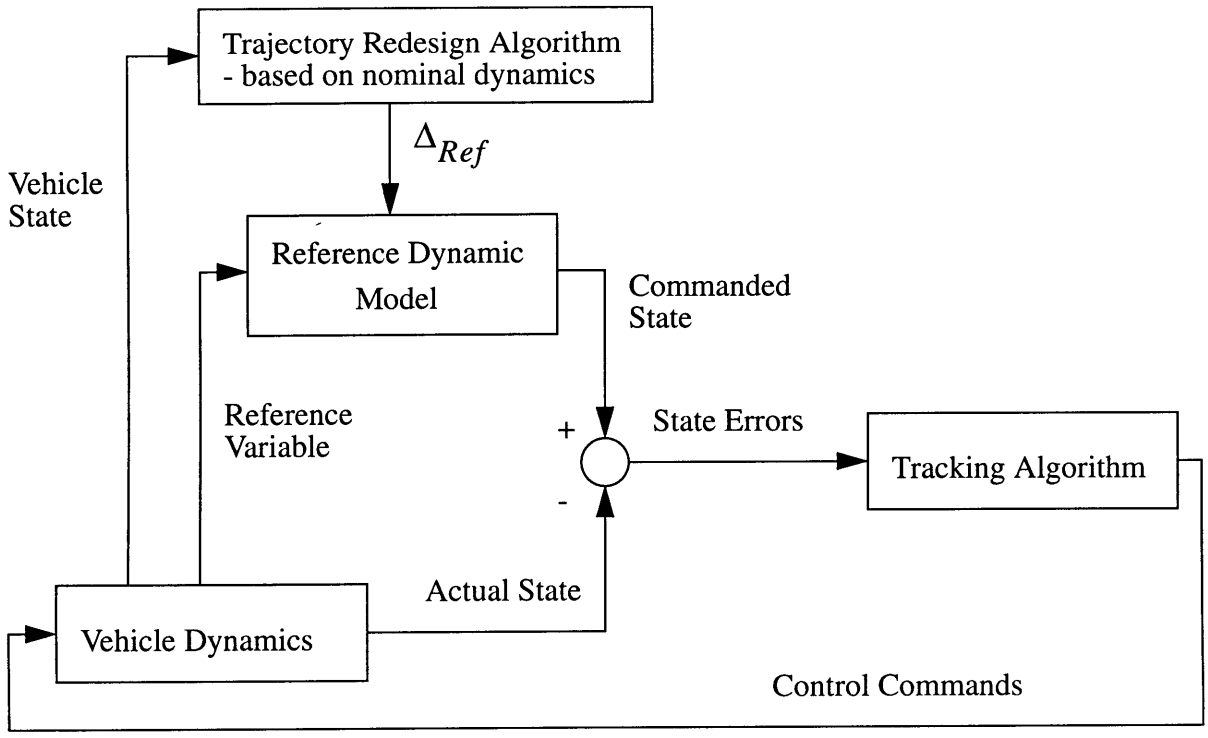

Figure 3.4 : Reference Dynamic Model Based Guidance

The difference between a predictor-corrector approach and a model based approach is subtle but, depending on the application, potentially significant. The most important fact to recognize is that both approaches accomplish the same goals but through different techniques. Define vehicle range as a "long-term" control output. Final range is a function of the entire vehicle trajectory. Tracking of state errors are "short-term" control objectives. In general, rejection of parametric uncertainties is best handled from a short-term perspective. This is especially true if the uncertainties are uncorrelated in time. A predictor-corrector approach makes long-term control decisions based on the current estimate of parametric uncertainties. A model based approach makes long-term control decisions based only on the best knowledge of the nominal dynamics. The model based approach accomplishes short-term control and rejects uncertainty through closed loop rejection of short-term state errors. A predictor-corrector approach accomplishes short-term control based on long term prediction. A final distinction is that because the predictor-corrector approach makes short-term control decisions based on long-term outputs, the number of control variables must be limited to make the correction numerically feasible in real time. A

model based approach can use all of the available control variables to track the reference model states because the problem can be posed as a multivariable regulator problem.

In summary, the predictor-corrector approach is estimation based while the model based approach is control based. They both accomplish the same goals and ultimately both approaches are limited by the same factor: control saturation. When using reference profile based approaches in applications with large variations in initial conditions, control saturation is frequent because it is difficult to guarantee realistic profiles. A reference profile based approach assumes that enough control authority is present to fly the desired profile. Predictor-corrector and model based approaches both successfully eliminate this problem by making predictions as a function of the current vehicle state. For the model based approach, control saturation only occurs when the parametric uncertainties are so great that the desired target is completely not achievable. This is due to the fact that the reference model, because it represents the best knowledge of the vehicle dynamics, is effectively the center of the achievable corridor. This is also the case for the predictor-corrector approach. This is a useful fact. The only performance limitation for the guidance system is now control saturation. The guidance system is not limited by the constraints of a profile based approach and now the guidance system maximizes the use of vehicle capability. The potential advantage of a predictor-corrector approach is that although it is still limited by control saturation, at least the predictor-corrector based guidance algorithm knows that a particular target site is not achievable due to a large parametric uncertainty.

Predictor-corrector guidance has generally been applied to low to mid *L/D* vehicles in low density environments [4]. The author would argue that in these cases estimation of parametric uncertainties becomes more important. Overall range control authority is relatively small so it is important to have knowledge of how parametric uncertainties affect the trajectory. For high *L/D* applications, there is more range control authority and a model or profile based approach makes more sense. A combination of the two approaches could serve as a highly effective guidance system. Uncertainty estimation could be applied to trajectory design, footprint definition, and site selection, while reference model tracking guarantees convergence to the target states.

The above discussion is very general. The details of the implementation and advantages of a

model based approach are addressed throughout the remainder of this thesis. Several needs have been identified in the above discussion. The first is a nominal guidance algorithm. The nominal guidance algorithm controls the reference model states. In addition the nominal guidance algorithm defines the framework of the trajectory design algorithm. The nominal guidance algorithm is defined by the engineer before the vehicle leaves the ground by examining the vehicle properties and trajectory constraints. A real time range control feedback law for trajectory design is necessary. The tracking law drives the vehicle state to the model state. This guarantees that the actual vehicle behaves like the nominal vehicle. This simplifies the trajectory design problem and allows the use of only nominal dynamics for trajectory design. The reference model propagates real time throughout the flight. The trajectory design and tracking laws run real time. The trajectory design algorithm meets the long-term control objectives (primarily range control) while the tracking algorithm meets the short-term control objectives (rejection of parametric uncertainties).

3.2 Space Shuttle Glide Return to Launch Site Guidance

The vehicle nominal trajectory is defined from the general framework of the shuttle Glide Return to Launch Site (GRTLS) guidance system. GRTLS is used for shuttle aborts. In a shuttle abort, it is assumed that one or two engines are still firing. Range control is accomplished using the powered phase of the abort guidance and thus the design requirements on GRTLS are simplified. This simplification causes a great deal of the guidance to be essentially open loop. The critical useful aspect of GRTLS is that it is designed to deal with the specific problem of recovering from a ballistic trajectory. The powered phase delivers the shuttle to the glide portion on a ballistic trajectory so it is difficult to regain vehicle control. GRTLS handles this problem using three guidance phases: Alpha Recovery, Nz Hold, and Alpha Transition. Brief descriptions are provided below of each phase to introduce the basic problems of dealing with entry from a ballistic trajectory. A more detailed introduction is available in the *RTLS Abort Training Manual* [17].

3.2.1 Alpha Recovery

As the vehicle enters the atmosphere on a ballistic trajectory, there is virtually no vehicle

controllability. The only goal is to kill off the massive sink rates and to regain vehicle control as rapidly as possible. The shuttle angle of attack is increased as much as possible to generate the maximum lift and bring the flight path angle back to roughly near zero.

3.2.2 Nz Hold

The shuttle builds up dynamic pressure and normal load increases rapidly in the process of reducing the sink rate. Eventually the normal load limit (2.0 g's for the shuttle) is reached and the angle of attack is reduced to maintain a normal load of 2.0 g's. Once the sink rate is sufficiently reduced to a predefined limit and the normal load constraint is no longer applicable, then the shuttle transitions to the alpha transition phase.

3.2.3 Alpha Transition

As explained before, vehicle range control for the shuttle is provided by the powered phase. This allows the alpha transition phase to be flown open loop. Angle of attack is simply commanded by a fixed angle of attack vs. mach profile to roughly follow maximum L/D. As the vehicle was put on the proper initial condition for entry by using the powered portion, no closed loop ranging is necessary. Furthermore, the aerodynamic properties of the shuttle do not cause large trajectory oscillations even though the angle of attack command is open loop. The end of alpha transition is defined by the vehicle's velocity reaching Mach 3.2 where the Terminal Area of Energy Management (TAEM) phase guidance takes over and guides the vehicle to a safe landing. TAEM guidance is described in [15].

3.3 X-34 Nominal Entry Guidance

This section defines the nominal guidance algorithm which controls the reference model trajectory. The nominal guidance algorithm defines the framework for both trajectory design and tracking. Although GRTLS is a good starting point for robust abort guidance, it is insufficient for dealing with the range of possible initial conditions and landing sites that are possible in an X-34 abort. In addition, the aerodynamic properties of the X-34 are different enough to require a modified approach to nominal trajectory design. Although the X-34 and the shuttle are different vehicles there is an important similarity: the powered phase of X-34 flight puts the vehicle on a

ballistic trajectory. This similarity requires retaining the alpha recovery phase guidance as described below. The constraints are monitored and controlled during alpha recovery so the Nz Hold phase is not required. The second phase is Closed Loop Alpha Transition. It is called closed loop because even for the nominal case, closed loop control is necessary to deal with the vehicle aerodynamic properties.

3.3.1 Alpha Recovery

To kill off the initial high sink rates associated with a ballistic trajectory, the vehicle is pitched up to generate maximum lift. This is accomplished by commanding maximum achievable angle of attack (generated by maximum elevon deflection). As the vehicle enters the atmosphere and generates more and more lift, the normal acceleration and dynamic pressure build up. In some cases, depending on initial conditions and environment and aerodynamic uncertainties, the normal acceleration limit is reached and then the vehicle angle of attack is reduced to follow the normal acceleration limit of 4.0 g's. Once the vehicle sink rate is killed off (measurable by reducing the altitude rate to an acceptable level) and the vehicle is no longer on the constraint limit, guidance switches to Closed Loop Alpha Transition. For the nominal case, no banking is used during alpha recovery.

Figure 3.5 summarizes the features of the angle of attack guidance law during alpha recovery phase guidance. The angle of attack guidance law used for nominal design uses perfect aerodynamic knowledge. The linearized change in normal acceleration with respect to angle of attack is computed and this sensitivity is used to generate the new angle of attack command. In actual implementation, the guidance issues a normal acceleration command to the flight control system, not an angle of attack command. A 6DOF flight control system then uses the vehicle control surfaces to achieve the desired normal acceleration command of 4.0 g's. The normal acceleration command is filtered as the load builds up to prevent control saturation. The sudden application of a 4.0 g command right when the limit is reached could cause control saturation as the flight control system attempts to immediately respond to the command. For the purposes of nominal trajectory definition and 3DOF guidance analysis the "perfect" angle of attack guidance law shown below is sufficient. To prevent unrealistic control commands the angle of attack rate response is limited to 2.0 deg/sec.

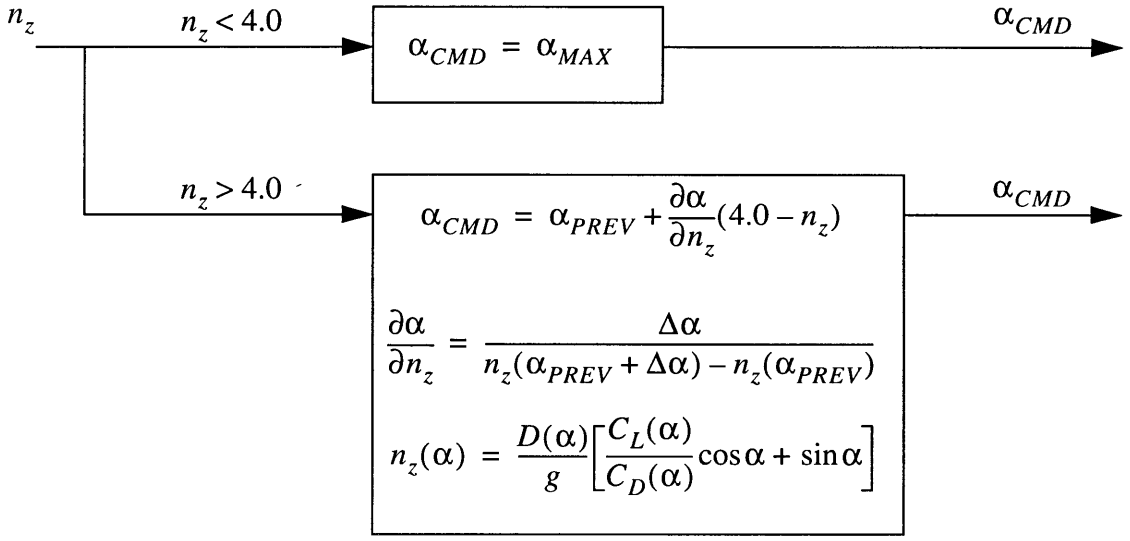

Figure 3.5 : Alpha Recovery Guidance - "Perfect" Angle of Attack Control Law

3.3.2 Closed Loop Alpha Transition (CLAT)

The goal of alpha transition for the shuttle is simply to fly at max L/D, point towards the target, and deliver the vehicle on the front side of the L/D curve for TAEM guidance to take over and fly the vehicle to a safe landing. Although an open loop alpha transition was sufficient for the shuttle, an X-34 abort leaves the vehicle with no engine. With no engine to make range adjustments, closed loop control of the glide during alpha transition is necessary. Closed loop angle of attack control is used to maintain a smooth trajectory while banking is used to point the vehicle toward the target and control vehicle range.

Angle of Attack Nominal Guidance Law

Angle of attack follows a constant pitch command until an upper limit angle of attack vs. velocity profile is reached. The upper limit profile smoothly transitions the angle of attack to the front side of the *L/D* curve at TAEM interface. The constant pitch command is necessary to prevent the vehicle from oscillating up and down throughout the trajectory. A fixed angle of attack profile proved insufficient for smoothing out the trajectory. The only closed loop element in the nominal case is the pitch command following. The CLAT angle of attack guidance law is summarized in

Figure 3.6 below. The "*midval*" refers to middle value. This function is used to define upper and lower limits on a quantity. Like the normal acceleration command guidance above, this guidance law assumes a perfect attitude response. To prevent unrealistic attitude responses the angle of attack command is again rate limited to 2.0 deg/sec.

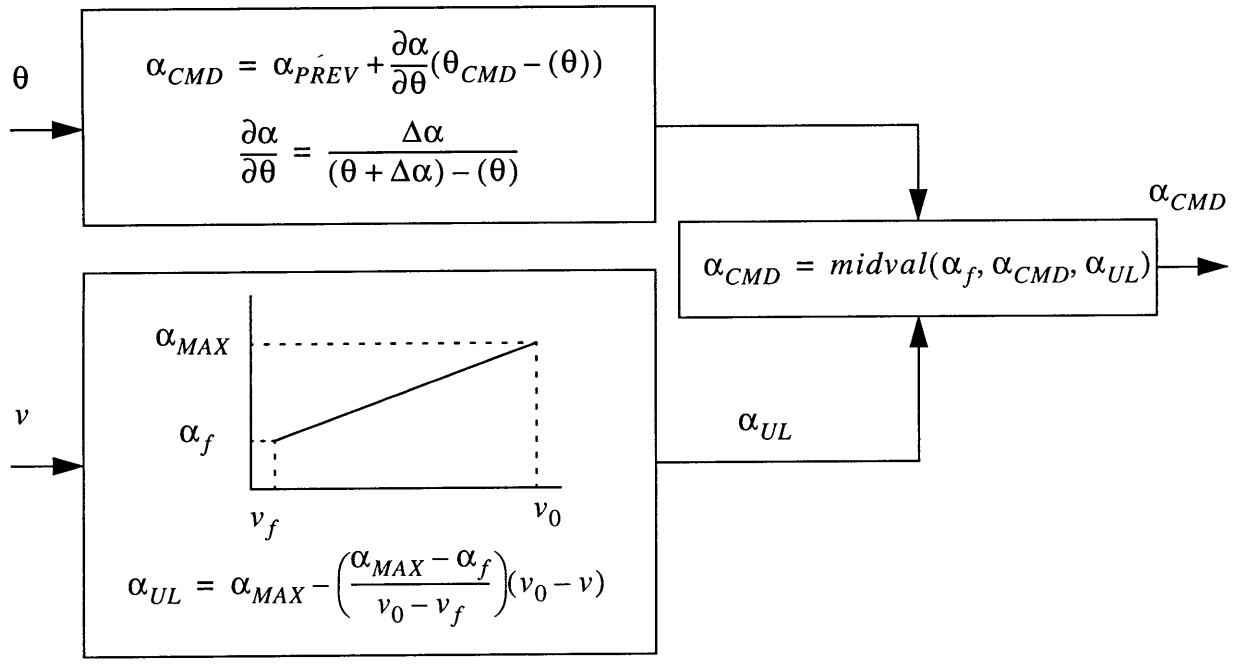

Figure 3.6 : CLAT Angle of Attack Nominal Guidance Law

Bank Angle Nominal Guidance Law

The bank angle nominal guidance law presented here is only used for azimuth angle control. This guidance law assumes that a constant bank command designed to meet minimum crossrange requirements and final range target requirements has already been defined. Azimuth angle control is very simple and is accomplished by simply reversing the direction of bank when an azimuth deadband is exceeded. The deadband size is defined as a function of the bank angle command with an upper limit. Deadband definition was accomplished empirically. The bank angle command is rate limited to 10.0 deg/sec. Defining the magnitude of the bank angle command for range control is addressed in detail in Chapters 4,5, and 6. Figure 3.7 below summarizes the bank angle azimuth guidance law.

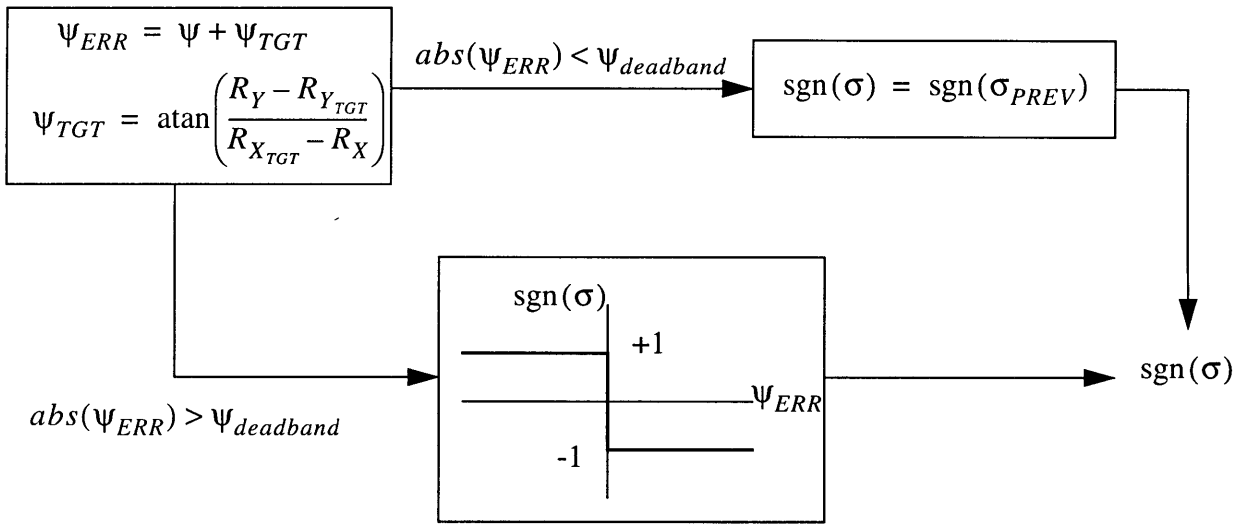

Figure 3.7 : Bank Angle Azimuth Guidance Law

Nominal Vertical Profile

The nominal vertical profile with no banking is illustrated in Figure 3.8. The fixed angle of attack command for alpha recovery is shown and the reduction of angle of attack to follow the normal load limit is highlighted. The immediate reduction in angle of attack upon entering alpha transition is caused by the constant pitch command. Without this reduction the vehicle lobs back up into the atmosphere and the trajectory is not smooth. Next the angle of attack gradually increases to maintain the constant pitch. Finally the upper limit profile is reached and the vehicle is pitched down to enter TAEM. To demonstrate the use of roll reversals to control crossrange, a nominal vertical profile with a constant bank command of 30 degrees is shown as well. Bank rate limited roll reversals are used to keep the vehicle pointed towards the target. For simplicity, the target in this case is defined as the final downrange of the no banking case. The crossrange target is zero. The azimuth error is kept within the deadband by reversing the direction of bank. The trajectory with banking has increased dynamic pressure in the latter portion of flight but dynamic pressure is still not close to the constraint.

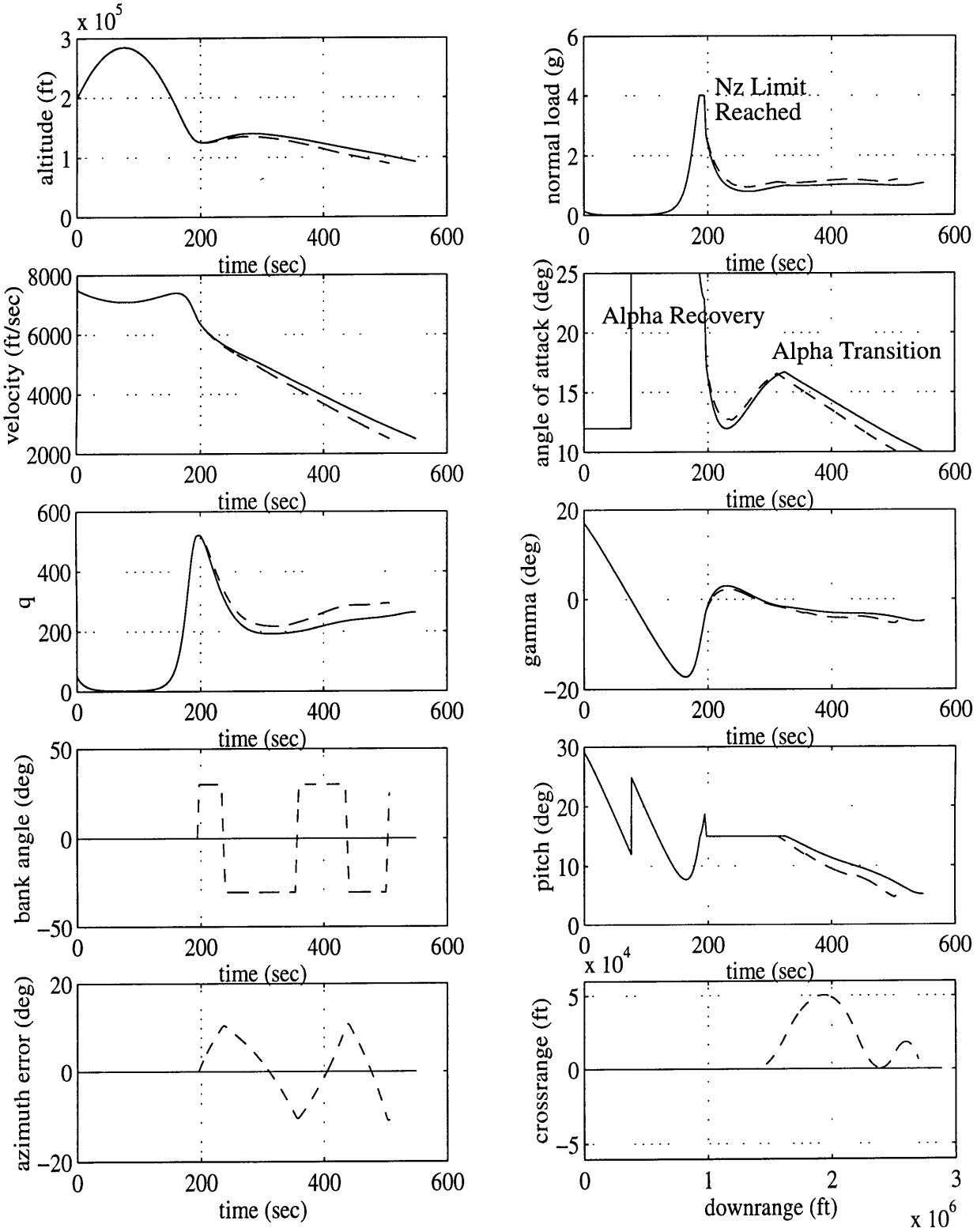

Figure 3.8 : Nominal Vertical Profile with 0° bank('-') and 30° bank ('--')

3.4 X-34 Reference Dynamic Model Definition

One of the principal advantages of using a reference model rather than a reference profile is that the nominal guidance algorithm precisely defines reference model behavior. The flight characteristics of the reference model are defined by the nominal vehicle equations of motion and the nominal guidance laws defined above. In each phase of flight the reference model is characterized by several parameters. Some of the free parameters are defined prior to the mission while other free parameters of the reference model become the control parameters of the trajectory design algorithm. They are presented here in the context of reference model design but the reader should keep in mind that the reference model and the nominal vehicle and guidance are one and the same. Chapter 4 addresses how changes in each of these parameters effects the vehicle trajectory (or the reference model trajectory). The results in chapter 4 provide rationale for selecting some parameters prior to the mission while using other for real time range control.

3.4.1 Alpha Recovery Reference Dynamic Model

The heavily constrained nature of the alpha recovery phase makes design and tracking of a reference model difficult. Chapter 4 addresses many of the difficulties associated with alpha recovery design. The possible design options are presented here as a basis for analysis. The alpha recovery reference dynamic model can be summarized by the following block diagram:

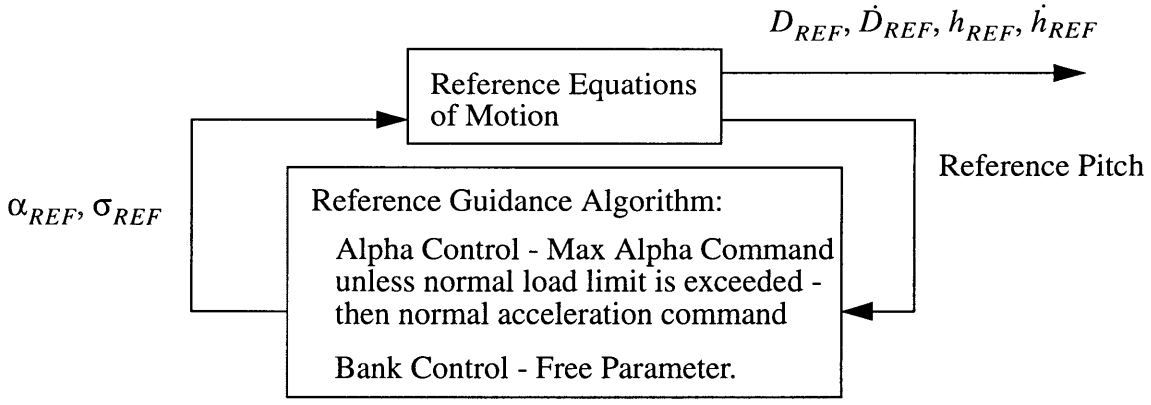

Figure 3.9 : Alpha Recovery Reference Dynamic Model

The reference model presented here has two free parameters for design consideration. The first is the maximum angle of attack command. The constrained nature of alpha recovery requires that

the maximum angle of attack command be determined through pre-mission analysis. Second, the bank angle can be varied during alpha recovery to maximize the use of the vehicle footprint. Bank angle is a potential real time range control free parameter. Due to the highly constrained nature of the alpha recovery phase, bank angle control during alpha recovery is not specifically addressed in this thesis. The algorithms developed for CLAT bank angle control could be extended for alpha recovery if a capacity for constraint monitoring is included. Again, the details of these problems are addressed in chapter 4.

3.4.2 Closed Loop Alpha Transition Reference Dynamic Model

During CLAT, the constraints are no longer as much of a concern and the flexibility of the guidance system is increased. The reference model has three free parameters as shown in Figure 3.10 below. The first parameter is the magnitude of the constant pitch command to guarantee a smooth trajectory. The constant pitch command is chosen prior to the mission according to the results presented in chapter 4. Second, a bias to the upper limit angle of attack profile is used for final altitude corrections. Again, the angle of attack upper limit profile bias is selected prior to the mission according to the results presented in chapter 4. Last, a constant bank angle command subject to an azimuth deadband is used. The magnitude of the constant bank angle command during CLAT is the primary real time range control parameter. The angle of attack and bank angle commands are rate limited.

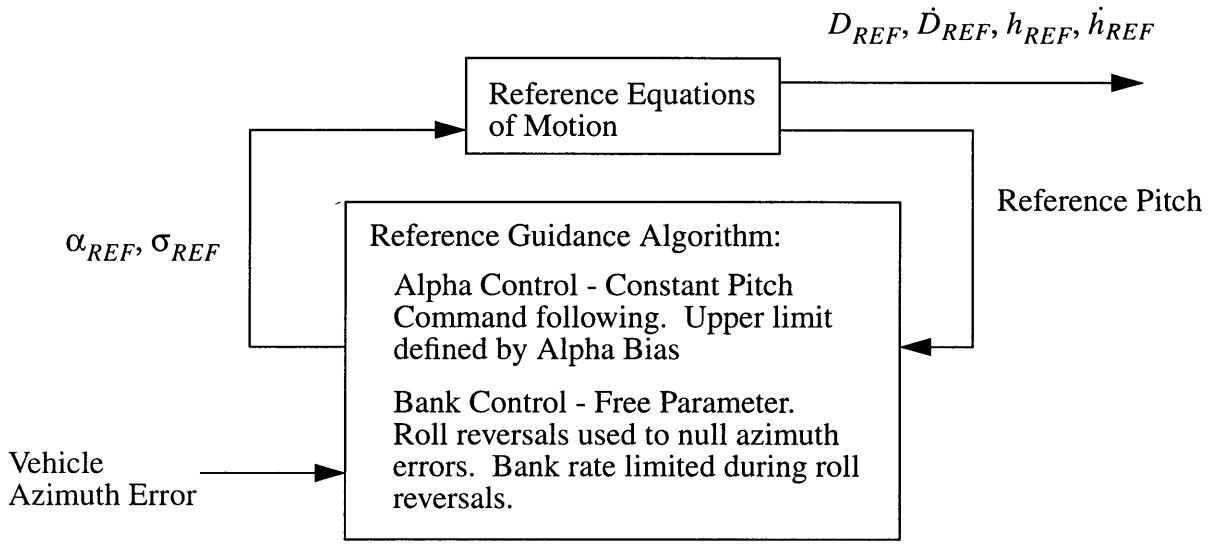

Figure 3.10 : Closed Loop Alpha Transition Reference Dynamic Model

Note that the actual vehicle azimuth error is used to determine roll reversals. This is required because in the process of tracking the commanded reference parameters the actual azimuth may vary greatly from the reference azimuth. Environment uncertainties and disturbances make it impossible to track all reference parameters perfectly. This is addressed further in chapters 6 and 7.

3.4.3 Summary of Guidance and Reference Dynamic Model Free Parameters

The nominal vehicle and the reference dynamic model share the free parameters available for trajectory design. In alpha recovery, two parameters are used: nominal angle of attack command and bank angle. CLAT has three parameters: magnitude of the constant pitch command, angle of attack bias on the angle of attack vs. velocity upper limit profile, and bank angle. The effects of these parameters on nominal vehicle behavior define the approach used to select the reference model parameters to meet the desired performance goals. Also the nominal effects provide rationale for definition of some parameters prior to the mission and others in real time. The guidance system functions table is updated below to reflect the definition of the reference dynamic model.

Table 3.1 : Guidance System Functions

	Trajectory Design	Reference Dynamic Model	Trajectory Tracking
Alpha Recovery	Footprint definition and site selection Determine baseline CLAT plan - i.e. generate reference model parameters	Set to measured environment State	Nominal Alpha Recovery Guidance
Angle of Attack	Select reference angle of attack command		Fly commanded reference angle of attack unless normal load constraint is violated
CLAT	Generate Reference Dynamic Model parameters	Propagates nominal dynamics to current vehicle velocity.	Track Reference Dynamic Model
Angle of Attack	Select Constant Pitch and Alpha Bias reference commands	Constant Pitch Command following to a biased upper limit profile.	
Bank Angle	Select reference bank angle command	Constant bank command defined by the Trajectory Design Algorithm.	
Roll Reversals		Controls roll reversals by measuring vehicle azimuth.	Performs roll reversals when commanded by Reference Dynamic Model.

Chapter 4

Vehicle Capability Analysis

Before defining a trajectory design or trajectory tracking strategy it is important to gain a solid understanding of the available controls and how their application throughout the flight will effect vehicle constraints and performance. The control variables are the reference model free parameters. The controls are applied through design and tracking of the reference model. The free parameters of the reference model are the free parameters available for nominal trajectory design. For alpha recovery phase the nominal angle of attack command and the bank angle can be varied. CLAT uses a constant pitch command, a bias on the angle of attack upper limit profile, and bank angle. Each parameter has different effects on the vehicle performance and constraints. These effects vary in the presence of environment and vehicle uncertainties. The evaluation of the effects of the guidance free parameters on final range and altitude lead to the definition of a vehicle footprint. This vehicle footprint is not the true footprint, rather it is the achievable footprint within the parameters available to the guidance algorithm. This chapter examines the individual effects of the control variables and their overall effects on vehicle footprint. Examining these effects constitutes the "pre-mission analysis" necessary to define the individual parameters of the reference model (excluding CLAT bank angle). The effects of the CLAT bank angle provide insight for definition of a guidance algorithm which maximizes performance without constraint violation in the presence of uncertainty and disturbances.

4.1 Effects of Modifying the Nominal Trajectory

From the entry guidance standpoint, nominal vehicle capability is defined as the footprint of achievable TAEM initial conditions [15]. TAEM requires the vehicle to arrive near an altitude and range target. TAEM is actually a very robust guidance algorithm and can handle a reasonable array of initial conditions provided that the vehicle is initially in an equilibrium condition. The vehicle footprint is defined by the vehicle aerodynamic properties, by the initial conditions, and by the desired TAEM altitude and range targets. It is also desirable to arrive at TAEM interface in

equilibrium flight. Flying at maximum L/D with zero bank defines the maximum range capability. This is a hard and fast rule defined by aerodynamic laws. However, most aborts will require some reduction in range and/or some minimum crossrange to meet a TAEM target for a landing site. The footprint also may be restricted by the vehicle constraints. These constraints are especially important in the alpha recovery phase and severely limit the guidance system in terms of range control authority.

Nominal Abort Trajectory Final States

Throughout this chapter results are presented in terms of their effects on the nominal trajectory. All results due to open loop bank angle and angle of attack perturbations are presented in terms of difference from the nominal values. The nominal final altitudes, final ranges, and maximum dynamic pressures are presented in Table 4.1 below to serve as a reference for comparison. Nominal final states represent a trajectory with nominal alpha recovery guidance and nominal CLAT guidance. The commanded angle of attack during alpha recovery is 25 degrees and this is reduced if the normal acceleration limit is reached. During CLAT, the nominal bank angle is zero and the constant pitch command is 15 degrees. Note that the abort velocity of 7500 ft/sec corresponds to a maximum speed of mach 8 (the nominal trajectory).

Table 4.1 : Nominal abort trajectory final states

Abort Velocity (ft/ sec)	Altitude (ft)	Downrange (ft)	Max q
7500	92053	2.885×10^6	521.4
7000	93056	2.484×10^6	442.5
6500	93570	2.135×10^6	399.7
6000	91741	1.776×10^6	358.7
6500	88662	1.473×10^6	319.3
5000	90656	1.160×10^6	306.6

The forthcoming results are presented as errors rather than actual values to emphasize that the

goal of this chapter is to identify systematic methods for selecting reference model parameters.

4.1.1 Alpha Recovery

As discussed earlier, alpha recovery is characterized by generating the maximum lift force available to kill off the high sink rate resulting from the ballistic entry trajectory. For higher mach number aborts, the normal acceleration limit will almost always be reached and the dynamic pressure limit must be monitored as in some cases it can actually be reached prior to the normal load limit. From examining the nominal mach 8 trajectory it is clear that the vehicle covers a large downrange distance during the alpha recovery. Some closed loop angle of attack control or closed loop banking could be desirable for range control. However, the close proximity of the constraints makes this a difficult control problem. To understand the difficulties in this design and control problem, examine the results of the following experiments.

Nominal Angle of Attack Perturbation

As an experiment, the nominal angle of attack during alpha recovery was varied to observe the effects on the trajectory. If the normal acceleration limit was reached, then the angle of attack is reduced to track the limit. Figure 4.1 below shows the changes in downrange and maximum dynamic pressure with respect to varying the nominal alpha recovery angle of attack. Results are shown for all abort velocities.

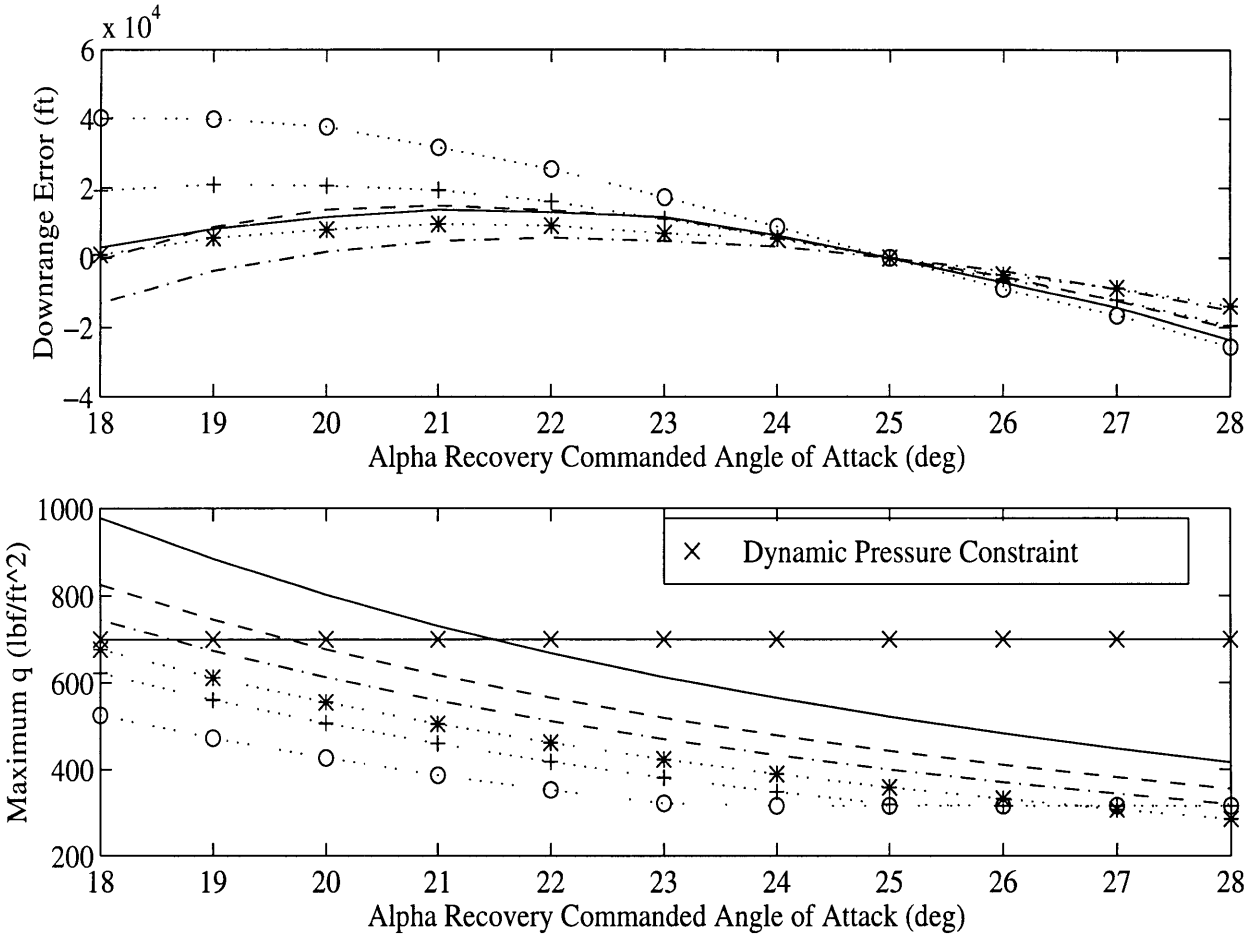

Figure 4.1 : Downrange and Dynamic Pressure wrt Nominal Angle of Attack in AR - 7500 ft/sec, -- 7000 ft/sec, -. 6500 ft/sec, + 6000 ft/sec, o 5500 ft/sec, * 5000 ft/sec

Although reducing the angle of attack can increase the final range by increasing vehicle *L/D*, for higher velocity aborts the maximum dynamic pressure is quickly exceeded by reducing the angle of attack too much. This is due to the fact that not enough lift is generated and the vehicle falls too low into the atmosphere at high velocities, thus causing dynamic pressure to increase. Additionally, if more angle of attack (i.e. more lift) is achieved then the range decreases due to reduced *L/D* but the dynamic pressure limit is not active. Note that the nominal angle of attack of 25 degrees is limited by the maximum achievable moment generated by the control surfaces to maintain equilibrium flight. So a greater angle of attack may not even be achievable. At lower

velocities, the constraint limitations are not as great a problem. These results indicate that some closed loop angle of attack control may be desirable for low mach number aborts. For higher abort velocities, the sensitivity of the dynamic pressure constraint to any perturbations from the nominal makes allowing angle of attack control during alpha recovery risky at best.

All of these factors combine to require that the nominal alpha recovery angle of attack be fixed through pre-mission analysis. All analysis from this point assumes that the alpha recovery angle of attack command is fixed to 25 degrees. This minimizes potential problems in dealing with the dynamic pressure constraint. In addition the effects of the alpha recovery angle of attack command on final range are relatively small and do not add to vehicle capability.

Alpha Recovery Banking

The effects of banking during alpha recovery are not as potentially hazardous as angle of attack variations. To illustrate the trends, a constant bank command is applied during alpha recovery (with a nominal angle of attack of 25 degrees) for the different aborts. The ground track range and maximum dynamic pressure effects are illustrated in Figure 4.2. Ground range is measured as the range along the earth's surface from the vehicle position at the initiation of banking to the vehicle's final position at TAEM interface. Note that ground range is roughly equivalent to downrange if roll reversals are performed to maintain a straight ground track. Ground range errors represent final range difference from the nominal. The bank command during CLAT is zero. Once alpha recovery is finished the vehicle returns to wings level flight.

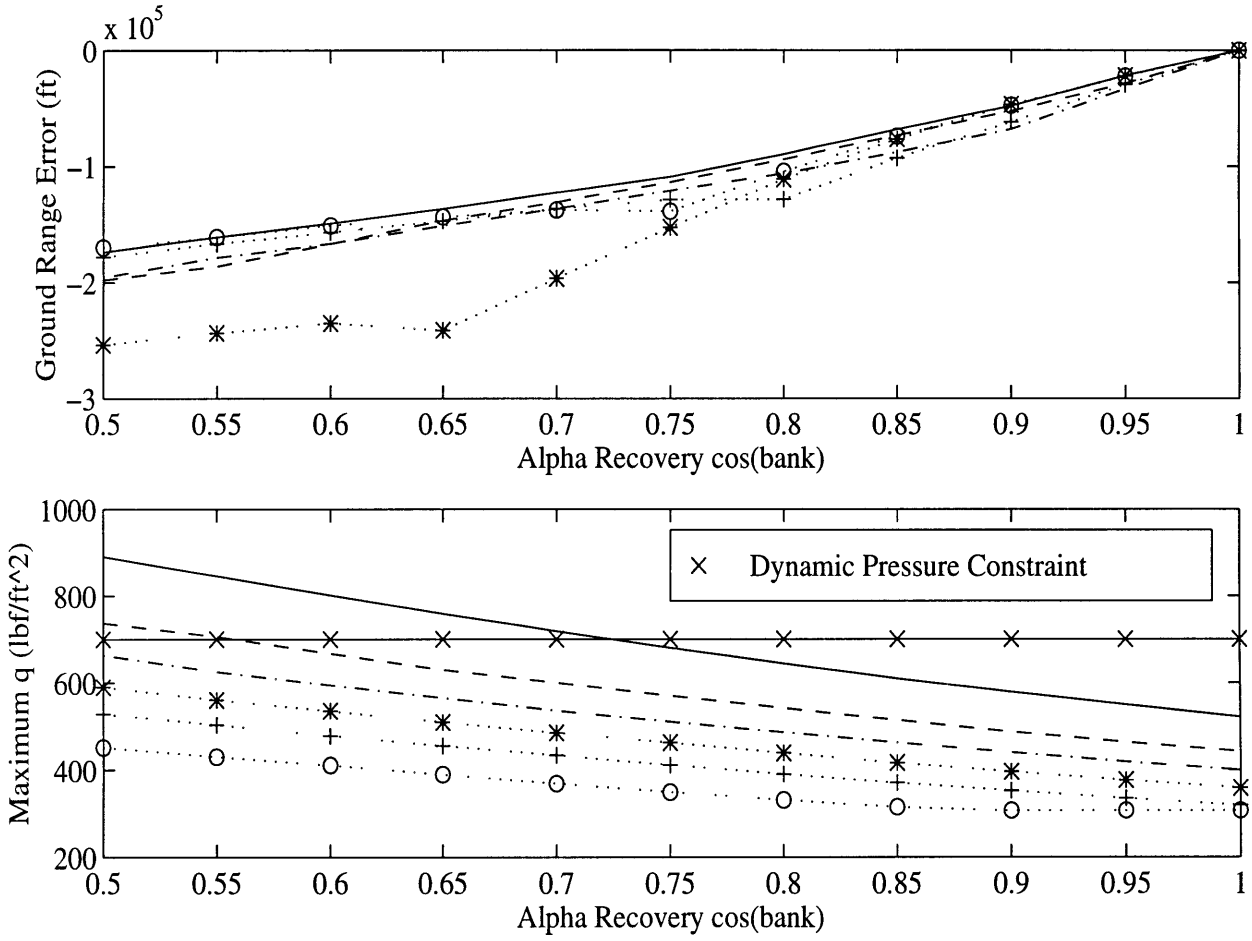

Figure 4.2 : Ground range and maximum dynamic pressure wrt alpha recovery bank angle

- 7500 ft/sec, -- 7000 ft/sec, -. 6500 ft/sec, + 6000 ft/sec, o 5500 ft/sec, * 5000 ft/sec

For higher abort velocities, the dynamic pressure limit is encountered as the bank angle increases. At lower abort velocities the constraint is not a factor. It is clear from this analysis that a robust guidance system must include the capacity for closed loop alpha recovery control and allow for variations from the nominal for trajectory design purposes. Allowing bank angle and angle of attack perturbations during alpha recovery would fully utilize vehicle capability during an abort. However, the optimization problem for trajectory design is difficult due to the proximity of the nonlinear state constraints. In addition, the control problem is complicated by the nonlinear state constraints.

The potential problems associated with closed loop bank control during alpha recovery led the author to initially constrain the bank angle to zero during alpha recovery. The framework developed for closed loop bank control during CLAT easily extends to alpha recovery if a constraint monitoring capability is added to the algorithm. This becomes more evident through the development of the trajectory design and tracking algorithms in chapters 5 and 6.

4.1.2 Closed Loop Alpha Transition

While alpha recovery is characterized by a guidance system designed to avoid constraints, CLAT is much more flexible, allowing the guidance system a number of options for meeting altitude and range requirements without danger of constraint violation. To review the nominal CLAT guidance profile, the angle of attack is commanded to maintain a constant pitch attitude until an upper limit angle of attack vs. velocity profile is reached. For the nominal case, no banking is used. The constraints are no longer a concern. To simplify the design problem, the options for CLAT guidance are limited to three items. First, the effects of constant bank angle perturbations are examined. The second design option is varying the commanded pitch for closed loop angle of attack control. Last, the angle of attack upper limit profile is allowed to be shifted by a bias up or down. Note that no results are presented for the effects on the vehicle constraints, this is because the analysis did not reveal significant increases in the constrained variables beyond the maximum values from alpha recovery.

Open Loop Constant Bank Commands

Banking is the workhorse for downrange control for entry guidance. Also, any crossrange errors must be nulled out by banking. The CLAT reference bank angle command is chosen as the primary range control parameter because of its large control authority and the lack of any adverse effects on vehicle constraints. The results presented here demonstrate a large capability from just bank control for downrange and crossrange control. Intuitively this makes a lot of sense. By banking, the vehicle can directly control the effective lift of the vehicle and increase or decrease the flight path angle. Note that banking is accomplished without pitching up to maintain altitude. In fact, the objective is to reduce the altitude by reducing lift. This in turn increases the vehicle drag and the velocity is reduced at a faster rate. By increasing the vehicle drag through banking,

the final range and altitude targets can be met. Figure 4.3 illustrates ground range capability with respect to the cosine of the bank angle. Also shown are final altitude errors. The ground range capability using only bank angle control during CLAT is far greater than the alpha recovery ground range effects.

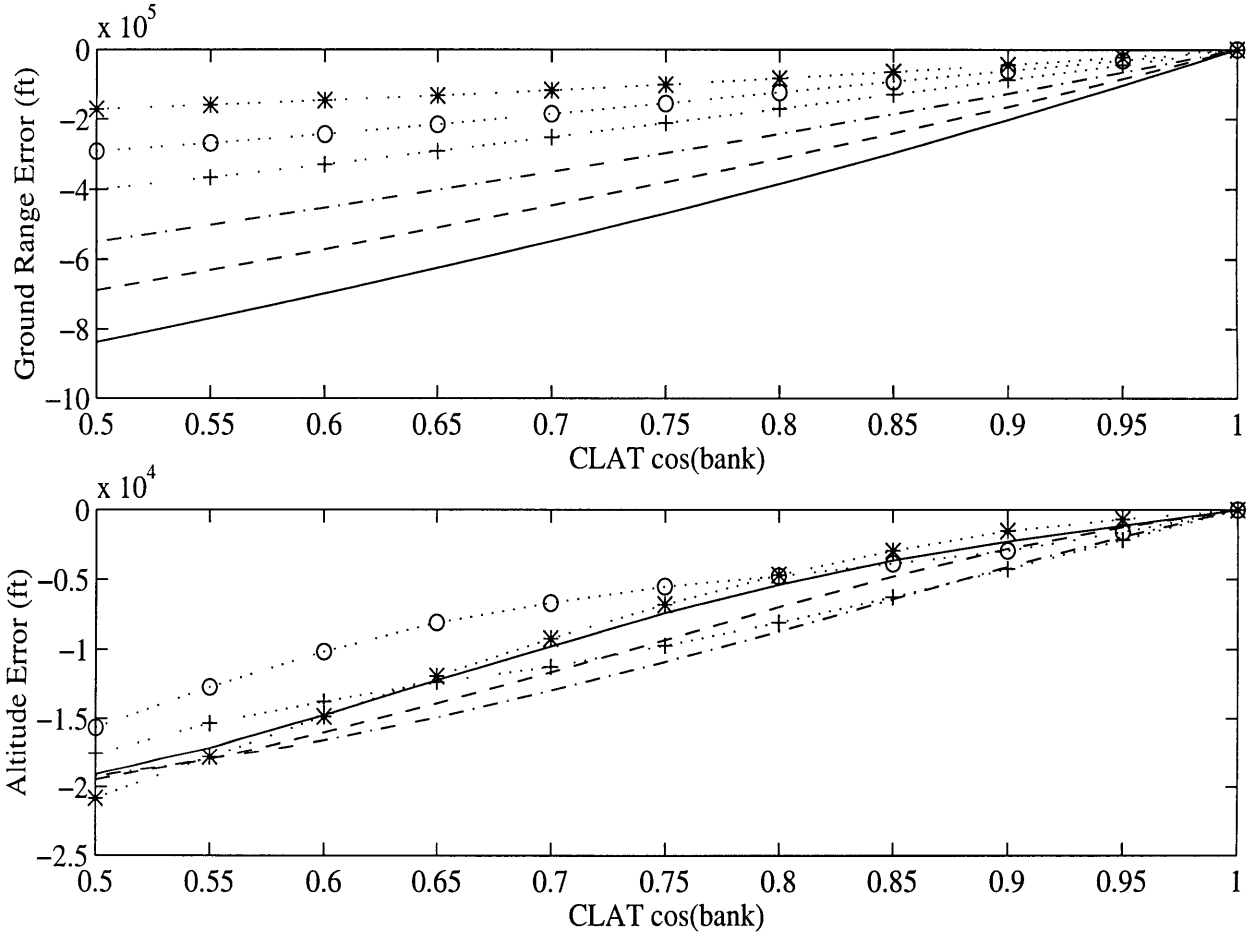

Figure 4.3 : Ground range and altitude errors due to CLAT bank angle

- 7500 ft/sec, -- 7000 ft/sec, -. 6500 ft/sec, + 6000 ft/sec, o 5500 ft/sec, * 5000 ft/sec

The effects of bank angle on the final altitude and the final ground range are nearly linear. This linearity is very important for trajectory design. Also note the reduction in final altitude caused by banking - clearly this is not desirable if the TAEM interface conditions are to be met. This

reduction in final altitude will be addressed through a simple relationship used by the trajectory design algorithm. Crossrange control is illustrated by figure 4.4 below.

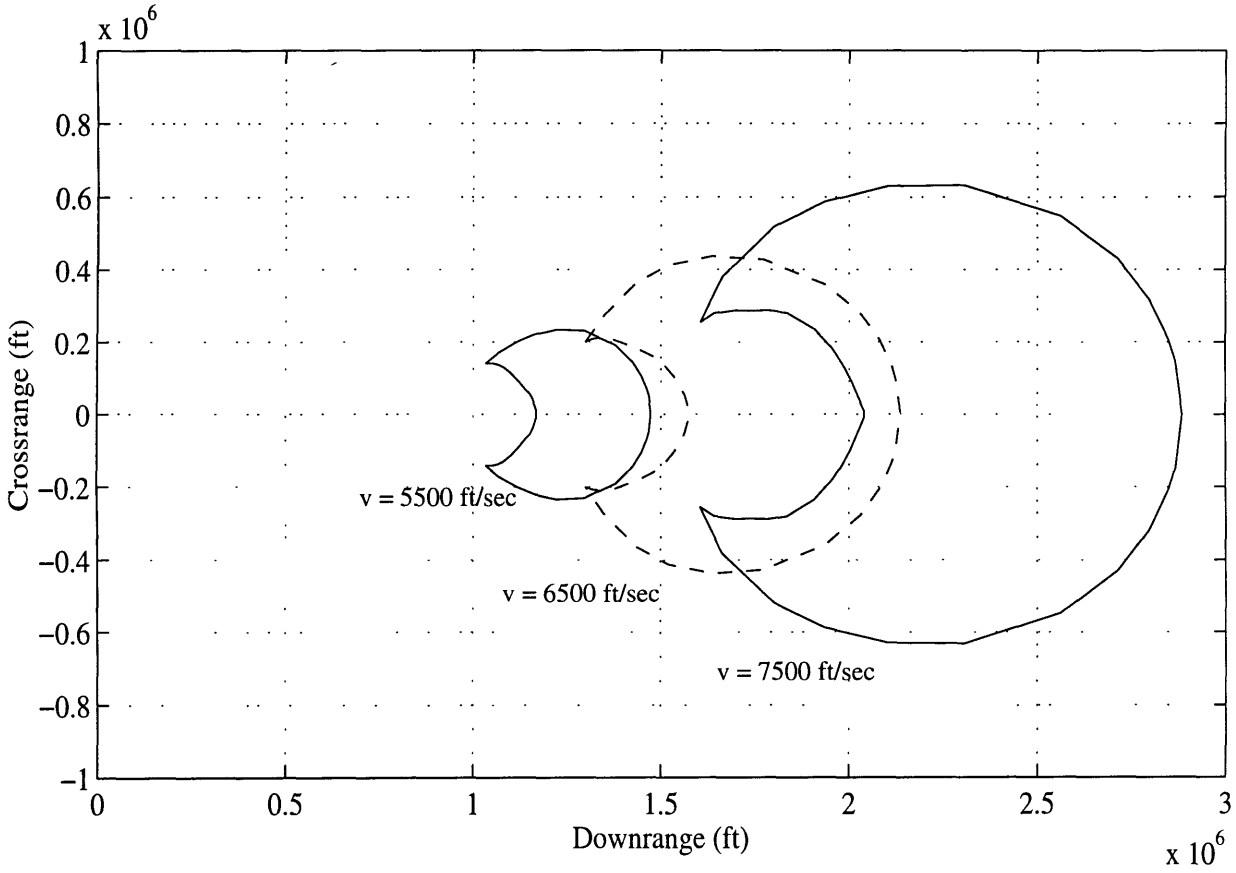

Figure 4.4 : Downrange and crossrange CLAT banking effects

Results for other abort velocities are not shown for improved clarity. The important (and expected) result is that vehicle capability increases with increased abort velocity.

Constant Pitch Command Variations

The constant pitch command was primarily used to prevent the large trajectory oscillations associated with a fixed angle of attack profile. Keeping this in mind, examine Figure 4.5 which illustrates several items. First the final downrange and altitude changes are shown with respect to the constant pitch command. Also included is a "trajectory quality index." This is simply a

measure defined to give an indication of the oscillations of the profile for the different pitch commands. This index is generated by taking the variance of the vehicle drag during alpha transition with respect to the linear regression of the vehicle drag. Vehicle drag is a good indicator of trajectory quality as it is sensitive to dramatic changes in altitude (density effects drag) and angle of attack (changes the coefficient of drag). The nominal pitch command is 15 degrees.

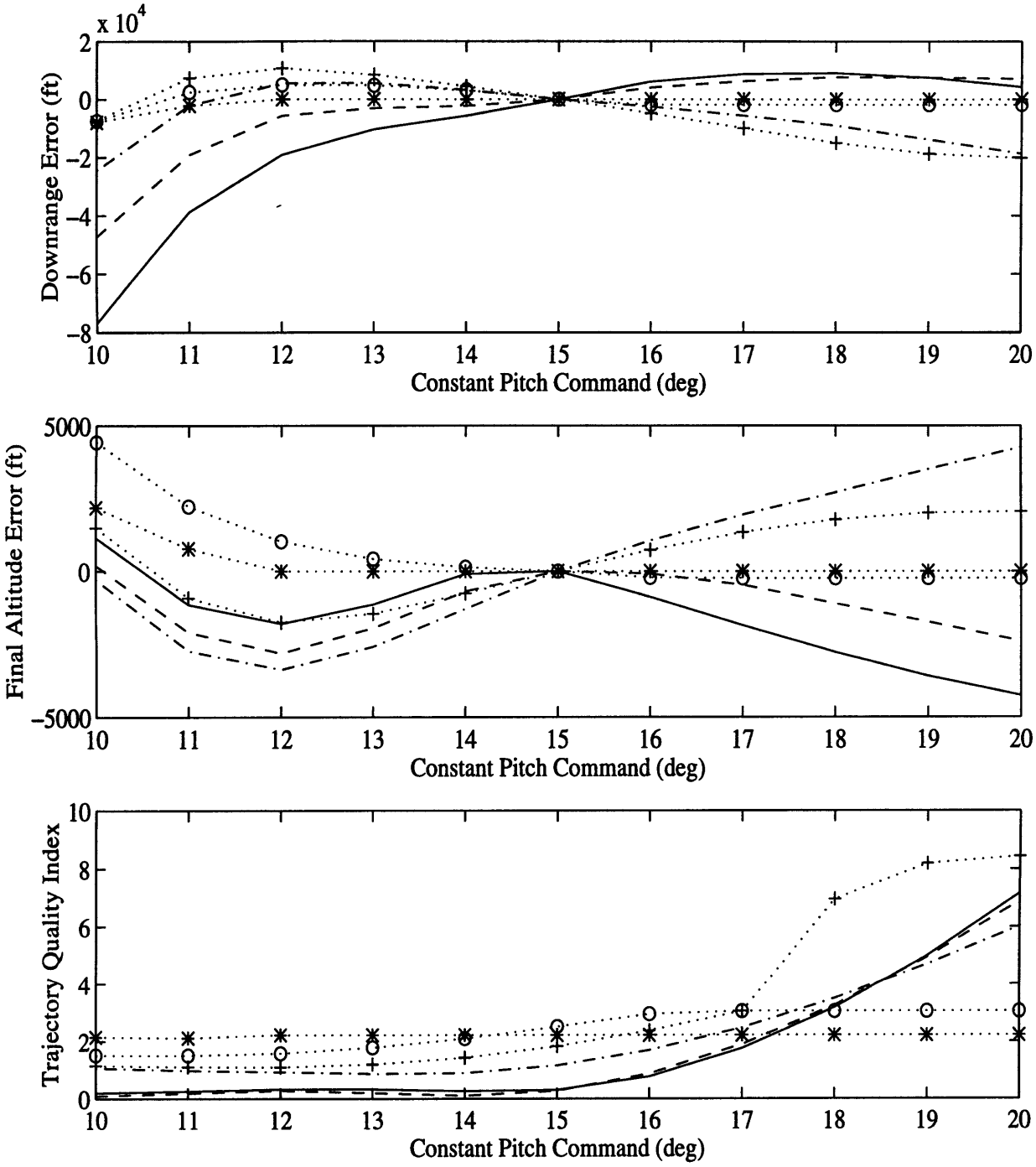

Figure 4.5 : Downrange and altitude errors, and trajectory quality index wrt constant pitch command

- 7500 ft/sec, -- 7000 ft/sec, -. 6500 ft/sec, + 6000 ft/sec, o 5500 ft/sec, * 5000 ft/sec

The changes in altitude are generally uncorrelated and are not very significant in terms of magnitude. The constant pitch command has a clear contribution to trajectory quality. Below a 15 degree pitch command the quality is greatly improved. Also below 15 degrees the final range is reduced. Generally the pitch command should be chosen to not reduce the final range while maintaining good trajectory quality. Thus a 15 degree constant pitch command is used for all abort velocities for CLAT angle of attack control.

Alpha Bias Variations

The alpha bias factor is introduced to help counteract some of the reduction in altitude caused by constant bank commands for range control. Again, the intuition is simple - pulling up increases the lift and thus the final altitude will be higher. Furthermore, pulling up reduces the *L/D* (backside of the *L/D* curve) thus reducing the final range. Figure 4.6 illustrates these expected results for downrange and altitude.

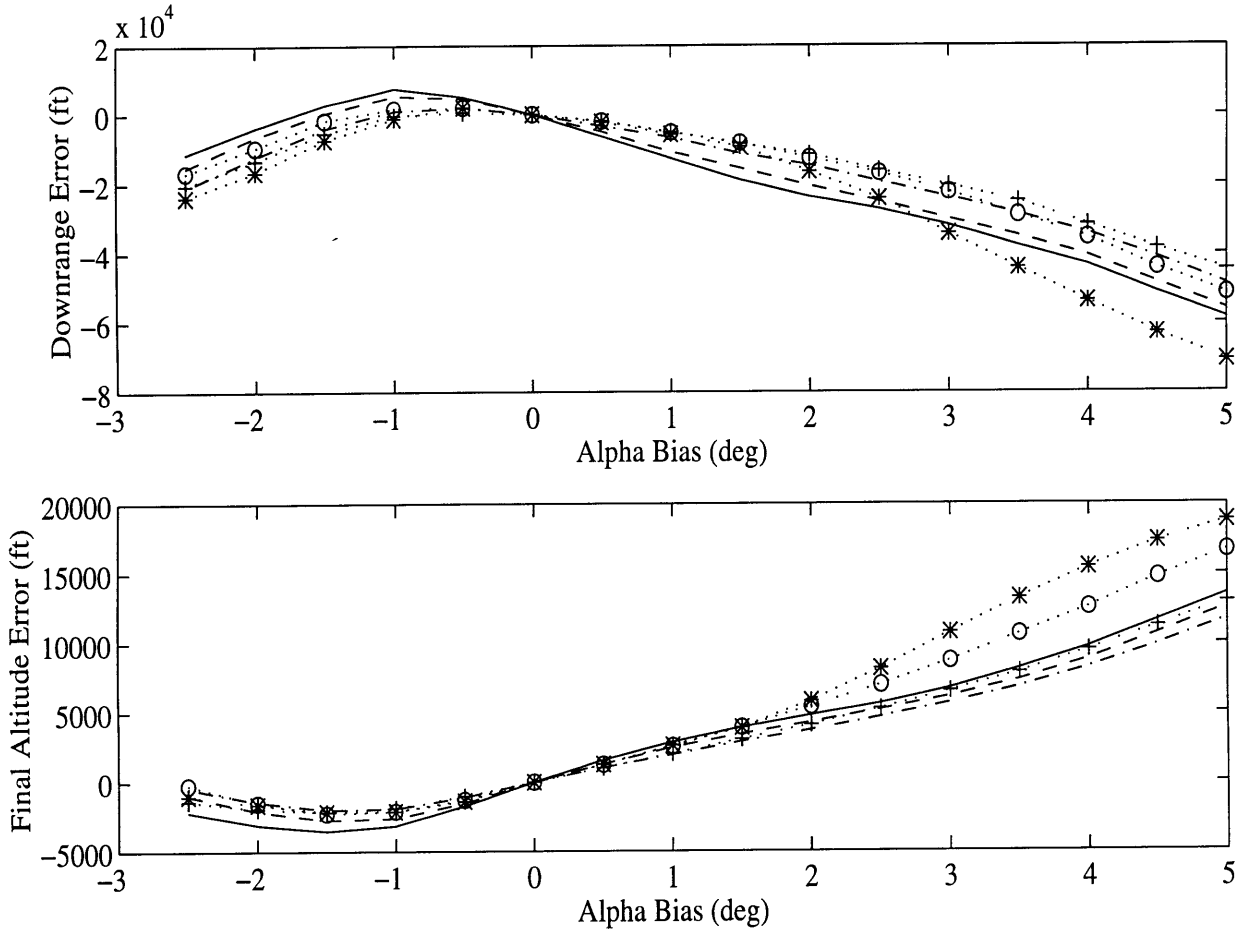

Figure 4.6 : Downrange, Altitude vs. Alpha Bias

- 7500 ft/sec, -- 7000 ft/sec, -. 6500 ft/sec, + 6000 ft/sec, o 5500 ft/sec, * 5000 ft/sec

It is evident that the alpha bias is useful in meeting target altitude requirements without significantly reducing the vehicle range. The altitude target used for this thesis is 100000 feet. The nominal abort trajectories all terminate at an altitude of approximately 90000 feet so the alpha bias command is fixed to +4.0 degrees. This adds the necessary altitude to ensure that the TAEM energy target is met. Fine tuning of the selection of the alpha bias may be necessary as further knowledge of the nominal vehicle aerodynamic properties is gained. Alpha bias could be scheduled as a function of abort velocity using this knowledge.

4.2 Guidance-Limited Footprint Definition

Given the accumulated information on vehicle capability, a graphical representation of the footprint provided by the above options is possible. This is not completely representative of the vehicle footprint. A complete trajectory optimization routine could provide a better description. An optimization routine allows much greater flexibility in angle of attack commands to increase the footprint size. The goal being development of a real time abort guidance system, a full trajectory optimization is not possible and it is best to limit the design to a parameter optimization. In addition, limiting the guidance options provides some measure of conservatism. To measure this degree of conservatism would require the use of an optimization routine to set a standard for comparison of guidance algorithms. The conservatism is likely to be negligible due to the fact that bank angle has much more range control authority than angle of attack.

Figure 4.7 illustrates the footprints for three different abort velocities. Footprints represent both CLAT open loop bank commands and combined alpha recovery and CLAT bank commands. An array of bank commands from 0 to 80 degrees show the maximum downrange and crossrange capability. To graphical represent the minimum range capability, the maximum bank angle is commanded for CLAT but roll reversals are used. The sign of the bank angle is controlled by the normal azimuth deadband logic with target sites chosen along the maximum range contour. Note that during alpha recovery the maximum open loop bank angle command is chosen to avoid violating the maximum dynamic pressure constraint. The maximum bank angle corresponds to the results in figure 4.2. For the 7500 ft/sec abort the maximum bank angle is 41 degrees while the 6500 ft/sec and 5500 ft/sec aborts use a maximum of 60 degrees (the dynamic pressure constraint is not active).

Although no closed loop range control is used during alpha recovery in this thesis, the comparison is included for two reasons. The first is to show potential for increased abort capability if closed loop range control is added to alpha recovery. Second, although there is increased capability, the majority of range control authority is still provided by CLAT bank commands.

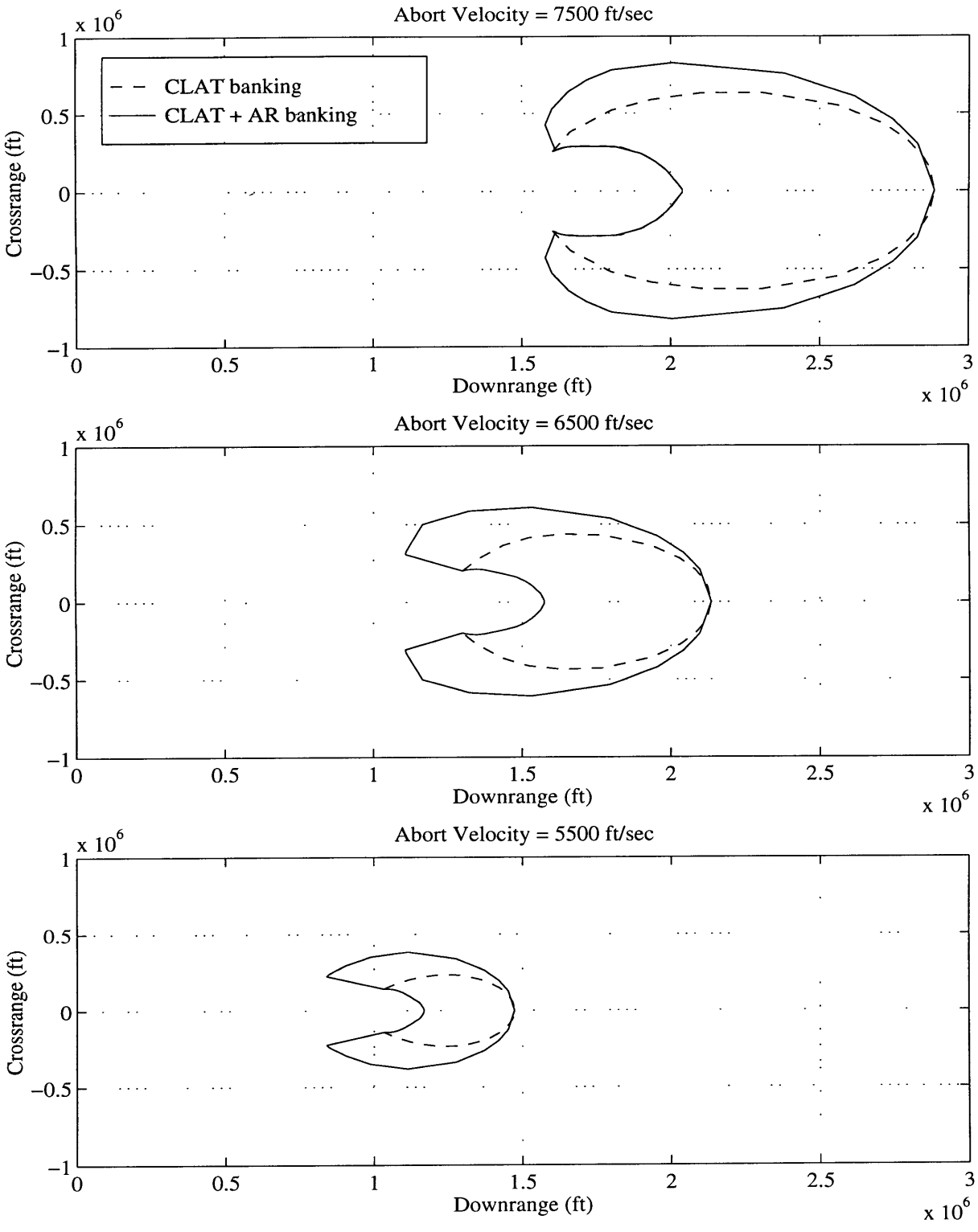

Figure 4.7 : AR + CLAT footprints

4.3 Implications for Trajectory Design

The pre-mission analysis results presented here outline a structure for designing trajectories which meet the TAEM target conditions. This is especially true for the CLAT phase. By working within the free parameters of the reference dynamic model, a wide variety of abort situations can be handled. Over the next chapters, trajectory design and trajectory tracking algorithms are developed in full for the CLAT phase using reference model based guidance. The CLAT reference bank command is used to control final range. The constant pitch and alpha bias commands are fixed according this chapter's analysis.

The results for the alpha recovery phase indicate a need for caution. The proximity of the constraints makes definition of a real time robust alpha recovery design and tracking algorithm difficult. Furthermore, vehicle capability (i.e. footprint size) is not necessarily greatly increased by modifying the alpha recovery phase. Thus alpha recovery will only use the nominal algorithm (maximum angle of attack subject to normal acceleration limiting). As the CLAT algorithm is developed and presented, possible extensions for closed loop alpha recovery control will be considered.

Chapter 5

Trajectory Design

The atmospheric entry guidance problem can be formulated as two subproblems: trajectory design and trajectory tracking. These work together to achieve the desired target condition. In turn, trajectory design is divided into three major functions. The first is pre-mission analysis to define some reference model parameters and determine methods for defining the other parameters. Pre-mission analysis was completed in chapter 4. The second function is initial reference dynamic model design. Here the nominal reference model bank angle is computed to meet range and altitude requirements. Included in the initial design is vehicle footprint definition and site selection. The third function is the closed loop redesign capability which adjusts the reference dynamic model to account for major disturbances and uncertainties which the tracking algorithm is unable to reject. The initial design algorithm utilizes the nearly linear relationship between the cosine of the bank angle and the total glide range for both footprint definition and initial reference bank angle command computation. The redesign algorithm makes use of energy-range basis trajectories to modify the reference bank angle command during the flight.

5.1 Design Algorithm: General Approach

Thus far, discussion has focused on definition of the reference dynamic model and the effects of modifying its free parameters. This chapter addresses the problem of defining the parameters of the reference dynamic model. Recall that the reference dynamic model is simply the nominal vehicle dynamics subject to the nominal guidance propagated at each guidance step to match the current vehicle velocity. The states of the reference dynamic model are the commands for the vehicle to follow. The reference dynamic model has a limited number of free parameters. During alpha recovery, only the nominal guidance algorithm is implemented due to the potential for constraint violation. The reference dynamic states are not propagated during alpha recovery. Instead, they are set to the measured environment states. During alpha recovery the trajectory design algorithm selects the baseline values of the CLAT free parameters (bank angle, constant

pitch, and alpha bias). The constant pitch command and alpha bias command are both specified by the analysis in chapter 4. This leaves only the constant bank command for the reference dynamic model to compute in real time. At the initiation of CLAT, reference model propagation and closed loop tracking of the reference commences. Also at this point closed loop adjustment of the reference model begins. Table 5.1 below summarizes the functions of the reference dynamic model and the design and tracking algorithms as they have been defined thus far.

Table 5.1 : Guidance System Functions

	Trajectory Design	Reference Dynamic Model	Trajectory Tracking
Alpha Recovery	Footprint definition and site selection Determine baseline CLAT plan	Set to measured environment State	Nominal Alpha Recovery Guidance
CLAT	Generate Reference Dynamic Model bank angle command	Propagate nominal dynamics to current vehicle velocity	Tracking law to follow Reference Dynamic Model
Angle of Attack	Constant Pitch and Alpha Bias commands specified according to pre-mission analysis	Constant Pitch Command following to a biased upper limit profile	
Bank Angle	Closed-loop redesign of reference bank angle	Constant bank command defined by the Trajectory Design Algorithm	
Roll Reversals		Controls roll reversals by measuring vehicle azimuth	Performs roll reversals when commanded by Reference Dynamic Model

In the context of the above system, the trajectory design problem has been reduced to a single parameter: the reference model constant bank angle. Recall figure 5.1 which presents the nearly linear relationship between final range and the cosine of the bank command.

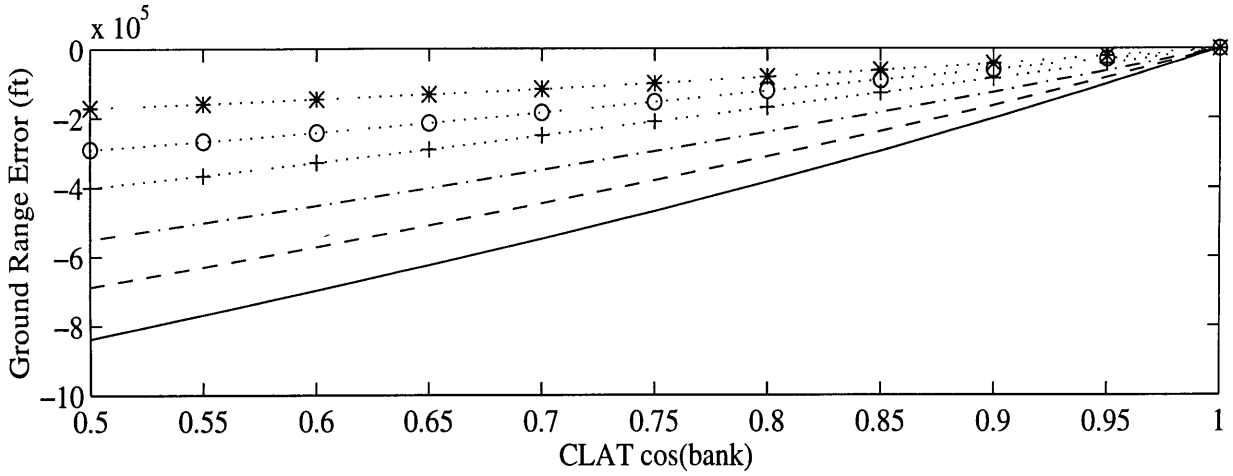

Figure 5.1 : Ground range effects due to CLAT bank angle

Because the relationships are so linear this is a simple parameter optimization problem. The range control problem is solved by linear approximations and assumes that the reference dynamic model can be tracked perfectly. Chapter 6 addresses the trajectory tracking laws. The trajectory design algorithm presented here assumes that the dynamic reference model can be tracked perfectly in the presence of uncertainty to guarantee that the design goals are met. By tracking the dynamic reference model's drag and altitude the TAEM interface conditions are met. This fact is critical because it allows the design algorithm to only consider the nominal environment. No estimation of parametric uncertainties is necessary. The tracking law rejects the disturbances caused by parametric uncertainties.

The closed loop redesign algorithm must be capable of adapting to off-nominal environments. The lack of closed loop range control during alpha recovery creates huge variations in initial conditions which dramatically effect the approach for closed loop modification of the reference dynamic. The closed loop redesign algorithm uses an energy-range basis set to select the reference bank angle. The energy-range basis is robust to initial condition uncertainties.

5.2 Footprint Definition and Range Prediction: Reference Profile Based Approaches

Prior entry guidance algorithms rely on reference profiles for trajectory design and tracking. The basics of profile based range prediction and footprint definition are described here to serve as a reference point for analysis.

5.2.1 Analytic Approach: Drag-Velocity or Drag-Energy Approximation

The most developed and tested atmospheric guidance algorithm is space shuttle entry guidance [8]. Range prediction for space shuttle entry guidance is accomplished by analytic approximation of the range achieved by flying a drag vs. velocity profile. The drag vs. velocity profile can be modified to meet the final range requirements. A tracking law ensures that the shuttle flies the specified profile by modulating the bank angle. Range as a function of a drag-velocity profile is relatively easy to derive. Begin by combining equations 2.6, 2.3 and 2.4 to yield equations 5.1 and 5.2 for downrange and crossrange.

$$\Delta R_x = -\int_{v_0}^{v_f} \frac{v\cos\gamma\cos\psi}{D + g\sin\gamma} dv \qquad \textbf{5.1}$$

$$\Delta R_y = -\int_{v_0}^{v_f} \frac{v\cos\gamma\sin\psi}{D + g\sin\gamma} dv \qquad \textbf{5.2}$$

If the heading angle, flight path angle, and drag are specified with respect to velocity then integrating these equations with respect to velocity yields a predicted downrange and crossrange. For the moment assume that the flight path angle is small and that crossrange effects can be ignored. If the flight path angle is small then $\cos\gamma \sim 1$ and $D >> g\sin\gamma$. This yields the following expression for ground range (i.e. range along the ground track - ignoring heading changes and roll reversal effects):

$$\Delta R = -\int_{v_0}^{v_f} \frac{v}{D} dv \qquad \textbf{5.3}$$

This expression is only a function of drag and velocity. If vehicle drag is specified with respect to velocity then the above integration is simple. Furthermore, if the drag is specified in piecewise linear segments where for each segment in velocity $[v_i, v_{i+1}]$,

$$D_i = a_i(v - v_i) + b_i \tag{5.4}$$

then an analytical expression is obtained for ground range:

$$\Delta R = \frac{v_f - v_0}{a_i} - \left(\frac{b_i - a_i v_i}{a_i^2}\right)\ln\left(\frac{a_i(v_f - v_i) + b_i}{a_i(v_0 - v_i) + b_i}\right) \tag{5.5}$$

Analytic range prediction using piecewise linear drag-velocity profiles is the baseline for shuttle entry guidance and many other approaches (Note that shuttle guidance actually uses quadratic, linear, and constant segments for range prediction - see [8] for a detailed explanation).

Another approach (also used in the final phase of shuttle entry guidance) is to specify the drag as a function of energy. Energy is defined as:

$$E = gh + \frac{1}{2}v^2 \tag{5.6}$$

Differentiating equation 5.6 with respect to velocity and then combining with equations 2.3 through 2.6 yields the following expression for ground range:

$$\Delta R = -\int_{E_0}^{E_f} \frac{\cos\gamma}{D} dE \tag{5.7}$$

Assuming $\cos\gamma \sim 1$ and piecewise linear drag segments yields:

$$\Delta R = -\int_{E_0}^{E_f} \frac{1}{D} dE \tag{5.8}$$

$$\Delta R = \frac{1}{a_i}\ln\left(\frac{a_i(E_f - E_i) + b_i}{a_i(E_0 - E_i) + b_i}\right) \tag{5.9}$$

Both of the analytic range prediction expressions above assume that the flight path angle is small. The drag-energy approximation is generally much more accurate than the drag-velocity approximation owing to the fact that $\cos\gamma \sim 1$ is a better approximation than $\sin\gamma \sim 0$. In any case, the X-34 nominal trajectory generally has large flight path angles during the ballistic portion of the trajectory so these approximations are not valid for X-34 trajectories. Furthermore, analytic approximations do not account for the prediction errors caused by banking away from the target or by roll reversals. Analytic prediction approaches rely on closed loop feedback over the course of the trajectory to null range errors. Further, analytic approaches rely on a predictable smooth trajectory where the initial conditions make the tracking of a reference profile achievable.

Analytic drag-velocity approximations can easily be extended to a footprint definition algorithm. However, the author does not know of an existing reference for such an approach.

5.2.2 Exact Solution of Families of Drag-Velocity Profiles for Footprint Definition

Deutsch presents a method for footprint definition which eliminates the small flight path angle assumption in solving for the range [3]. In addition, crossrange effects are included by numerically integrating the heading angle, downrange, and crossrange with respect to a drag vs. velocity profile. The key points of this approach for range prediction are included in Appendix A. This approach is much more accurate for nominal range prediction and eliminates errors resulting from the small flight path angle approximation. Deutsch extends the exact solution to a footprint definition algorithm which is based on a family of drag-velocity reference profiles. This family of nominal profiles is used to define a footprint of achievable targets and a reference profile is generated to be used by the tracking algorithm. This approach was successfully demonstrated in a 3DOF simulation environment for demonstration of an abort planning algorithm.

5.3 Footprint Definition and Range Prediction for a Reference Model

The quasi-linear relationships between ground range and CLAT bank commands (with linear reduction of bank at low velocities) form the basis of the X-34 trajectory design algorithm. By recognizing that the problem is nearly linear the trajectory optimization is defined as a one parameter optimization. Parameter optimization problems are generally easier to solve and faster to converge than a trajectory optimization problem. In addition the footprint definition is defined purely in terms of the single parameter.

The problems of footprint definition and range prediction for a reference model are closely linked. Fast range prediction is required for accurate assessment of possible landing sites. Traditional range prediction methods are not easily applied to a reference model based guidance system. This is due to the fact that only a single parameter, the reference bank angle command, must be

selected rather than an entire reference profile. A numerical trajectory integration approach is used for range prediction and footprint definition for reference model based guidance. A small number of basis trajectories are generated through integration of the nominal dynamics and nominal guidance with a constant bank angle command. The basis trajectories are used to define a footprint of achievable TAEM initial conditions. The reference bank angle command is selected by interpolation between the basis trajectories in one form or another to meet final range requirements.

After defining the reference model parameter optimization problem, the tools to accomplish footprint definition and range prediction through numerical integration are presented here. These include the definition of basis trajectories and methods for weighting sites for their feasibility.

5.3.1 Reference Dynamic Model Parameter Optimization Problem

Reference model design has been reduced to a one parameter optimization problem. Although the reference model has three free parameters (constant pitch, alpha bias, and constant bank), the constant pitch and alpha bias commands are already specified by the analysis in chapter 4. This leaves only one parameter for final range control: the constant bank angle command. Section 5.3.5 demonstrates how final altitude can actually be controlled by a linear reduction in the bank angle just prior to TAEM interface. Because the final altitude is specified by a linear reduction in bank angle, the only objective of the optimization is to meet range requirements. The cost function is defined as follows:

$$J = \min_{\sigma_{REF}} \left[\sqrt{(R_X - R_{X_{TGT}})^2 + (R_Y - R_{Y_{TGT}})^2} - R_{TGT} \right]^2 \qquad \textbf{5.10}$$

Although this is the actual cost function for minimizing the final range error, the implementation used to solve for the reference bank angle is not based directly on minimizing this cost function. The implementation takes advantage of the linear relationship between $\cos(\sigma)$ and the ground range and actually solves the following cost function:

$$J = \min_{\cos\sigma_{REF}} \left| \sqrt{(R_X - R_{X_{TGT}})^2 + (R_Y - R_{Y_{TGT}})^2} - R_{TGT} \right| \qquad \textbf{5.11}$$

As long as the target ground range is within the vehicle footprint then the cost function has a minimum and is convex. The minimum value is actually zero because there is an exact bank angle corresponding to the desired ground range. To obtain derivative information some time domain integration of trajectories is required. This is because to determine final range the entire trajectory must be evaluated. The derivative is found by interpolation between known trajectories:

$$\frac{\partial J}{\partial \cos\sigma} = \frac{\Delta R_{ERR}}{\Delta \cos\sigma} = \frac{(R(\sigma + \Delta\sigma) - R_{TGT}) - (R(\sigma) - R_{TGT})}{\Delta \cos\sigma} \qquad \textbf{5.12}$$

Interpolation between known nominal trajectories is used in several forms for both footprint definition and reference bank angle command generation.

5.3.2 Minimum and Maximum Range Prediction - Baseline Footprint

The minimum and maximum achievable range can be predicted for the nominal case by numerical integration of the guidance frame equations of motion subject to the nominal guidance algorithm. Chapter 4 describes the effects of the CLAT bank angle command on final range. The maximum range is determined for a CLAT bank command of zero. Minimum range is defined by the maximum CLAT bank angle. For analysis here, a maximum CLAT bank angle of 80 degrees is used. Roll reversals are used to control crossrange. The azimuth deadband in this case is defined by defining the maximum range to be the target.

The minimum and maximum straight ahead range trajectories form an initial footprint approximation. By viewing the minimum and maximum range trajectories as minimum and maximum radii at azimuths from +60° to -60° originating at the start of CLAT, an approximate footprint is defined. Note that this footprint is not realistic as crossrange effects are ignored. However, the site weighting procedure in section 5.3.3 takes care of this problem by eliminating sites which are not achievable. Figure 5.2 illustrates this initial footprint approximation and includes the actual guidance limited footprint. The minimum and maximum range ground tracks are included.

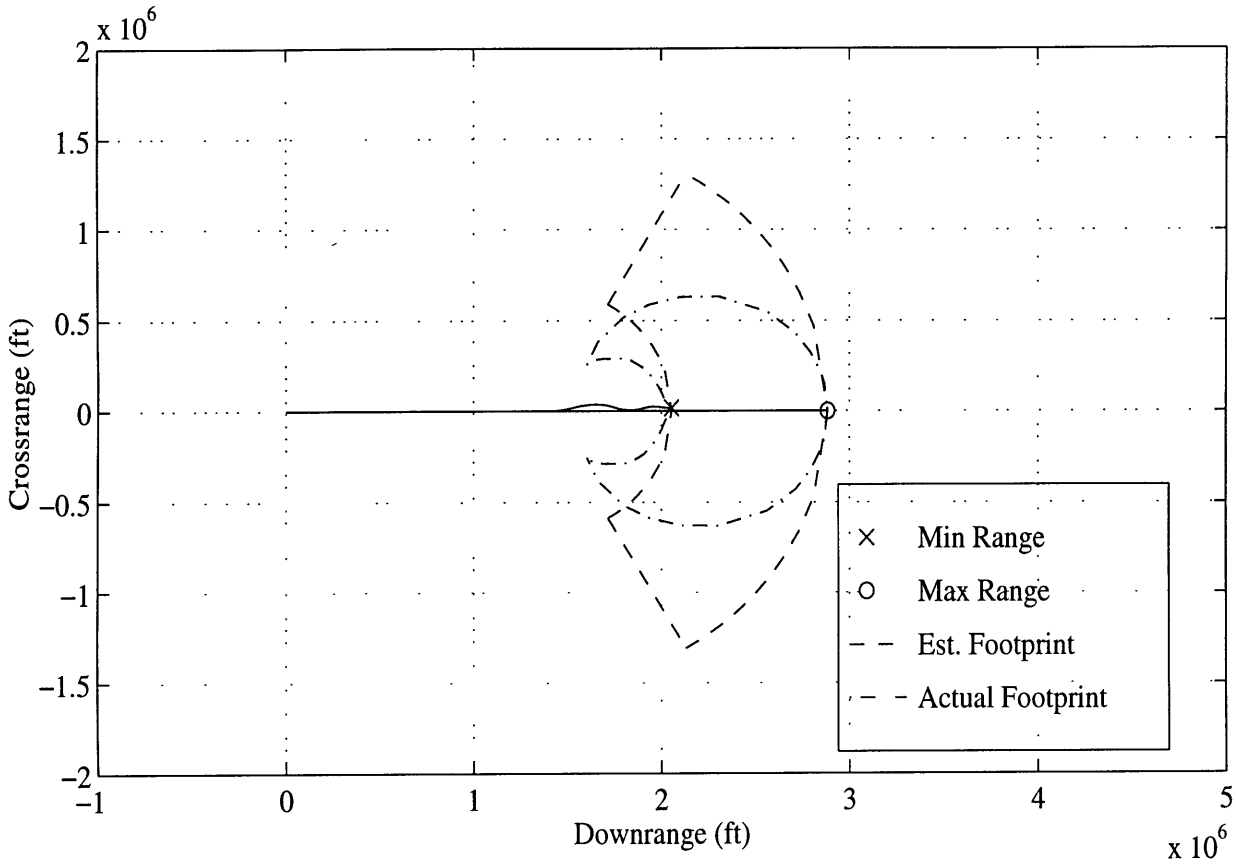

Figure 5.2 : Footprint approximation using minimum and maximum range trajectories

Clearly the estimated footprint is much larger than the actual footprint. However, the site weighting procedure defined below is designed to eliminate the sites which are in the estimated footprint but outside of the actual footprint. As for sites which are in the actual footprint but outside of the estimated footprint, these sites are generally outside of acceptable robustness margins as will be further explained below.

5.3.3 Site Weighting

A basic site weighting procedure to evaluate the candidate sites within the initial estimated footprint is defined here. This weighting procedure is primarily concerned with defining feasibility of a candidate landing site. Feasibility is defined by the minimum bank angle required to meet crossrange requirements for that site and by the bank angle necessary to meet ground range requirements for that site. Out of the feasible sites, a landing site must be chosen based on

some cost function. The cost function could include factors such as runway length, proximity to populations, etc. Deutsch has addressed the development of these aspects of the cost function for an abort planning algorithm [3]. A robustness weighting for a site is introduced here in terms of the reference bank angle and its proximity to the bank angle saturation constraints. The actual development of the correspondence of bank angle saturation and robustness is included in Chapters 6 and 7.

Crossrange Requirement: Minimum Bank Angle Estimate

Crossrange feasibility for a given site can be determined by defining an estimated minimum bank angle corresponding to that site's crossrange position. The minimum bank angle is approximated by assuming equilibrium glide from the velocity at the end of alpha recovery. The method used to approximate minimum bank angle is similar to the ground track prediction routine used in TAEM [15].

Assuming a point mass, the free body diagram for equilibrium flight is shown below in the lvlh frame.

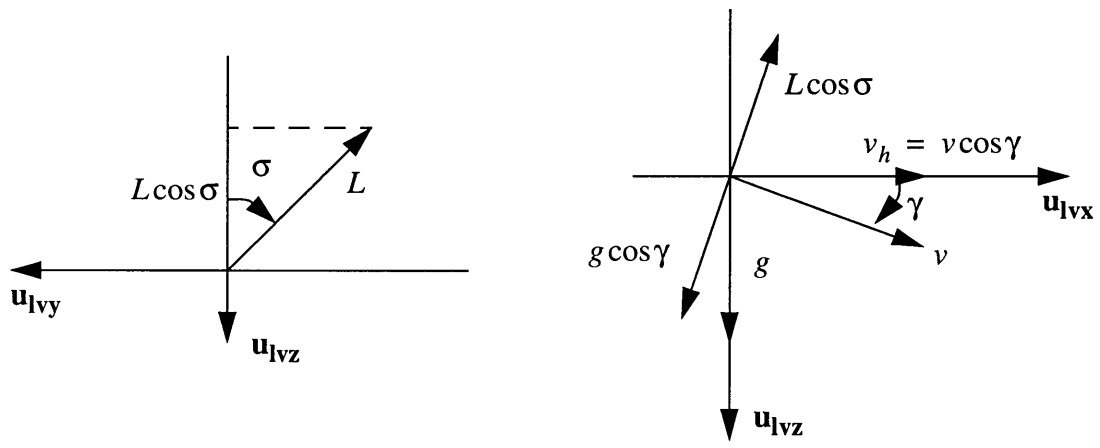

Figure 5.3 : Minimum bank angle computation free body diagram

In equilibrium, the sum of the forces in the body frame is zero. Summing forces yields:

$$\sum F_z = L\cos\sigma - g\cos\gamma = 0 \tag{5.13}$$

$$\sum F_y = L\sin\sigma - \frac{v_h}{R_{cir}} = 0 \tag{5.14}$$

The radius, R_{cir}, can be approximated by dividing the ground range to the target by the azimuth error (note that the "0" subscript refers to quantities at the start of CLAT):

$$R_{cir} = \frac{\sqrt{(R_{X_0} - R_{X_{TGT}})^2 + (R_{Y_0} - R_{Y_{TGT}})^2}}{\Psi_{err}} \tag{5.15}$$

Assuming small flight path angle, v_h can be approximated by v_0. Combining equations 5.13 through 5.15 yields the following approximation for the minimum bank angle to meet cross range requirements assuming equilibrium flight.

$$\sigma_{CROSS} = \text{atan}\left(\frac{v_0^2}{gR_{cir}}\right) \tag{5.16}$$

The minimum bank angle given by equation 5.16 is conservative because is does not account for changing velocity over the course of the trajectory. In practice it serves as a good approximation for the minimum necessary bank angle to meet the necessary crossrange requirement of the target site. This is verified experimentally by flying out several constant bank angle command trajectories with no roll reversals and computing a minimum bank angle estimate to meet the crossrange requirement resulting from that trajectory. Table 5.2 below summarizes these results:

Table 5.2 : Actual vs. Estimated Bank Angles

σ_{actual}	$\sigma_{estimate}$	$\Delta\sigma$
0	0	0
5	4.366	0.634
10	8.791	1.209
15	13.324	1.676
20	18.008	1.992
25	22.883	2.117
30	27.946	2.054
35	33.200	1.800
40	38.606	1.394
45	44.134	0.866
50	49.667	0.333
		$\overline{\Delta\sigma}$ = 1.280

The evidence above shows that the equilibrium glide assumption used to estimate the minimum bank angle to meet cross range requirements is a valid assumption. This is because CLAT trajectories are relatively smooth and the vehicle is in or nearly in equilibrium glide for the entire trajectory.

Ground Range Requirement: Bank Angle Estimate

In addition to the crossrange requirement, each site has a ground range requirement. Recall that ground range is nearly linearly related to the CLAT bank angle command. Thus the bank angle command necessary to meet ground range requirements for a site can be approximated by interpolation between the minimum and maximum ranges.

The bank angle estimate is made for each site by linear interpolation between the final ranges to

choose the bank angle such that the range-to-go error is zero (assuming all properties are linear between bank angles). The following equation solves for the each site's initial CLAT bank angle command (note σ_{CROSS} corresponds to maximum range and vice versa):

$$\cos\sigma_{SITE} = \cos\sigma_{max} + \frac{\cos\sigma_{CROSS} - \cos\sigma_{max}}{R_{GO_{max}} - R_{GO_{CROSS}}}(R_{GO_{TGT}} - R_{GO_{CROSS}}) \qquad \textbf{5.17}$$

Site Feasibility

Given the minimum bank angle for cross range requirements, σ_{CROSS}, and the bank angle necessary to meet ground range requirements, σ_{SITE}. A site is nominally feasible if the following condition is satisfied:

$$\sigma_{CROSS} < \sigma_{SITE} < \sigma_{max} \qquad \textbf{5.18}$$

It is assumed that σ_{CROSS} is greater than zero (the minimum bank angle).

Site Robustness Assessment

Equation 5.18 only assesses nominal feasibility. If parametric uncertainties are present the tracking algorithm must use a different bank angle to reflect the uncertainty. A more detailed discussion of how uncertainties relate to bank angle commands is included in Chapters 6 and 7. However, site robustness is an important aspect of site selection and is thus included here to emphasize this importance. If σ_{SITE} is exactly equal to σ_{CROSS} then there is very little robustness margin. A parametric uncertainty which requires a reduction of the bank angle to meet tracking requirements and guarantee the ground range requirement is met will cause the crossrange requirement to be violated. This indicates a desire to define performance robustness bounds in terms of control saturation. Equation 5.18 should actually be rewritten to include robustness bounds for feasibility:

$$\sigma_{CROSS} + \Delta\sigma_L < \sigma_{SITE} < \sigma_{max} + \Delta\sigma_U \qquad \textbf{5.19}$$

Two approaches can now be taken for including robustness as part of footprint definition. The

first includes the robustness bound in the site feasibility evaluation. A minimum robustness requirement is defined pre-mission and included in evaluation of candidate sites. In this manner a robustness guarantee is met.

An alternative approach is to include robustness as part of the cost function for site selection. An upper and lower $\Delta\sigma$ can be computed for each site and included as part of the weighting function. Now all nominally feasible sites are included but the most robust site can be selected. Of course the two methods can be combined to provide minimal robustness guarantees and then further information is gained by including robustness as a cost function term.

5.3.4 Range Prediction Fine Tuning and Initial Reference Bank Angle Command

Once the site is selected, a more accurate bank angle reference can be determined. The ground range approximation for a straight ahead trajectory does not correspond as well to high cross range trajectories. So once the site is selected, two basis trajectories must be generated for the site. Basis trajectories are generated by flying nominal guidance with CLAT bank angle commands given by:

$$\sigma_1 = \sigma_{SITE} - \Delta\sigma_{INIT} \qquad \textbf{5.20}$$

$$\sigma_2 = \sigma_{SITE} + \Delta\sigma_{INIT} \qquad \textbf{5.21}$$

The parameter $\Delta\sigma_{INIT}$ is designed to capture the range of initial condition variations possible due to parametric uncertainties resulting from the open loop nature of alpha recovery. This parameter is specified by pre-mission analysis as a function of abort velocity. The procedure to define this parameter is to fly out alpha recovery trajectories in the presence of some desired minimum and maximum density and *L/D* uncertainties. These uncertainties results in range variations at the initiation of CLAT. The worst case range errors resulting from the uncertainties are applied to equation 5.17 to solve for the changes in bank angle necessary to capture the possible variation.

Now the reference bank angle command is generated as a function of the basis trajectories:

$$\cos\sigma_{CMD} = \cos\sigma_1 + \frac{\cos\sigma_2 - \cos\sigma_1}{R_{GO_1} - R_{GO_2}}(R_{GO_{TGT}} - R_{GO_2}) \qquad \textbf{5.22}$$

In addition, generating the above two trajectories provide basis energy vs. range to go profiles which are used by the closed loop redesign algorithm to modify the reference bank angle to adjust for initial condition uncertainties.

5.3.5 Final Altitude Control Using Bank Angle

An important point described in Chapter 4 was the fact that the final altitude is also affected by the constant bank variations. Drag-velocity relationships are helpful in defining a solution to controlling the final altitude via bank angle. Altitude can be defined as a function of a position in drag-velocity space if the angle of attack is known:

$$r = r_S - H\ln\left(\frac{2Dm}{\rho_S S_a v^2 C_D}\right) \qquad \textbf{5.23}$$

This equation indicates that with a fixed angle of attack vs. velocity profile, the final altitude is a direct function of the position in drag-velocity space. Figure 5.4 shows the effects of CLAT constant bank variations on the vehicle trajectory in drag-velocity space

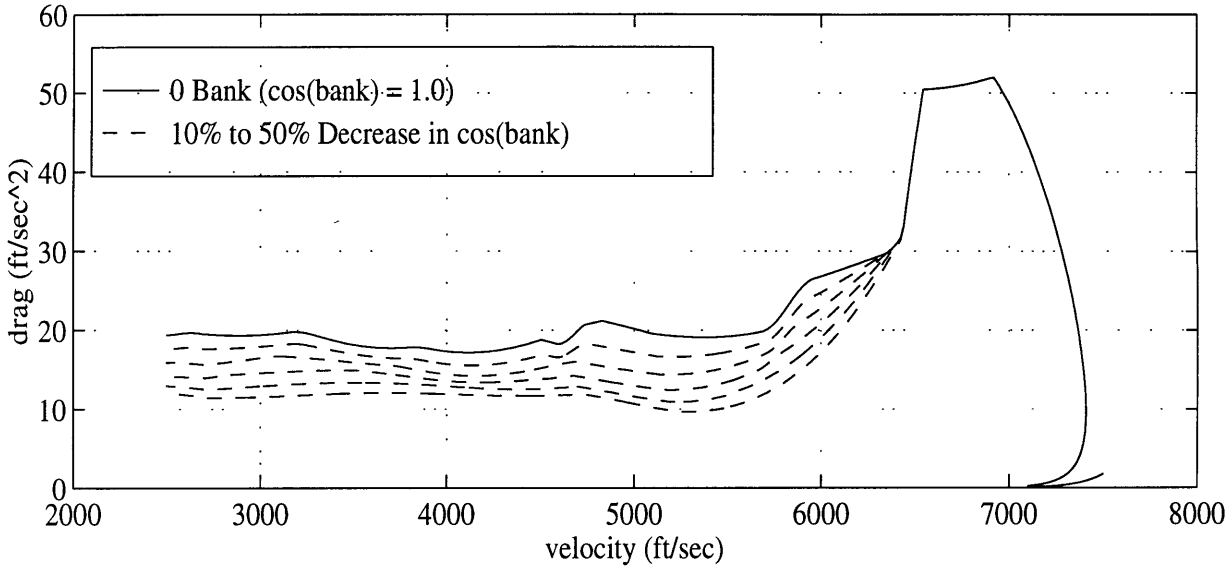

Figure 5.4 : Constant bank variations on X-34 D-V trajectories

Note that in Figure 5.4, the drag-velocity trajectories diverge at lower velocities. This divergence demonstrates the reduction in final altitude as a function of constant bank angle commands. Appendix A derives the following relationship between a position in drag-velocity space and a commanded bank angle:

$$u = \left(\frac{1}{b}\right)(\ddot{D}_{Ref} - a) \qquad \textbf{5.24}$$

$$\sigma = \text{acos}\left(\frac{u}{L/D}\right) \qquad \textbf{5.25}$$

Recognizing that, assuming a known angle of attack profile, a position in drag-velocity space can be used to define an altitude and bank angle it should be relatively easy to "shape" the trajectory to meet final altitude requirements. Recall that the angle of attack profile in the later portion of the trajectory is fixed by a known upper limit profile. Now final altitude control is achieved by modifying the constant bank command to linearly reduce the bank angle to zero at the lower velocities. The bank angle commands and corresponding drag-velocity trajectories are illustrated in Figure 5.5.

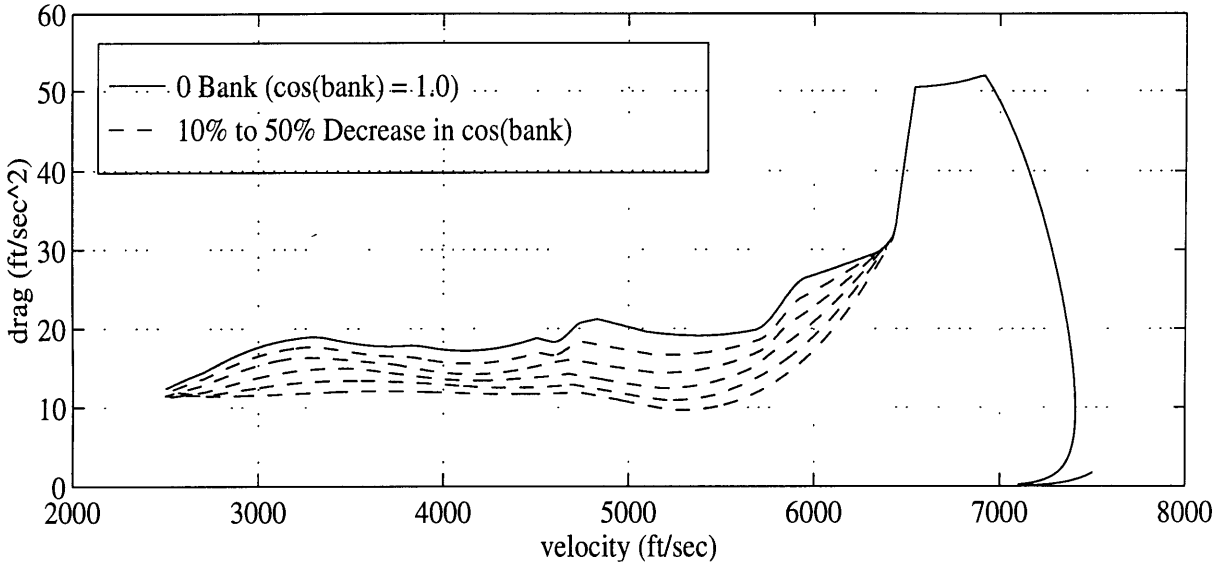

Figure 5.5 : Altitude "shaped" trajectories via bank command only.

The actual final altitudes both with and without the linear reduction in bank angle are shown below. The improvement using the linear reduction in bank angle is clear.

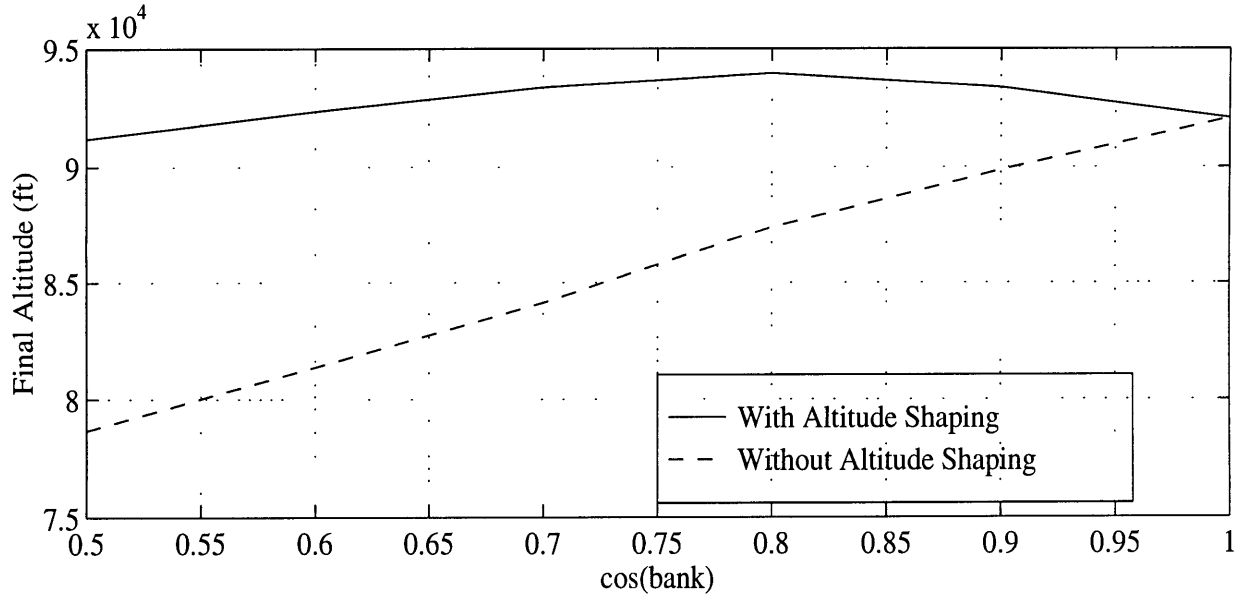

Figure 5.6 : Final Altitude vs. cosσ with and without altitude shaping

All of the above techniques for footprint definition are unaffected by the use of a linear reduction in bank angle to meet altitude requirements. From this point on assume that the nominal guidance algorithm and reference model guidance algorithm include the linear reduction in bank angle over the final portion of the trajectory.

5.4 Initial Trajectory Design Algorithm

The initial trajectory design is very important. A gross error in the initial design can result in large changes in the range because of the high velocities early in the trajectory. Even more importantly, the initial design algorithm also builds up the framework for the CLAT redesign algorithm. Recall that during alpha recovery the closed loop trajectory design functions are not operating. Also the reference dynamic model is not propagating but is just being set to the measured vehicle state. Although this reduces vehicle capability, the lack of closed loop redesign during alpha recovery actually makes CLAT design easier. Upon initiation of an abort, the vehicle is traveling upwards on a ballistic trajectory. During this ballistic portion and the alpha recovery phase, the guidance laws are relatively fixed. While lacking closed loop control limits the flexibility of the design algorithm, it also buys time. The trajectory design algorithm has a great deal of time (20 to 40 seconds depending on the abort initial conditions) to generate an initial plan. The design algorithm presented here only requires four trajectory integrations to completely define the vehicle footprint, select a site, select the initial reference bank angle, and define the basis set used for closed loop redesign.

The design algorithm is outlined below.

1. Evaluate Nominal Alpha Recovery Trajectory - Compute Alpha Recovery Angle of Attack Command
2. Footprint Definition and Site Selection
3. Compute Alpha Bias and Constant Pitch Commands
4. Define Basis CLAT Trajectories and Compute Initial Reference Bank Angle Command

1. Evaluate Nominal Alpha Recovery Trajectory - Compute Alpha Recovery Angle of Attack Command

The ascent portion of flight and alpha recovery are both relatively fixed. For the initial design a nominal ascent and alpha recovery are flown out using time integration to determine the nominal initial condition for CLAT. The constant angle of attack command is computed by a table lookup of maximum achievable angles of attack with respect to initial abort velocity. The maximum achievable angle of attack is computed pre-mission assuming maximum elevon deflection and solving the rigid body equations of motion for the steady state angle of attack given the moments generated by the maximum elevon deflection. Also determined here are estimates of the possible final alpha recovery range error due to parametric uncertainties. These estimates are determined by flying out alpha recovery trajectories in the presence of some desired minimum and maximum density and *L/D* uncertainties. The maximum range error estimate is used in selecting the basis trajectories.

2. Footprint Definition and Site Selection

Footprint definition uses the tools defined in section 5.3. The steps are outlined below:

2. a. Fly out minimum and maximum range trajectories to define baseline footprint.

2. b. Determine which sites are inside the baseline footprint.

2. c. Evaluate each site's feasibility and robustness using equations 5.15 through 5.19.

2. d. Select site based on robustness and other specified criteria (runway length, proximity to populations, etc.)

Steps 2.a-d provide simple and fast footprint definition based on only two trajectory integrations.

3. Compute Alpha Bias and Constant Pitch Commands

The angle of attack bias and constant pitch commands are specified with respect to abort velocity through pre-mission analysis. These parameters are defined by using information about vehicle capability. The angle of attack bias is selected to meet final altitude requirements for a zero bank trajectory and the constant pitch command is selected to minimize altitude oscillation for a zero bank trajectory. For simplicity, an angle of attack bias of 4.0 degrees and constant pitch command

of 15.0 degrees are used in the included performance analysis. These parameters were chosen from the vehicle capability analysis.

4. Define Basis CLAT Trajectories and Compute Initial Reference Bank Angle Command

As described in section 5.3.4, the minimum and maximum bank angle trajectories are not perfect representations of the actual range - especially for high cross range requirements. Now that the site has been chosen, basis trajectories for more accurate design can be defined in the actual direction of the target site. The basis trajectories are integrated out using the CLAT bank commands defined in section 5.3.4. These provide basis energy vs. range-to-go profiles for closed loop reference model redesign. In addition, a more accurate initial reference bank angle command is defined by equation 5.22:

$$\cos\sigma_{CMD} = \cos\sigma_1 + \frac{\cos\sigma_2 - \cos\sigma_1}{R_{GO_1} - R_{GO_2}}(R_{GO_{TGT}} - R_{GO_2}) \qquad \textbf{5.22}$$

5.5 Closed Loop Reference Model Redesign Using Basis Energy vs. Range-to-Go Trajectories

To motivate the difficulties in defining a robust closed loop redesign function a digression is necessary. X-34 trajectories present very specific problems for closed loop redesign. The highly uncertain nature of alpha recovery phase makes definition of an effective basis set difficult. Traditional reference profile approaches effectively provide a drag-velocity basis set of desired trajectories. The initial condition robustness of drag-velocity reference profile based approaches is evaluated and compared to the robustness of an energy-range basis. Drag-velocity based approaches are not robust to initial condition uncertainties and reliance on drag-velocity approximation for redesign can lead to definition of unachievable trajectories. Once the utility of energy-range based redesign is established, the closed loop reference model redesign algorithm is presented.

5.5.1 Robustness of Drag-Velocity Based Range Prediction

The basis trajectories defined in the initial design could be used to define drag vs. velocity

reference profiles. Using either analytic approximation or exact solution the drag vs. velocity basis could be used to predict the final range by integrating the drag-velocity profile from the current velocity to the final velocity (as explained in Appendix A). Unfortunately, this method is only effective in the nominal case. Drag-velocity based range prediction is not robust to initial condition uncertainties. The dynamic interactions caused by parametric uncertainties during alpha recovery create such a wide variety of initial conditions in the drag-velocity space that simply relying on the nominal set of drag-velocity profiles for range prediction is useless. From a trajectory design standpoint, during alpha recovery vehicle guidance is open loop. Thus CLAT redesign robustness to initial condition uncertainties is very important. When initial condition uncertainties are introduced the nominal set of drag-velocity trajectories is invalid as much of the nominal set is no longer achievable.

During alpha recovery, guidance is effectively open loop. Alpha recovery guidance is concerned with constraints - not with performance. This causes wide variations in the initial conditions at the start of CLAT when parametric uncertainties are present. The variations in initial conditions completely alter the drag-velocity space in which CLAT operates and the nominal basis set becomes completely unrepresentative of the achievable vehicle dynamics. Because the reference model is initialized at the start of CLAT it is still representative of achievable vehicle dynamics. However, the reference model drag-velocity trajectory is completely different from the nominal based basis trajectories due to these initial condition variations. Examine figure 5.7 below. The drag-velocity space effects of multiple uncertainties are shown. To simulate perfect CLAT tracking of the reference dynamic model, the uncertainties are only applied during alpha recovery and then the nominal dynamics are propagated during CLAT. This simulates the actual vehicle behavior because at the start of CLAT closed loop drag tracking begins and the actual vehicle drag-velocity trajectory will match that of the reference dynamic model. This is because the dynamic model propagates the nominal vehicle dynamics and the tracking algorithm controls the vehicle to track these dynamics. The example shown below is for a straight ahead flight with 30° constant bank command. Roll reversals are used when the azimuth deadband is exceeded. Note that the nominal drag-velocity trajectory is shown for each case as well.

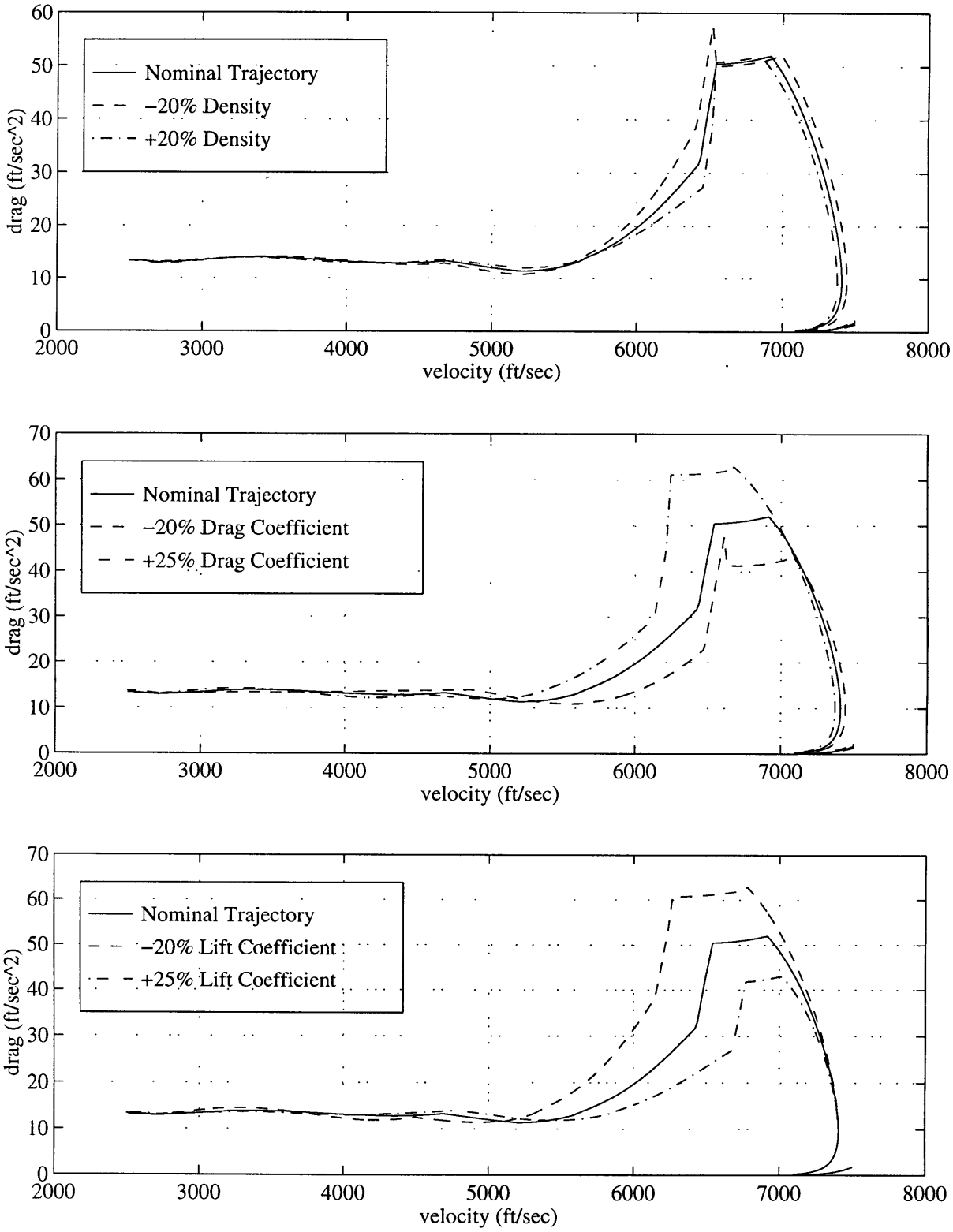

Figure 5.7 : Drag-Velocity Space Variations due to Parametric Uncertainties

For density uncertainties the trajectory variations are relatively small and quickly the perturbed trajectories converge to the nominal and ostensibly within the effective region of the basis trajectories. However, for aerodynamic variations the initial condition perturbations cause huge variations from the nominal trajectory. There is a large portion of the flight at high velocities when any closed loop redesign using drag-velocity basis trajectory interpolation is completely invalid. At high velocities errors in commands from the redesign function will cause large range errors. These errors can be so great that even when the trajectory reaches the desired nominal it is impossible to recover from earlier errors.

An important point to note is that an uncertainty in an aerodynamic coefficient corresponds to an *L/D* bias. Although an increase in C_D and an increase in C_L both result in a reduction in *L/D*, the dynamic behaviors in drag-velocity space resulting from the different biases are not always the same. The peak drag level during the normal acceleration limiting phase is correlated directly to the *L/D* bias. However, the dynamic behavior once the normal load limit is no longer active is not simply correlated with the *L/D* bias. The dynamic behavior is significantly different for C_D and C_L biases. This fact is illustrated below. Note that although the peak drag levels are linked to the *L/D* bias the drag-velocity space behavior varies according to the source of the *L/D* bias.

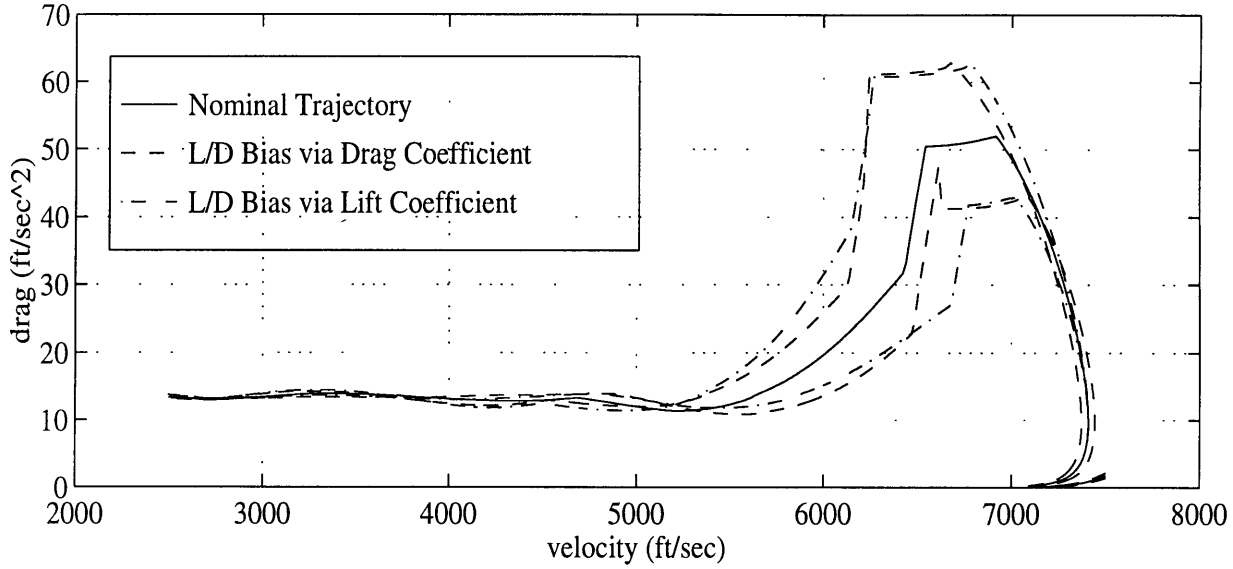

Figure 5.8 : Drag-Velocity Space Variations due to L/D Uncertainties

A closed loop redesign algorithm using the nominal drag-velocity basis set does not effectively capture vehicle capability or use realistic profiles. Propagating the dynamics in drag-velocity space based on interpolations within the nominal basis results in completely inaccurate range predictions early in the trajectory. The actual trajectory is so far from the nominal that any guidance decisions based on a drag-velocity nominal basis are highly inaccurate.

An attempt could be made at uncertainty estimation and modifying the basis trajectories according to the estimated bias. However, there would be a need to estimate both C_D and C_L rather than just *L/D*. An accurate measurement of *L/D* is possible, as is a measurement of atmospheric density. Unfortunately separating the aerodynamic coefficients would be a difficult estimation task.

All of these factors compound against the feasibility of closed-loop redesign using a drag-velocity basis set. There is simply not enough accurate information available to the design algorithm to effectively accomplish robust redesign. Fortunately, a better redesign option is available by taking advantage of linear relationships in the energy vs. range state space.

5.5.2 Energy-Range Space Variations due to Parametric Uncertainties

The lack of robustness of using a drag-velocity nominal basis set for closed loop redesign of the reference dynamic model necessitates the development of a more robust approach. The use of energy vs. range relationships provides a simple and robust method for real-time reference dynamic design. Ishimoto uses energy management for range control in an entry guidance algorithm [9].

The reference dynamic model free parameter is the CLAT bank angle command. Examine Figure 5.9 below which illustrates the linear relationships of the nominal energy-range profiles as a function of the cosine of the reference bank angle. The slope of the energy-range profile is determined by the bank angle command.

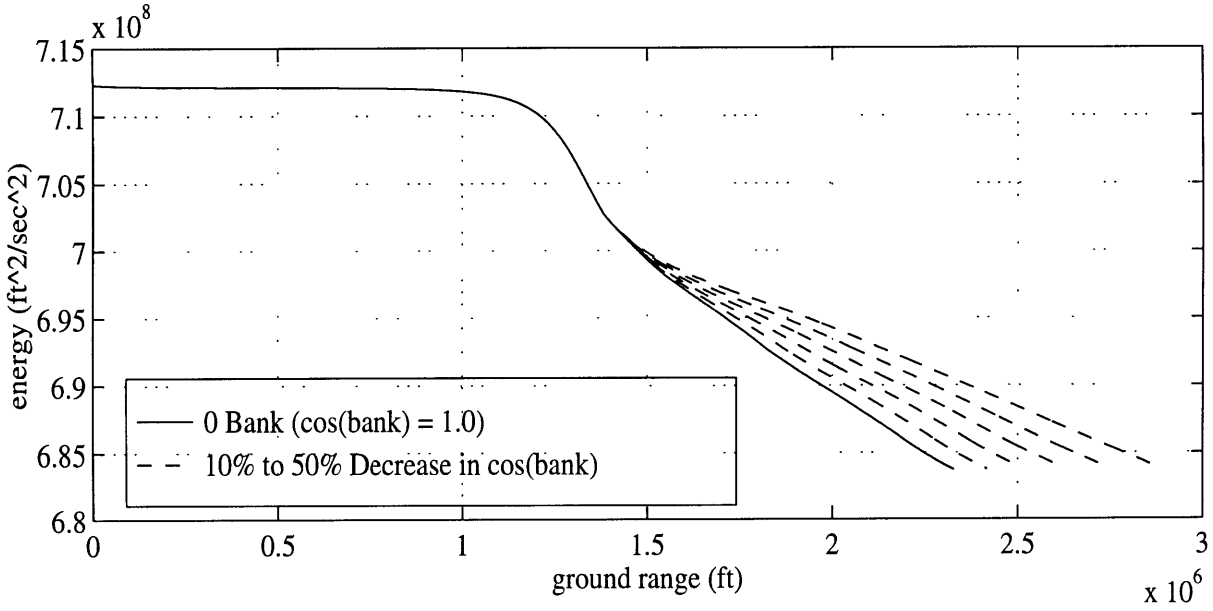

Figure 5.9 : Constant Bank Variations in Energy-Range Space

The energy-range space linear relationships imply a potentially useful approach for closed loop redesign of the reference model. Energy-range basis trajectories can be defined and the reference bank angle determined as a function of the final ground ranges of the basis trajectories and the actual current vehicle energy. The slope of the energy-range profile is modified by the reference

bank angle command to guide the vehicle to the desired range.

While similar to the drag-velocity reference profile approach, this approach is very different: it is robust to parametric uncertainties and initial condition variations due to parametric uncertainties. The slope of the energy range profile is maintained and can still be adjusted by the constant bank command. Figure 5.10 illustrates this fact. As in section 5.5.1 parametric uncertainties are applied to a constant bank trajectory during alpha recovery and then removed during CLAT to simulate perfect tracking of the dynamic reference. Again density and aerodynamic uncertainties are examined.

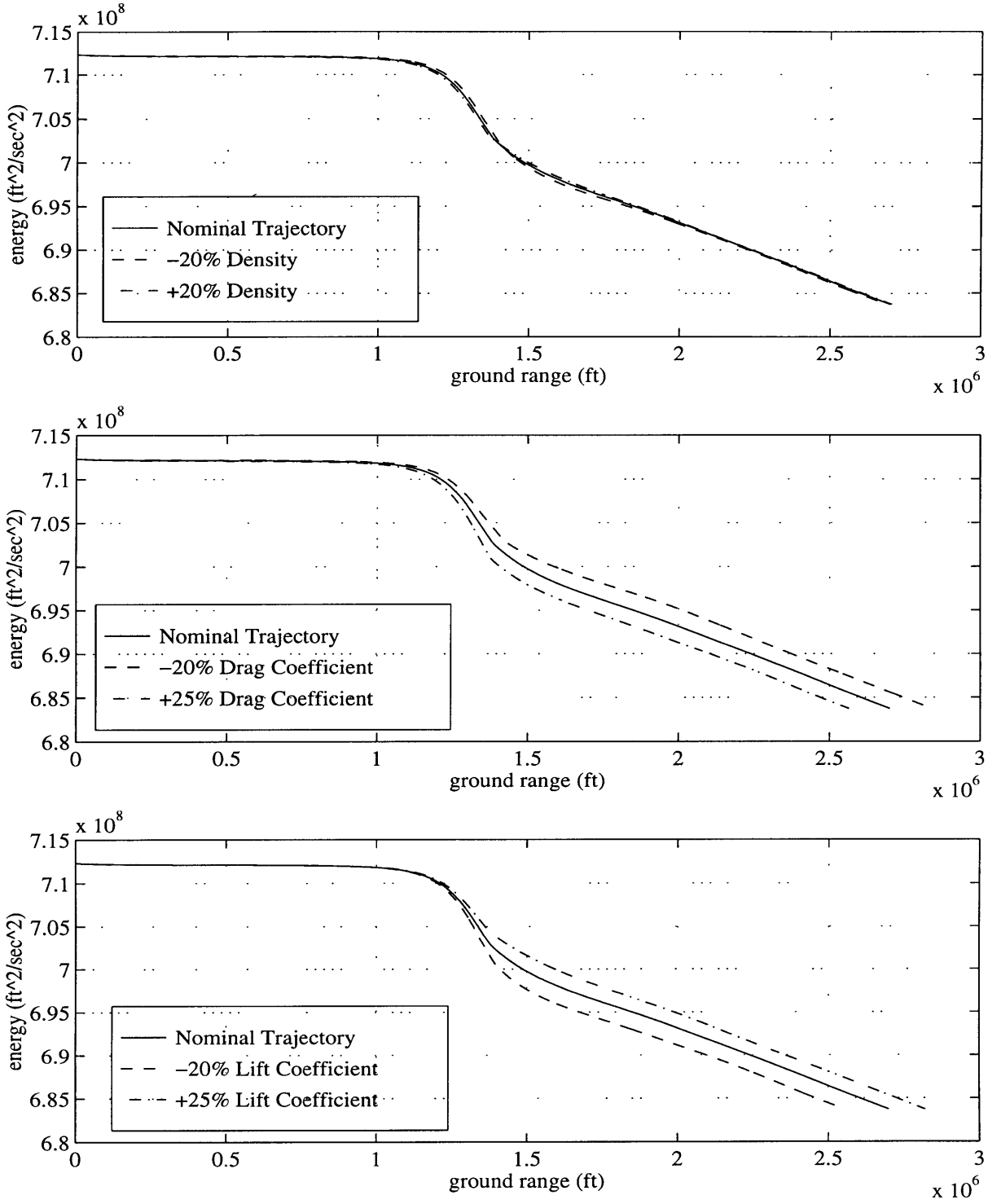

Figure 5.10 : Energy-Range Space Variations due to Parametric Uncertainties

The slope of the energy-range profile is maintained. The perturbed trajectories parallel the

nominal trajectory. The unpredictable drag-velocity trajectory behaviors are not evident.

Again correlation of aerodynamic uncertainties is important. Now the trajectory effects due to *L/D* biases are much more closely correlated as indicated below in figure 5.11. Unlike drag-velocity space trajectories, energy-range trajectories are much more "well-behaved" and provide a simple framework for real-time reference dynamic modification.

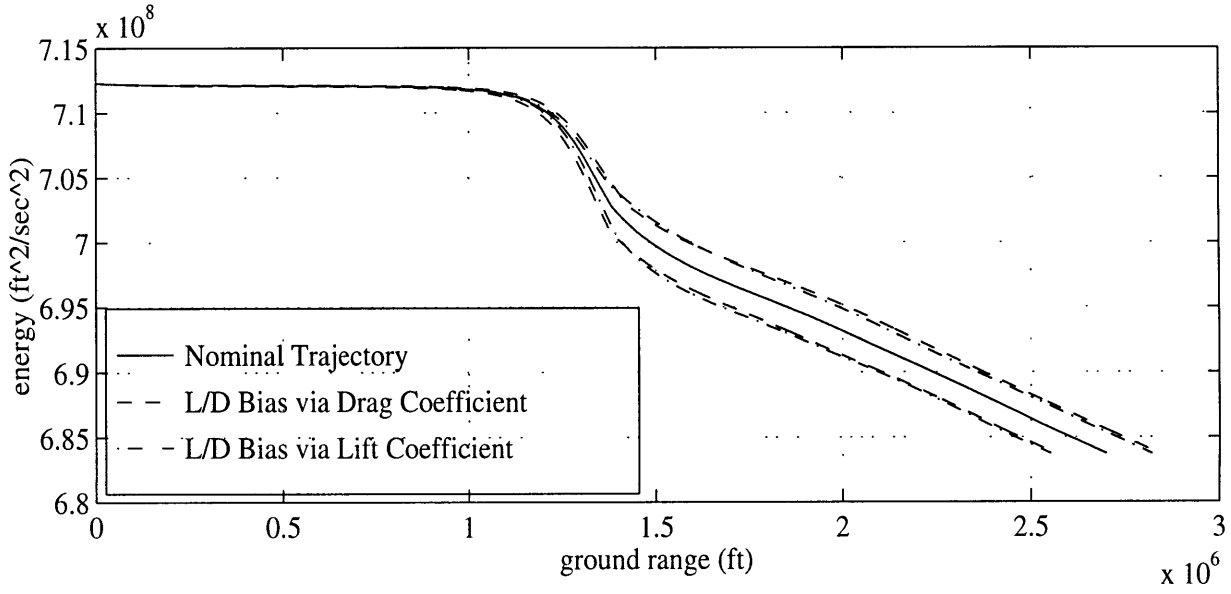

Figure 5.11 : Energy-Range Space Variations due to L/D Uncertainties

5.5.3 Implication for Closed-Loop Trajectory Design

All of the above factors point to the utility of an energy-range basis set for modification of the reference dynamic to meet range requirements. The drag-velocity approach is not robust to initial condition uncertainties. An energy-range approach is much more intuitive and robust. No parameter estimation is required. Note that the above results are very specific to X-34 trajectories. The need for reference model based guidance modified by energy-range feedback arises directly from the constrained nature of X-34 trajectories. Although the need is specific, the application is very general. The reference model approach subject to energy-range redesign covers a much larger class of problems than a reference profile approach.

5.5.4 Closed Loop Redesign: Energy-Range Feedback

The closed loop redesign algorithm is conceptually similar to the initial design algorithm. Energy-range profiles are used as the basis set for interpolation and the bank angle command is adjusted as a function of final range to go on the basis profiles. No integration or iteration is used because the basis set can simply be shifted according to the current energy and range state. The algorithm is as follows:

1. Determine range to go on each basis profile for the current vehicle energy. This is determined as illustrated below. The vehicle is outside of the basis energy range trajectories due to a parametric uncertainty. The current basis range to go is solved by determining the range to go of the basis trajectories at the vehicle energy level.

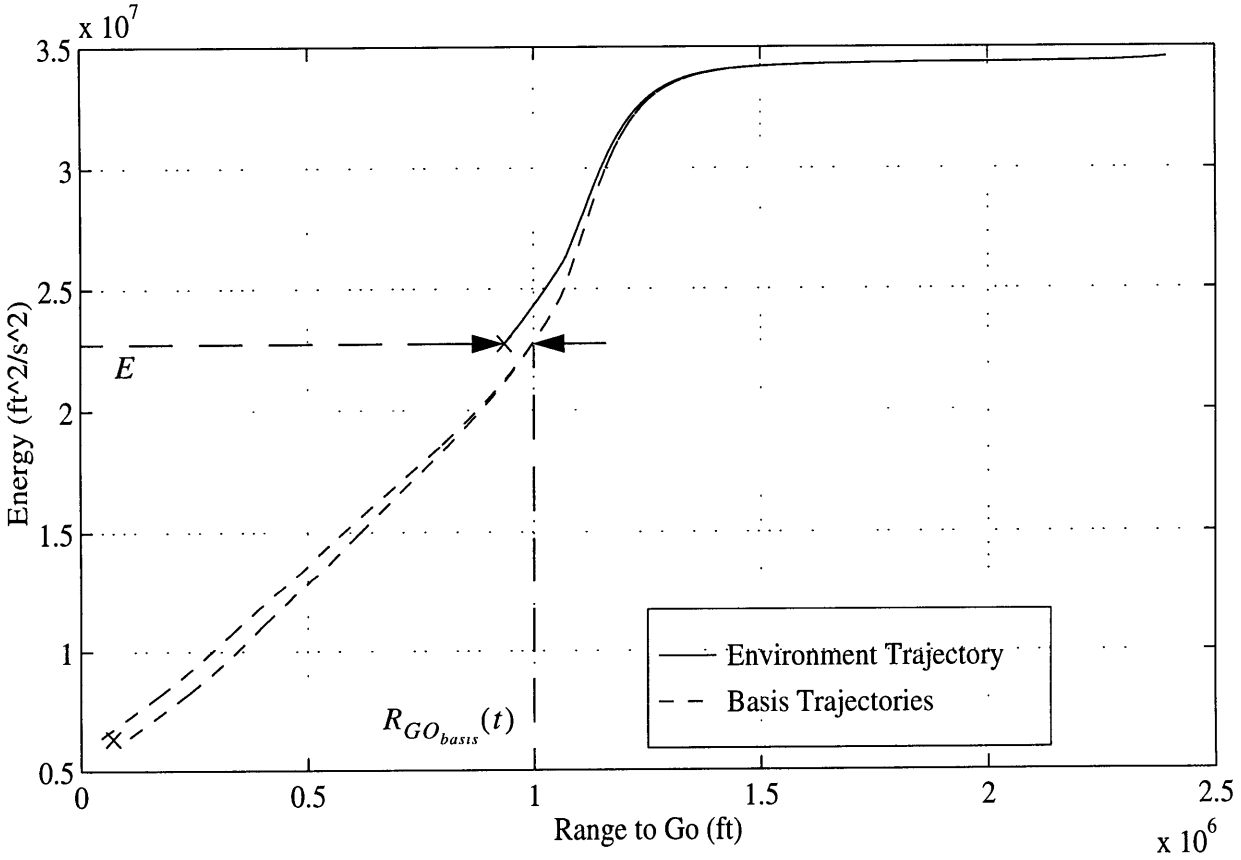

Figure 5.12 : Basis R_{GO} Computation

2. Shift final basis range to go according to current range to go differences.

$$R_{GO_{shift}} = R_{GO}(t) - R_{GO_{basis}}(t) \quad \textbf{5.26}$$

$$R_{GO_{ShiftBasis}}(t_f) = R_{GO_{basis}}(t_f) + R_{GO_{shift}} \quad \textbf{5.27}$$

3. Predict final range to go using current bank angle and interpolating between the shifted basis trajectories:

$$R_{GO_{PRED}} = R_{GO_{ShiftBasis1}}(t_f) + \left(\frac{\cos\sigma_{CMD} - \cos\sigma_{basis1}}{\cos\sigma_{basis2} - \cos\sigma_{basis1}}\right) \cdot (R_{GO_{ShiftBasis2}}(t_f) - R_{GO_{ShiftBasis1}}(t_f)) \quad \textbf{5.28}$$

4. Compute new bank angle reference by interpolation between basis final range to go profiles:

$$\cos\sigma_{CMD} = \cos\sigma_{CMD_{prev}} + \left(\frac{\cos\sigma_{basis2} - \cos\sigma_{basis1}}{R_{GO_{basis2}} - R_{GO_{basis1}}}\right)(R_{GO_{TGT}} - R_{GO_{PRED}}) \quad \textbf{5.29}$$

Steps 3 and 4 can be combined but they are separated for clarity. Also, separating steps 3 and 4 clearly specifies the reference bank angle selection algorithm as an integral range controller.

5.6 Trajectory Design Algorithm Summary

The trajectory design algorithm presented above is viewed as the outer loop in a model based compensator for range control. The goal of the design algorithm is to specify a reference dynamic model which is guaranteed to reach the desired target conditions in the nominal case. There are three functions for trajectory design: pre-mission analysis, initial design, redesign.

Pre-mission analysis was completed in chapter 4. The reference model alpha recovery angle of attack command of 25°, the alpha recovery bank angle command of 0°, the CLAT constant pitch command of 15°, and the alpha bias command of 4° were all chosen according to the results presented in chapter 4.

Initial design is carried out while the vehicle is in alpha recovery. Initial design accomplishes footprint definition by integrating out a zero bank CLAT trajectory and an 80° bank trajectory.

The full vehicle state is integrated and is initialized at the measured states at the initiation of the abort. Both trajectories are flown out straight ahead. The 80° trajectory uses roll reversals to maintain a (roughly) constant azimuth. Interpolating between the ground ranges of these trajectories and determining a minimum bank angle to meet crossrange requirements defines site feasibility and thus defines the vehicle footprint. The target site is chosen according to some cost function. Now, two more CLAT trajectories are integrated with constant bank angle commands chosen near the expected bank angle command to reach the target site. Again the full vehicle state is integrated and is initialized at the measured states at the initiation of the abort. Roll reversals are used to point the vehicle towards the target site and maintain the vehicle within the azimuth deadband. Interpolating between the ground ranges of these trajectories generates the initial reference bank angle command. Initial design is now complete.

At the completion of alpha recovery and the start of CLAT, the reference dynamic model is initialized to the current measured vehicle state. The reference model is not initialized again during CLAT. From this point on, closed loop tracking of the reference model ensures that the vehicle behavior is nominal. This allows range control to only be concerned with the nominal dynamics. Range control is accomplished by interpolating between the energy vs. range to go profiles generated during the initial design. The current vehicle energy is matched to the basis profiles and final range is predicted for the current reference bank angle. At every guidance cycle the redesign algorithm computes a perturbation to the reference bank angle to drive the predicted range error to zero. The sensitivity of the range to the bank angle is computed as a function of the basis energy-range profiles. Note that the redesign algorithm is able to use only nominal energy-range profiles because the behavior of the reference model is, by definition, nominal. In terms of range control, closed loop tracking of the model also makes the behavior of the actual vehicle appear nominal.

Table 5.3 is updated below to reflect the current guidance system. The trajectory tracking algorithm completes the guidance system by providing the inner loop tracking of the reference model to reject disturbances and uncertainties.

Table 5.3 : Guidance System Functions

	Trajectory Design	Reference Dynamic Model	Trajectory Tracking
Alpha Recovery	Footprint definition and site selection Determine baseline CLAT plan	Set to measured environment State	Nominal Alpha Recovery Guidance
CLAT	Generate Reference Dynamic Model bank angle command using interpolation between basis trajectories	Propagate nominal dynamics to current vehicle velocity	Tracking law to follow Reference Dynamic Model
Angle of Attack	Constant Pitch and Alpha Bias commands specified according to pre-mission analysis	Constant Pitch Command following to a biased upper limit profile	
Bank Angle	Closed-loop redesign of reference bank angle using interpolation between energy-range basis trajectories	Constant bank command defined by the Trajectory Design Algorithm	
Roll Reversals		Controls roll reversals by measuring vehicle azimuth	Performs roll reversals when commanded by Reference Dynamic Model

Chapter 6

Trajectory Tracking

In the nominal case where all aerodynamic data is perfectly accurate, the atmosphere is modeled exactly, there are no winds, and initial conditions are exactly as expected, no tracking laws are necessary. The vehicle simply flies the designated profile open loop and reaches the target exactly as expected. Of course this is not realistic. Uncertainties abound, especially in atmospheric guidance problems. The ability to adjust for these uncertainties and reject disturbances is critical for any guidance system. Trajectory tracking fills the second major block in the guidance system. Traditional approaches rely on linearized methods with single-input-single-output (SISO) feedback loops to track a reference profile designed to meet the vehicle range requirements. New methods propose nonlinear tracking laws but still only track one reference profile. Predictor-corrector approaches rely on estimation of environment uncertainties. This chapter lays out the foundation and demonstrates the concept of tracking two reference variables using two control variables for atmospheric guidance. Multiple-input-multiple-output (MIMO) control theory has seen huge developments in the last several decades and has been applied successfully to linear and nonlinear control problems. The basis of the proposed guidance system is in tracking both drag and altitude by using variations on angle of attack and bank angle from the nominal. Accurate tracking of both reference variables improves guidance system robustness. The tracking problem is a two-input-two-output regulator problem. The reference model provides the nominal controls and commanded output states. Perturbations from the nominal controls are used to meet the commanded states in the presence of uncertainty and disturbances. Two tracking algorithms are presented and compared and contrasted through linearized analysis and through actual nonlinear simulation. Robustness properties are the focus of the analysis. The first algorithm treats the problem as an output feedback problem with pseudo-decoupled dynamics. The second algorithm uses linear quadratic regulator (LQR) theory to solve the problem by linearizing about the nominal model. Linearized analysis of both controllers shows that the LQR control algorithm can be made through weighting to match the frequency response of the decoupled algorithm. However, the LQR approach relies on state feedback. State feedback approaches have difficulty

in handling true output feedback problems when uncertainties exist in the output and feedforward matrices. For these reasons, despite the fact that all states are perfectly measured, a full state feedback LQR approach is not robust to uncertainties.

6.1 Traditional SISO Entry Guidance Approaches

The most thoroughly operationally tested example for high *L/D* glide return vehicles is the space shuttle. The entry guidance algorithm has proven enormously successful. The shuttle Glide Return to Launch Site (GRTLS) guidance is the starting point for abort guidance approaches while shuttle entry guidance is a starting point for closed loop guidance approaches. Several variations to the shuttle guidance algorithm have been proposed. All proposed methods tackle the same problem of SISO tracking but using nonlinear control methods to improve tracking performance.

6.1.1 Glide Return to Launch Site Open Loop Alpha Transition

GRTLS guidance is described in section 3.2 but some important points are reiterated here. While the alpha recovery phase with normal acceleration limiting handles the problem of recovery from a ballistic entry, the alpha transition phase allows no adjustment for range. Shuttle alpha transition is flown open loop with angle of attack at roughly maximum *L/D*. Range control is provided during the powered phase of flight and it is assumed that TAEM guidance is able to adjust for any dispersions. X-34 trajectories have too many possible abort scenarios and no powered phase of the abort to use this approach. Clearly some sort of closed loop control is required.

6.1.2 Entry Guidance Drag-Velocity or Altitude-Velocity Tracking

Drag-velocity based shuttle entry guidance was outlined in section 5.2. Tracking of the drag-velocity profile is accomplished through linear feedback control methods. The success of the shuttle entry guidance algorithm and recent interest in reusable launch vehicle technology has spurred the application of nonlinear control methods to tracking drag-velocity reference profiles as well. Alternative approaches utilizing altitude-velocity reference profiles have been proposed as well.

Drag-Velocity Tracking

The basis for controlling vehicle drag using bank angle to guarantee final range is well established in a number of applications. The shuttle entry guidance algorithm is described in full by Harpold and Graves in Shuttle Entry Guidance [8]. Another applicable method for drag-velocity tracking is proposed by Mease and Kremer in Shuttle Entry Guidance Revisited Using Nonlinear Geometric Methods [14]. Mease and Kremer propose a feedback linearization in a similar format as the shuttle entry guidance.

Drag is chosen as the command variable because of its explicit control of final range. This concept can be motivated by deriving an analytic approximation for vehicle range based explicitly on drag and velocity. Start with the equations of motion for radial position, velocity, and flight path angle:

$$\frac{dr}{dt} = v\sin\gamma \qquad \textbf{2.5}$$

$$\frac{dv}{dt} = -D - g\sin\gamma \qquad \textbf{2.6}$$

$$\frac{d\gamma}{dt} = \left(\frac{1}{v}\right)\left(L\cos\sigma - \left(g - \frac{v^2}{r}\right)\cos\gamma\right) \qquad \textbf{2.7}$$

The vehicle heading angle, downrange, and crossrange are actually outputs of the above dynamics and their equations of motion are:

$$\frac{d\psi}{dt} = \left(\frac{1}{v}\right)\left(L\frac{\sin\sigma}{\cos\gamma} - \frac{v^2}{r}\cos\gamma\sin\psi\right) \qquad \textbf{2.8}$$

$$\frac{dR_x}{dt} = v\cos\gamma\cos\psi \qquad \textbf{2.3}$$

$$\frac{dR_y}{dt} = v\cos\gamma\sin\psi \qquad \textbf{2.4}$$

Combining equations 2.6, 2.3 and 2.4 yields equations 5.1 and 5.2 for downrange and crossrange.

$$\Delta R_x = -\int_{v_0}^{v_f} \frac{v\cos\gamma\cos\psi}{D + g\sin\gamma} dv \qquad \textbf{5.1}$$

$$\Delta R_y = -\int_{v_0}^{v_f} \frac{v\cos\gamma\sin\psi}{D + g\sin\gamma} dv \qquad \textbf{5.2}$$

Assuming that flight path angle is small and only considering the range along the ground track

yields an approximation for range which is a function of drag and velocity:

$$\Delta R = -\int_{v_0}^{v_f} \frac{v}{D} dv \tag{6.1}$$

This relation is the motivation for tracking drag as a function of the reference velocity. The traditional approach to trajectory design and tracking is to design a drag-velocity profile which defines the current drag command. Then the tracking law determines the bank angle to meet this command. The trajectory design algorithm presented in Chapter 5 avoids this approximation by predicting and controlling final range as a function of exact nominal trajectory integrations. Deutsch's approach also avoids this approximation by actually solving the equations of motion for the flight path angle given a point along a drag-velocity profile.

The shuttle and feedback linearization methods are summarized here as an introduction to the drag-velocity tracking problem using bank angle. Both methods have a nominal bank angle command plus a feedback term. For both methods, the nominal bank angle command is determined in a similar manner as described in Appendix A and [14]. The current nominal bank angle command is determined as a function of the drag-velocity reference profile. The drag-velocity dynamic system is described by the equations given in Appendix A but with a small flight path angle assumption and the drag coefficient is assumed to be constant as in equations 6.2 to 6.5.

$$(z_1, z_2, z_3) = (D, \dot{D}, v) \tag{6.2}$$

$$\dot{z}_1 = z_2 = \dot{D} = -\frac{Dv}{H}\sin\gamma - \frac{2D^2}{v} \tag{6.3}$$

$$\dot{z}_2 = \ddot{D} = a + bu \tag{6.4}$$

$$a = \frac{D}{H}\left(g - \frac{v^2}{r}\right) + \dot{D}\left(\frac{\dot{D}}{D} - \frac{3D}{v}\right) - \frac{4D^3}{v^2}$$

$$b = -\frac{D^2}{H} \qquad u = \frac{L\cos\sigma}{D}$$

$$\dot{z}_3 = \dot{v} = -D + gH\left(\frac{\dot{D}v + 2D^2}{Dv^2}\right) \tag{6.5}$$

The nominal control can be determined by solving the equations of motion (the "r" subscript

indicates reference):

$$u_r = \left(\frac{1}{b_r}\right)(\ddot{D}_r - a_r) \tag{6.6}$$

To correct for disturbances from the nominal both methods apply a feedback term. The feedback term is designed to follow desired error dynamics given by:

$$\Delta\ddot{D} + 2\zeta\omega\Delta\dot{D} + \omega^2\Delta D = 0 \tag{6.7}$$

Specify that

$$\nu = a + bu = \ddot{D}_r + 2\zeta\omega\Delta\dot{D} + \omega^2\Delta D \tag{6.8}$$

The shuttle entry guidance law uses linear corrections about ν to determine the gains on the errors. The linearized law is given by equation 6.9.

$$u_L = \frac{1}{b_r}(\ddot{D}_r - a_r) - K_p(v)\Delta D - K_d(v)\Delta\dot{D} \tag{6.9}$$

$$K_p(v) = \frac{1}{b_r}\left[\omega^2 + \left(\frac{\partial a}{\partial D}\right)_r + u_r\left(\frac{\partial b}{\partial D}\right)_r\right]$$

$$K_d(v) = \frac{1}{b_r}\left[2\zeta\omega + \left(\frac{\partial a}{\partial \dot{D}}\right)_r + u_r\left(\frac{\partial b}{\partial \dot{D}}\right)_r\right]$$

The feedback linearized method simply solves equation 6.8 for u to get:

$$u_N = \frac{1}{b_r}(\ddot{D}_r - a_r - \omega^2\Delta D - 2\zeta\omega\Delta\dot{D}) \tag{6.10}$$

Mease and Kremer show that for the nominal case the desired error dynamics are tracked exactly by 6.10 [14]. Because of the assumptions made in linearization the error dynamics are not tracked perfectly by the control law in 6.9. Mease and Kremer also show that the true constraint for asymptotic tracking of the desired reference is control saturation [14]. The only difference between the control laws is that the feedback linearization gives perfect tracking of the desired error dynamics.

An integral term is added to the shuttle control law to correct for steady state error in the presence of uncertainties and noise. Kremer and Mease also note the necessity of including an integral term in the control law [14].

Professor Ping Lu of Iowa State University proposes another drag-velocity tracking method in Entry Guidance and Trajectory Control for Reusable Launch Vehicle [10]. The control law is based on the nonlinear predictive control method presented in his paper Nonlinear Predictive Controllers for Continuous System [11]. The end result is similar to the feedback linearization method above. Following Lu's predictive control method leads to a control law of the form:

$$u = \frac{1}{b_r}\left(\ddot{D}_r - a_r - \omega^2\Delta D - 2\zeta\omega\Delta\dot{D} + \frac{1}{T}\left(-\Delta\dot{D} - 2\zeta\omega\Delta D - \omega^2\int_0^{\tau}\Delta D d\mu\right)\right) \qquad \textbf{6.11}$$

This controller is a nonlinear PID controller where the feedback linearized control law is a nonlinear PD controller. Bank angle control laws for drag-velocity tracking all generally reduce to the form of a linear or nonlinear PID controller. The addition of the integral term ensures zero steady state error in the presence of noise and uncertainty.

Altitude-Velocity Tracking

In addition to drag-velocity tracking, some entry guidance algorithms have been proposed which use altitude-velocity tracking. These algorithms recognize the relation between altitude and drag given by equation 5.23 to define the altitude reference profile.

$$r = r_S - H\ln\left(\frac{2Dm}{\rho_S S_a v^2 C_D}\right) \qquad \textbf{5.23}$$

Shinji Ishimoto, of Japan's National Aerospace Laboratory, proposes an entry guidance algorithm based on altitude-velocity tracking [9]. The altitude command is generated from a drag command which is computed as a function of range to go. The drag command is formulated as a function of range to go by using the relationship of drag, energy, and range-to-go as long as $\cos\gamma \sim 1$. Ishimoto notes that equation 5.8 can also be expressed as:

$$E_0 - E_F = \int_{R_F}^{R_0} D_r dR \qquad \textbf{6.12}$$

Expressing the drag command as a quadratic function of range-to-go and defining a final drag and final energy target leads to the following linear system of equations which defines the coefficients

of the quadratic drag function:

$$D_0 = C_{20} + C_{21}R_0 + C_{22}R_0^2 \qquad \textbf{6.13}$$

$$D_F = C_{20} + C_{21}R_F + C_{22}R_F^2 \qquad \textbf{6.14}$$

$$E_0 - E_F = C_{20}(R_0 - R_F) + \frac{C_{21}}{2}(R_0 - R_F)^2 + \frac{C_{22}}{3}(R_0 - R_F)^3 \qquad \textbf{6.15}$$

Although this formulation assumes that the flight path angle is small and cross-range effects and roll reversals are only controlled through feedback, the linearity of the relationship between energy and range is captured. Recall that the linearity in the energy-range space forms the basis for the closed loop redesign function presented in the last chapter. The reference command is defined by altitude commands derived using equation 5.23. Bank commands are determined by a PID control law to drive altitude errors to zero.

Angle of Attack Modulation

All of the above methods rely principally on bank angle for trajectory control. However, every method also allows angle of attack modulation as well to control the vehicle drag during roll reversals and to correct for short period disturbances. Angle of attack modulation was first described by Harpold and Graves [8]. The angle of attack command perturbations are kept small so as not to affect the bank angle control law. The angle of attack control law is typically defined as a perturbation from the nominal angle of attack profile as follows:

$$\Delta\alpha = f_\alpha(D_r - D) \qquad \textbf{6.16}$$

A bias term is included in the bank angle logic to drive the angle of attack command back to the nominal and retain principal trajectory control via bank angle [8].

6.1.3 Robustness of Traditional Approaches

The above approaches with one exception (Ishimoto's algorithm controls altitude with bank angle and enforces drag tracking by adding angle of attack modulation) all focus on tracking of a single reference profile using bank angle control. Angle of attack control authority is limited to maintain the good qualities of the bank angle control law. The various new methods provide better tracking

performance by using nonlinear control methodologies but all ultimately can be viewed as some form of a PID controller tracking a single reference profile. The controllable subspace in the drag-velocity space is determined completely by control saturation rather than the method of control. In the steady state all control laws utilizing bank angle will reach the same values to compensate for disturbances. Barring extreme cases, for any reasonable control law global asymptotically stable convergence is guaranteed unless control saturation occurs.

Recognizing this fact, guidance must be examined from the overall effects rather than just tracking of a profile. In short, tracking the profile is "easy". The difficulty is in selecting and defining reference profiles that meet the target requirements. Assuming that tracking will be guaranteed, examine what a given profile provides. Tracking of a drag profile guarantees convergence of the desired range. However, a density bias will induce final altitude errors as the bank angle control law is using only altitude to generate the desired drag level. Tracking an altitude profile gives the desired altitude. However, now a density bias causes final range errors. Profile redesign functions can correct for some of these errors but the guidance system is not really utilizing it's full capability. Profile redesign functions must operate on a low bandwidth to prevent large incorrect decisions due to a high frequency disturbance. Thus not all errors induced by single profile tracking can be corrected. Performance robustness when tracking a single profile can not be guaranteed. Improved tracking performance is gained and the guidance system is simplified but the vehicle performance is limited by the framework of the guidance system.

6.2 Multivariable Approach - Drag and Altitude Tracking

Now the goal becomes to modify the framework of the guidance system to allow for improved performance robustness. This is accomplished by increasing the complexity of the system. Two reference variables are defined and the references are tracked using two control variables. When drag is tracked alone the altitude is sacrificed and vice versa. Bank angle control laws modify the vehicle lift to track a reference. Angle of attack can also be used to independently modify the vehicle *L/D* and also the lift and drag. It follows that angle of attack control could be allowed so that both drag and altitude reference could be tracked. Tracking of both profiles increases performance robustness of the guidance system. Increased performance is gained at the price of

increased complexity and difficulty in design.

Angle of attack's entrance into the equations of motion is nonlinear and the equations of motion must be linearized to put the state equations into a form which is affine in the control. Without linearization, angle of attack is not affine because of the quadratic effect on the drag coefficient. Bank angle control is feedback linearizable and affine. This makes bank angle guidance laws easy to define in comparison to angle of attack guidance laws. Add to this the potential problems for cross-coupling effects and now the reference profile tracking problem becomes very complicated. Although this is a difficult control problem, multivariable control has seen huge developments in the past several decades and more and more problems are being solved by multivariable methodologies with the goal of increased performance.

The dynamic reference model becomes even more useful for implementation of a multivariable design. Rather than performing transformations to generate multiple reference commands, the dynamic reference provides any desired commands and nominal controls simply by virtue of the reference state propagation. The reference model simplifies other implementation issues as well and these are noted below.

Comparison of Reference Dynamic Model Based Guidance to Ishimoto's Algorithm

The robust abort guidance system presented in this thesis is a natural extension of Ishimoto's algorithm. Ishimoto solves for the reference command by analytic approximation as a function of range to go and energy to be dissipated [9]. The design algorithm presented here also adjusts the reference by energy management. Ishimoto's guidance algorithm also tracks two reference profiles with two control variables. The bank angle uses a nonlinear PID control law to track vehicle altitude and the angle of attack is used to track the vehicle drag. The nominal bank angle is solved by nonlinear solution of the equations of motion. Ishimoto does not present the problem in a multivariable perspective or directly address any of the potential problems associated with such an approach [9].

In the algorithm presented here, use of a reference model eliminates the need to solve for the

nominal bank angle because it has been determined as a function of energy and range to go. The reference model generates the altitude and drag commands by integrating the nominal equations of motion to the vehicle's current velocity. The use of the reference model allows for application of linearized analysis about the nominal reference model while using reference profiles and nonlinear solutions of the equations of motion makes multivariable linearized analysis difficult. Ishimoto's algorithm was fully tested in a 6DOF simulation environment and robustness results are presented in the paper, so the success and utility of the method is fully documented [9]. These results begin to justify the concept of a multivariable tracking algorithm with reference adjustment based on energy and range to go. The ideas presented in Ishimoto's paper can be viewed as a baseline for the guidance system presented in this thesis.

6.3 Multivariable Reference Dynamic Model Based Entry Guidance

The purpose of the trajectory design function is to design a dynamic reference model which propagates the nominal vehicle dynamics to reach a desired target state. Tracking the drag and altitude of the reference model guarantees that the vehicle reaches TAEM interface at the desired energy and range condition. Although the reference dynamic model was introduced in Chapter 3, the key points are reiterated here to reflect the multivariable format and the use of a closed loop trajectory design function to modify the reference model.

6.3.1 Overview and Block Diagram Representation

In section 3.4 the reference dynamic model was described. The reference dynamic model propagates the nominal vehicle dynamics subject to the nominal guidance law with a variable bank command chosen to meet range requirements. In flight, the reference dynamic model propagates in the time domain up to the current vehicle velocity (during CLAT velocity is monotonically decreasing). The reference dynamic model issues a nominal angle of attack and bank angle. The current states of the reference model become the drag and altitude commands for the tracking algorithm. The tracking algorithm perturbs the angle of attack and bank angle to drive the drag and altitude errors to zero in the presence of uncertainties and noise. Because the

vehicle velocity is matched to the reference model velocity, tracking of altitude and drag yields the desired final range and altitude targets. Large initial condition uncertainties and large disturbances are corrected by an outer loop which modifies the reference bank angle command to meet target energy and range states. The reference model and its interactions with the multivariable guidance system are presented in Figure 6.1.

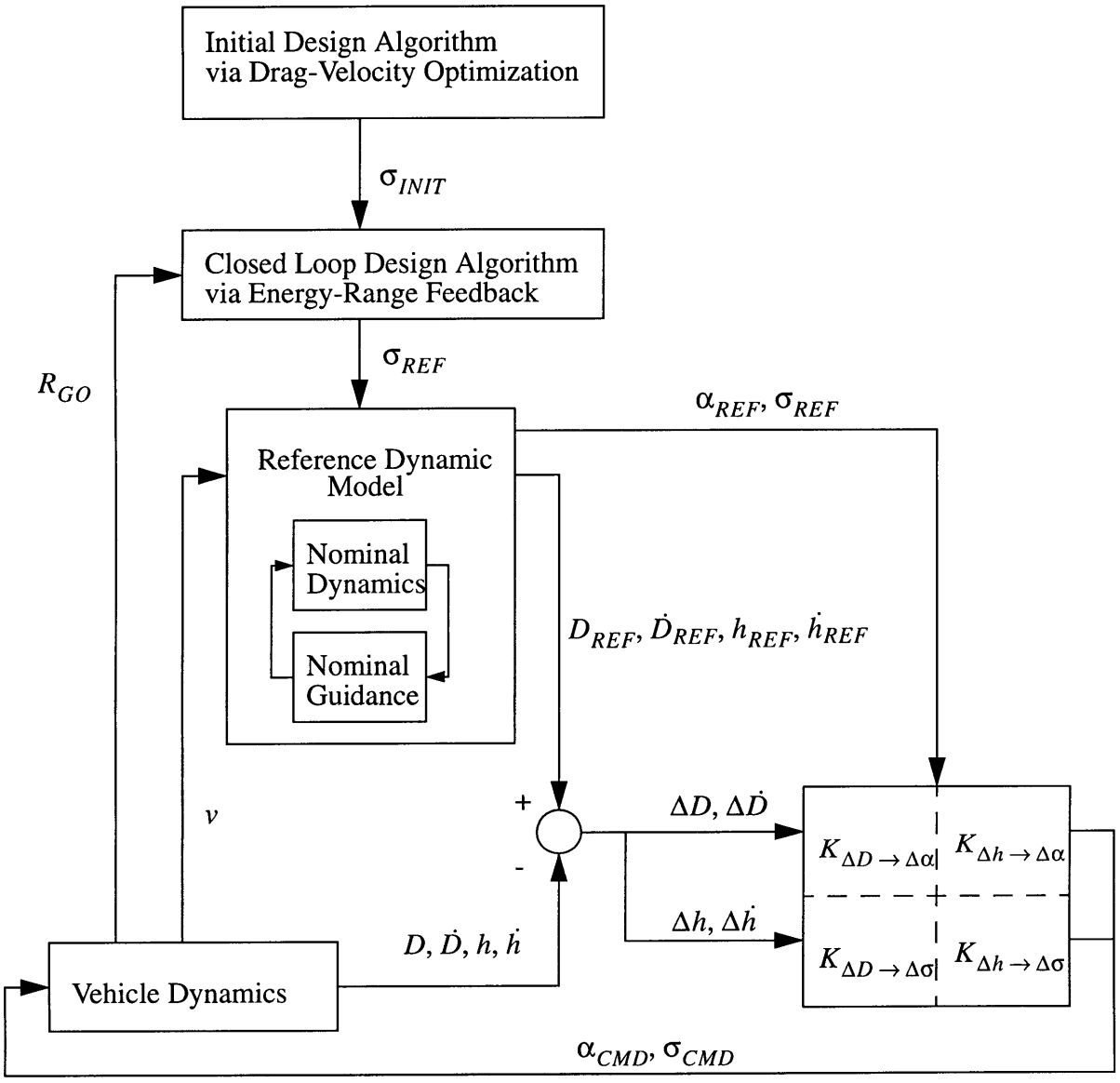

Figure 6.1 : Multivariable Reference Dynamic Model Based Guidance

6.3.2 Advantages of Reference Dynamic Model

The most important advantage of using a reference dynamic model as opposed to a reference profile is that the reference dynamic model is initialized at the start of closed loop control. Then it is propagated according to the nominal dynamics. This guarantees that control saturation only occurs when the desired profile is not physically achievable due to the uncertainties. When reference profiles are used it is difficult to define the profile to account for initial condition uncertainties. Initial condition uncertainties are very common in X-34 trajectories and the reference model eliminates this problem.

When considering the possibilities for control saturation the reference dynamic model provides an excellent framework for defining the performance robustness of a desired target site. Robustness is defined strictly by control saturation and the robustness bounds of a given candidate target site can be quickly characterized in terms of the limits provided by control saturation.

Another advantage is that during fast-dynamic maneuvers such as roll reversals it is difficult to define a realistic reference profile. The reference dynamic model is an exact representation of the fast dynamics.

From an overall strategy point of view it is easy to implement guidance commands such as the constant pitch command used during CLAT. Designing a feedback control loop to follow a guidance command is simple when only the nominal dynamics are considered. This allows for easy generation of the reference guidance commands.

6.4 Control Laws

Two tracking laws are presented here and compared and contrasted for stability and performance robustness. The first control law treats the problem as an output feedback problem. The control law assumes that the drag dynamics can be decoupled from the altitude dynamics. Because of the feedforward nature of the angle of attack control law on the vehicle drag, this is potentially a valid statement. The dynamic system between angle of attack and drag can almost be treated as a feedforward plant. Recognizing this fact, primary drag control is provided by angle of attack PID

control. A bank angle control PD law is defined for altitude tracking. By treating the problem as an output feedback problem very good robustness results are achieved.

The second control law takes on the problem using linear quadratic regulator (LQR) theory. LQR is the full state feedback control half of the H_2 (or linear quadratic gaussian - LQG) optimal control and estimation problem. H_2 optimal control seeks to minimize the mean squared error of the error states of a linear system. A summary of H_2 and LQR theory is available in [12]. The LQR has been applied to numerous control problems. An attractive feature of the LQR is that it has very good robustness properties when all states are perfectly measured. For model based guidance, the availability of a nominal reference model indicates that the LQR has potential to work very well to account for the coupling effects between drag and altitude. A time-varying LQR solution must be considered as a candidate tracking law. Unfortunately, despite the guaranteed robustness properties of the LQR, when uncertainty exists in the output and/or feedforward matrices, the LQR tracking algorithm is highly nonrobust. The results presented here show that although linearized performance measures and nominal simulations may indicate the superiority of the full state feedback LQR law, the actual nonlinear simulation results favor the output feedback approach.

6.4.1 Introductory Control Problem Definition

Before defining the individual control algorithms, the open loop dynamic system and the general framework of the control approaches must be examined. The nonlinear dynamics of interest are the altitude and the flight path angle. The drag is an output of these dynamics. Note that the vehicle velocity is always matched to the reference model velocity so the velocity dynamics are not important for the tracking problem. The nonlinear dynamic system is defined by:

$$\frac{dh}{dt} = v\sin\gamma \qquad \textbf{6.17}$$

$$\frac{d\gamma}{dt} = \left(\frac{1}{v}\right)\left(L\cos\sigma - \left(g - \frac{v^2}{r}\right)\cos\gamma\right) \qquad \textbf{2.7}$$

$$D = \frac{1}{2}\rho v^2 C_d \frac{S_a}{m} \qquad \textbf{2.2}$$

The above dynamic system has two states: altitude and flight path angle. A linearized system can

be formed by taking the first order expansion about some nominal point in the trajectory (in practice, the current reference model states). This yields a dynamic system with the following open loop block diagram:

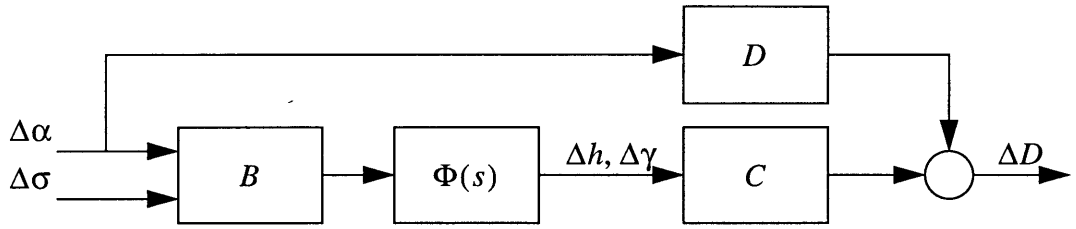

Figure 6.2 : Open Loop Block Diagram

Drag is purely an output of the altitude and flight path angle dynamic system and the above block diagram recognizes this fact. An output feedback approach recognizes this fact and the closed loop block diagram for an output feedback controller is represented by the following:

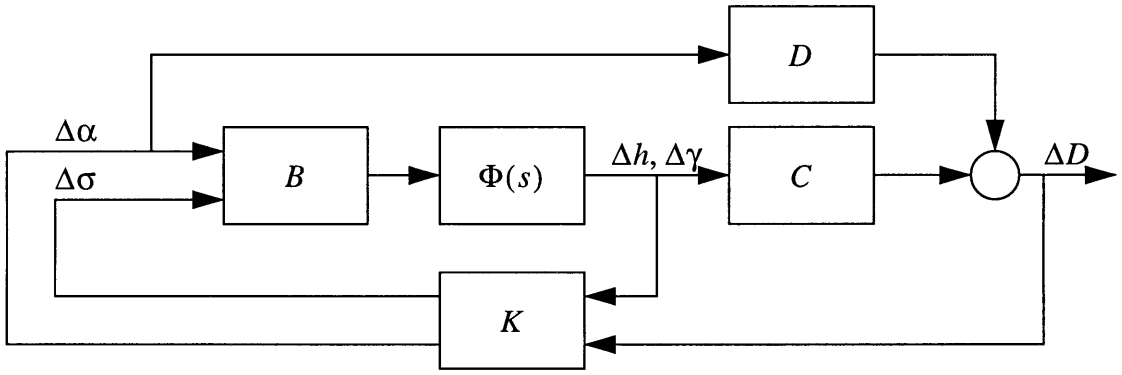

Figure 6.3 : Output Feedback Controller

A full state feedback control system feeds back altitude and flight path angle errors to meet tracking goals. LQR designs rely on full state feedback. This is problematic in dealing with uncertainties in the output matrices as there is no closed loop feedback to compensate. Examine the block diagram of a full state feedback controller with a feedforward multiplicative uncertainty. Physically this feedforward uncertainty could correspond to an error in the drag coefficient.

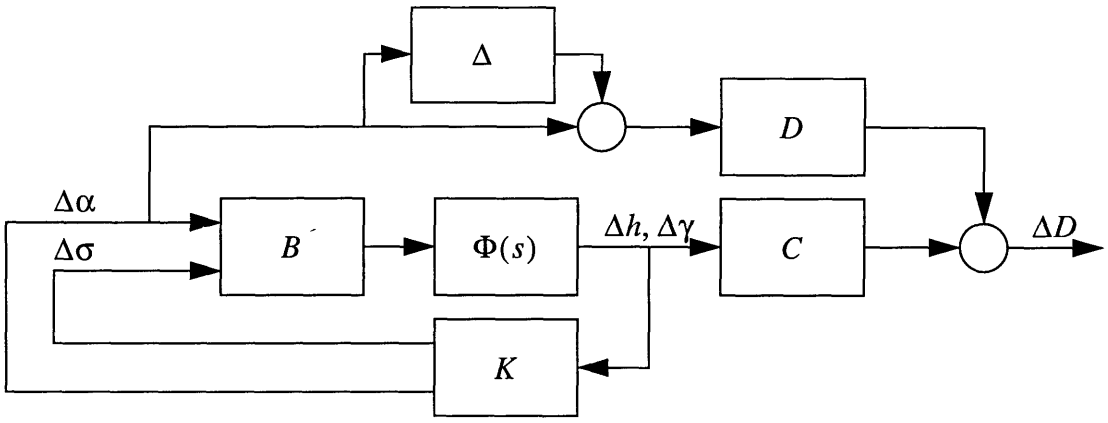

Figure 6.4 : Full State Feedback Controller

This controller will have steady state drag errors for any amount of uncertainty. The output feedback approach avoids this problem by feeding back the drag error directly. Modern control methodologies require the inclusion of any variable of interest as a state. Drag can be added as a state by augmenting the linearized drag rate dynamics. Drag rate is given by:

$$\dot{D} = -\frac{Dv}{H}\sin\gamma - \frac{2D^2}{v} - \frac{2Dg\sin\gamma}{v} \qquad \textbf{6.18}$$

The feedforward nature of the angle of attack can be recognized fairly accurately by the inclusion of the angle of attack error as a state. The angle of attack error state can only be modified by the application of a new control variable, Δu_α. The angle of attack error state is represented as the integral of the new control:

$$\Delta\dot{\alpha} = \Delta u_\alpha \quad \text{or} \quad \Delta\alpha = \int \Delta u_\alpha \qquad \textbf{6.19}$$

Although this does not agree perfectly with the nonlinear dynamic system it is actually slightly more realistic. The actual modification of the angle of attack is carried out by a flight control system to adjust the vehicle's control surfaces to meet the commanded angle of attack. The result is that in reality the effects of a control change are not feedforward. Rather there is a short time delay as the flight control system carries out the command. So the inclusion of the angle of attack as an error state modified by an integrated control is reasonable. In addition, integrating the angle of attack error state adds an integral to the control loop which is useful in increasing the loop gain at low frequencies and improving steady state error.

With the addition of the drag and angle of attack errors as states, full state feedback designs can theoretically provide perfect tracking:

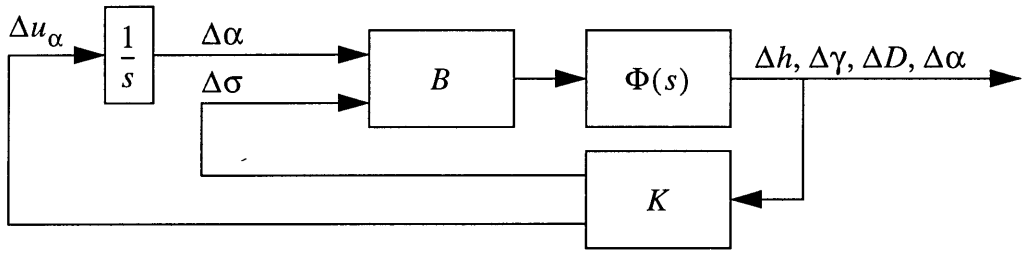

Figure 6.5 : Full State Feedback Control (Drag, Angle of Attack States Included)

The output feedback system can also be represented by augmenting the angle of attack and/or drag error states. Through linearization the control approaches are all interchangeable in the nominal case. In off-nominal scenarios the combination of states used for design becomes very important.

6.4.2 Output Feedback Approach

The output feedback approach presented here relies on separation of the drag-angle of attack system from the altitude-bank system. The output feedback control system with the angle of attack included as an error state is shown below:

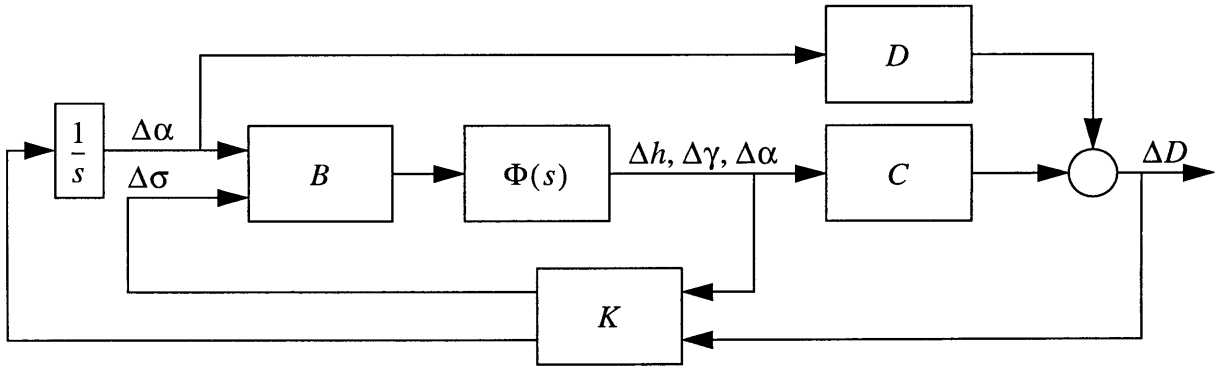

Figure 6.6 : Output Feedback Controller with Integrated Angle of Attack Control

This design framework provides robustness to uncertainties at any point in the loop without reliance on the accuracy of the linearized model. The control matrix, K, is defined by recognizing the most important properties of the dynamic system.

The angle of attack has a feedforward effect on the vehicle drag through the drag coefficient.

Vehicle drag can also be modified by adjusting the vehicle altitude (lower altitude = higher drag and vice versa). Changing the angle of attack also changes the lift coefficient. The vertical component of lift can also be modified by adjusting the bank angle. Without closed loop control the vehicle drag is completely governed by altitude control. However, angle of attack's feedforward effect on the drag can be used to separate the drag system from the altitude system. Examining the following singular value plots reveals some information to back this up. This frequency response represents the linearized dynamics from a point in the nominal trajectory during CLAT when the vehicle is in smooth equilibrium flight. The minimum singular value represents the gain from the controls to drag. The maximum singular value represents the gain from the controls to altitude. The singular values both with and without angle of attack integration are included.

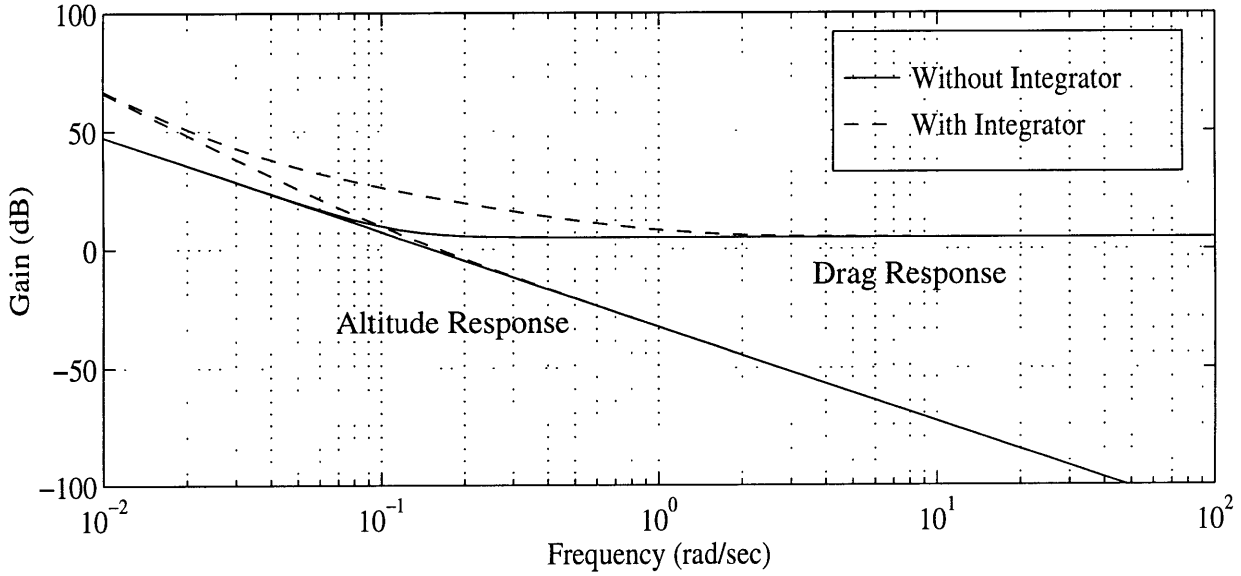

Figure 6.7 : Open loop frequency response with and without angle of attack integrator

The open loop frequency response of the system without integrators characterizes the system. At low frequencies the drag and altitude responses are perfectly coupled. At higher frequencies the feedforward effects of angle of attack on drag are evident. The high frequency feedforward effect indicates the potential to separate the altitude and drag responses. Integrating the angle of attack begins to separate the dynamics. The loop gain is increased at low frequencies. This will help drive steady state error to zero. The main advantage gained by integrating the angle of attack is that the altitude and drag responses are separated at lower frequencies than the system without integrated angle of attack.

Recognizing the feedforward nature of the drag response to angle of attack and the relatively inflexible nature of the dynamic system governing the altitude response is critical for design of a good tracking system. The output feedback tracking law is defined by two control laws. The angle of attack control law is simply chosen to guarantee that the gain magnitudes are much smaller than the feedforward gain magnitude, $\partial D/\partial\alpha$. It is also designed to given a smooth damped response. Some iteration was used to fine tune the control law.

$$\Delta u_\alpha = 0.2\Delta D + 0.7\Delta\dot{D} \qquad \textbf{6.20}$$

The drag command is issued from the reference model. The vehicle drag is measured as a function of the accelerations sensed by the inertial measurement unit (IMU). Drag rate is commanded and measured by the following equation (ignoring effects of velocity on C_D):

$$\Delta\dot{D} = -\frac{Dv}{H}\sin\gamma - \frac{2D^2}{v} - \frac{2Dg\sin\gamma}{v} \qquad \textbf{6.21}$$

The bank angle control law is actually formulated as a lift control law which is then transformed to a bank angle command. The desired response has a period of 90 seconds with critical damping. Shuttle entry guidance uses a period of 90 seconds for the bank to drag desired dynamics [14]. The bank angle control law is given by the following set of equations:

$$\Delta L = \omega_n^2\Delta h + 2\zeta\omega_n\Delta\dot{h} \qquad \textbf{6.22}$$

$$L_{Temp} = \left(\frac{L}{D}\right)_{ref} D_{ref}\cos\sigma_{ref} \qquad \textbf{6.23}$$

$$\sigma_{CMD} = \text{acos}(L_{Temp} + \Delta L) \qquad \textbf{6.24}$$

The closed loop system can be examined in the frequency domain to get a sense of the controller properties. The system and control law are linearized about the same nominal point to get an idea of the steady state properties. The first transfer function matrix to be considered is the loop transfer function, given by $T_L(s) = K\Phi(s)B$. Note that K in this case represents the linearized approximation of the control law and includes the output matrix. Figure 6.8 below shows the basic loop block diagram. The loop transfer function represents control to control gains (from 1 to 2). Two other transfer functions of interest are the sensitivity and complementary sensitivity

transfer function matrices. The sensitivity transfer function matrix is given by $T_S(s) = (I + T_L(s))^{-1}$ and the complementary sensitivity by $T_C(s) = T_L(s)(I + T_L(s))^{-1}$. The singular values of the sensitivity transfer function represent state to state disturbance rejection properties (from 2 to 2). The complementary sensitivity transfer function singular values characterize command following properties (from Δu_{ref} to 2) and noise response properties.

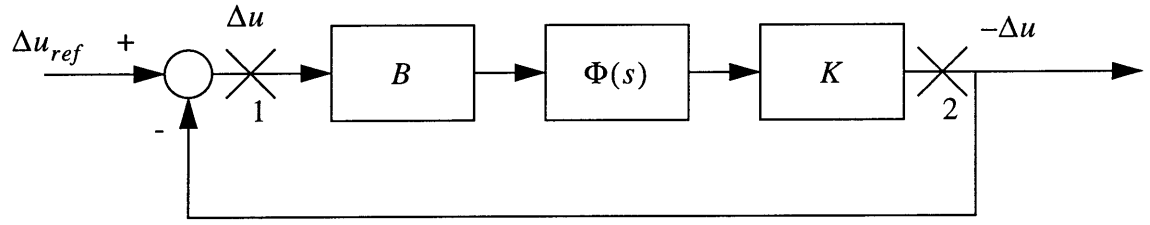

Figure 6.8 : Transfer Function Relationships

The singular values of the loop transfer function representing control to control gains are shown in figure 6.9 below.

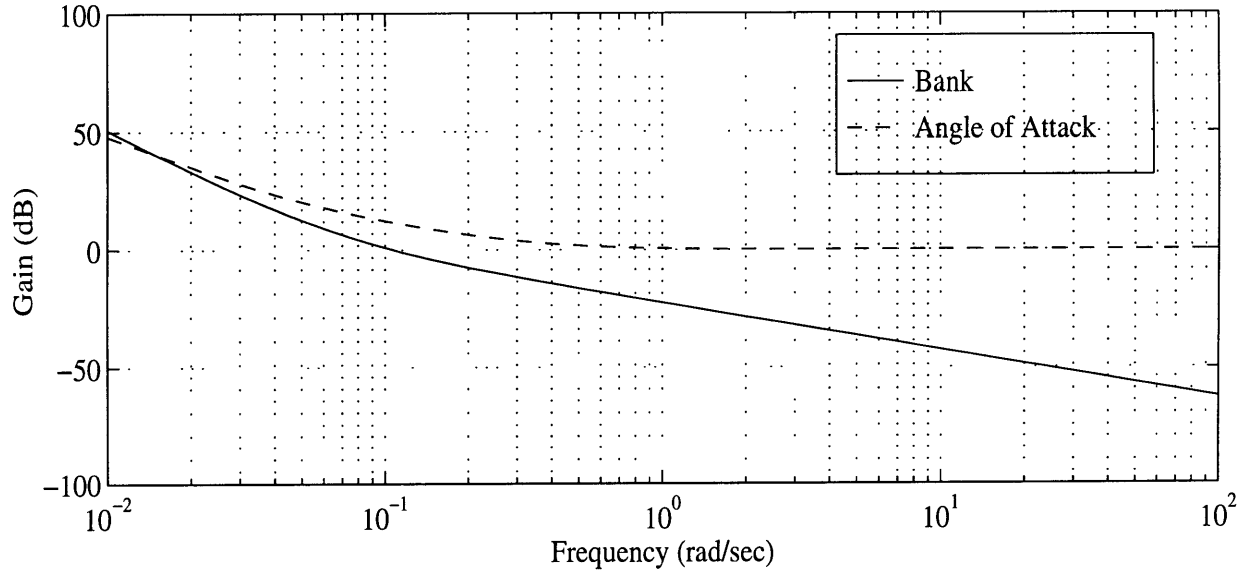

Figure 6.9 : Output Feedback Loop Transfer Function Singular Values

The singular values show that the responses are separated. The angle of attack system is faster than the bank angle system. For the output feedback compensator, the angle of attack system characterizes the drag response while the bank angle system characterizes the altitude response. The loop gains are high at low frequencies to drive steady state errors to zero. The bank angle control law treats the angle of attack effects on altitude as a disturbance. In practice, this control

law quickly reacts to drag errors with angle of attack control to reach a steady state and then the altitude errors are slowly corrected using the bank angle.

The sensitivity transfer function singular values representing state disturbance to state error gains are shown here:

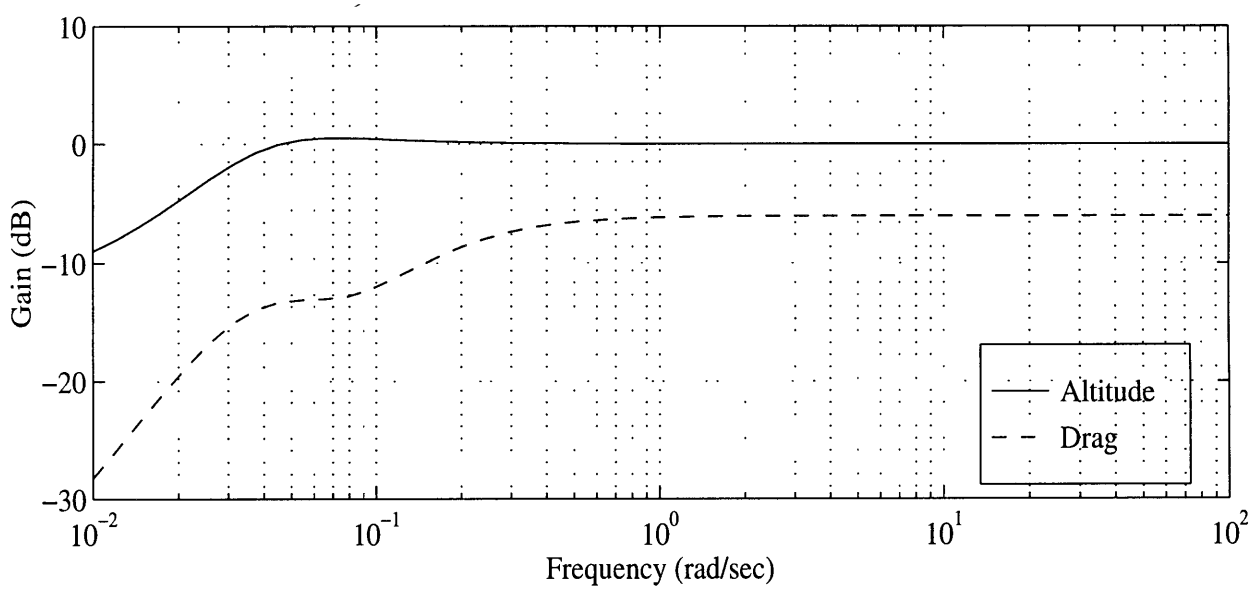

Figure 6.10 : Output Feedback Sensitivity Transfer Function Singular Values

The singular values indicate good disturbance rejection properties at low frequencies for drag. The altitude response singular value indicates that steady state errors will be present as some amplification of disturbances occurs at low frequencies. Although this is undesirable, the design is intended to focus on minimizing drag errors primarily. Some steady state altitude error is acceptable but small steady state drag errors can lead to large range errors.

Now examine the complementary sensitivity transfer function singular values:

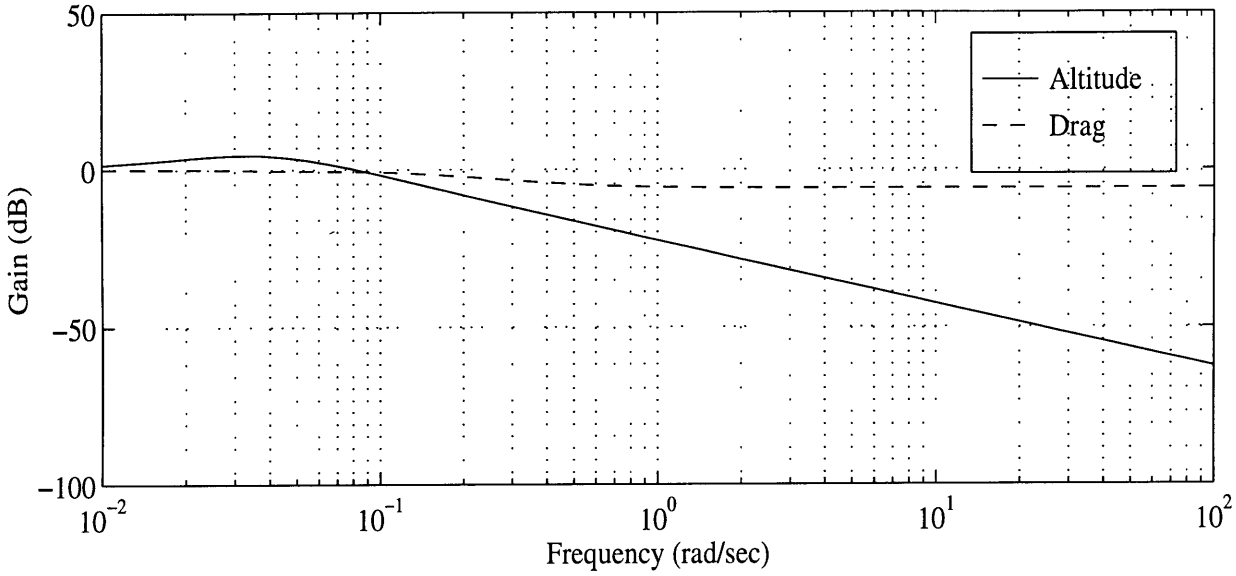

Figure 6.11 : Output Feedback Complementary Sensitivity Transfer Function Singular Values

The complementary sensitivity singular values reinforce that the dynamics have been separated. Steady state drag error is zero and high frequency noise is attenuated. Noise attenuation is not as good for the drag response due to the feedforward term. In practice, filtering the drag estimate prevents high frequency changes in the drag measurement. In turn this prevents high frequency control action. Again steady state altitude errors are indicated but the magnitudes are small enough to be acceptable.

The output feedback compensator recognizes the ability to shape the angle of attack to drag system response in any manner. Drag errors are recognized as more important than altitude errors (recall that range errors are the integral of the drag errors). The drag dynamics are successfully separated from the altitude dynamics and the drag response is faster than the altitude response. Most importantly, implementation of the output feedback compensator recognizes that drag is purely an output of the altitude, flight path angle, and angle of attack dynamic system. Actual measured drag errors are fed back and there is no reliance on accuracy of the dynamic model. All of these factors ensure that steady state tracking performance is maximized in the presence of uncertainty.

6.4.3 LQR Approach

The linear quadratic regulator is a full state feedback controller. It assumes that all states are perfectly measurable or that an accurate estimate is available. Figure 6.5 is included again to show the block diagram representation of the linearized model used to derive an LQR based guidance algorithm. Angle of attack and drag are included as states. The control on angle of attack is integrated for the same reasons as in the output feedback design (higher loop gain at low frequencies to guarantee zero steady state error and to help separate the drag and altitude dynamics).

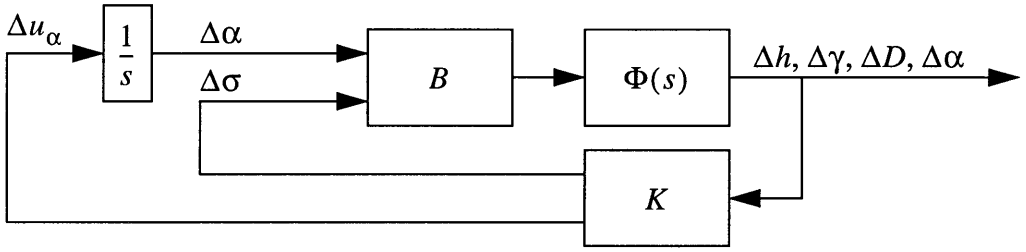

Figure 6.5 : Full State Feedback Control (Drag, Angle of Attack States Included)

The LQR solution methodology selects the gain matrix K to minimize the mean squared error of the performance variable and control perturbations. The performance variable is defined as a weighted output vector:

$$\Delta z = C_{LQ}\Delta x + D_{LQ}\Delta u = \begin{bmatrix} k_D & 0 & 0 & 0 \\ 0 & k_h & 0 & 0 \end{bmatrix} \begin{bmatrix} \Delta D \\ \Delta h \\ \Delta\gamma \\ \Delta\alpha \end{bmatrix} + \begin{bmatrix} k_{D\sigma} & k_{D\alpha} \\ k_{h\sigma} & k_{h\alpha} \end{bmatrix} \begin{bmatrix} \Delta\sigma \\ \Delta\alpha \end{bmatrix} \qquad \textbf{6.25}$$

The cost function is defined as:

$$J_{LQ} = \int (\Delta z^T \Delta z + \Delta u^T R_{LQ} \Delta u) dt \qquad \textbf{6.26}$$

$$J_{LQ} = \int (\Delta x^T C_{LQ}^T C_{LQ} \Delta x + 2\Delta x^T C_{LQ}^T D_{LQ} \Delta u + \Delta u^T (R_{LQ} + D_{LQ}^T D_{LQ}) \Delta u) dt \qquad \textbf{6.27}$$

The R_{LQ} and C_{LQ} matrices are used to define the cost function as a quadratic combination of state and control perturbations. The D_{LQ} matrix allows for the inclusion of cross weights between the states and controls. State weights penalize state errors. Control weights penalize control

application. Cross weights penalize the use of a control to influence a state. A good summary of weighting methods, including frequency dependent weights and cross state and control weights, can be found in [1]. For guidance system design the weights should be kept as simple as possible because the LQR solution relies on the accuracy of the current linearized model and introduction of complicated weights could create undesirable responses for a time-varying solution. The control weights are of the form:

$$R_{LQ} = \rho \begin{bmatrix} k_\alpha^2 & 0 \\ 0 & k_\sigma^2 \end{bmatrix} \qquad \textbf{6.28}$$

The most basic LQR approach uses no cross weights. Without crossweights the cost function has the form:

$$J_{LQ} = \int [k_D^2 \Delta D^2 + k_h^2 \Delta h^2 + \rho (k_\alpha^2 \Delta u_\alpha^2 + k_\sigma^2 \Delta \sigma^2)] dt \qquad \textbf{6.29}$$

Selection of weights is the most important part of the LQR design process. By adjusting the state and control weights the singular values can be shaped to meet the desired system response characteristics. Recognizing that the output feedback singular value responses are a good representation of the design goals, the LQR weights can be used to shape the singular values for a nominal point to be similar to the output feedback solution. The compensator should primarily reject drag errors using angle of attack and altitude errors using bank angle.

The LQR solution is only valid for a single nominal point along a trajectory but a time varying LQR solution is easily implemented by relinearizing at each guidance step and solving for new control gains. Time varying solutions and point solutions with many weighting strategies were implemented in an attempt to successfully define a compensator. The end result is that the most successful LQR designs were shaped in the frequency domain to match identically the output feedback singular values. However, nonlinear performance of all designs was unacceptable in off nominal cases. Uncertainties in the output or feedforward matrices created steady state errors. In general the LQR designs used too much angle of attack control to reject altitude rate errors. Even by applying heavy cross weights the LQR solutions still used a minimal amount of control to guarantee the optimum mean squared error. Attempts were made to optimize the control weights to minimize the angle of attack gain on altitude rate but always a minimum control application

was necessary.

As an interesting aside note, the most successful LQR solutions were actually not optimal LQR solutions at all. By removing the terms in the linearized dynamics which told the LQR solution that the angle of attack influenced the flight path angle, the LQR solution did not use angle of attack to control altitude rate. This is a theoretically unsound approach. However, this approach yielded stable time varying LQR solutions. Steady state errors were still present in the face of uncertainty but at least stable solutions were achieved. The author does not know of such an approach for control and would not recommend the practice. LQR solutions work best when full knowledge of the dynamics are present and removing this knowledge does not appear to be an acceptable approach.

The next section compares the LQR solution to the output feedback solution. A time varying LQR is designed which matches the output feedback exactly in the frequency domain when only linearized dynamics are considered. Despite the good appearances, the LQR solutions have steady state error and the use of angle of attack to control altitude rate causes undesirable control transients.

6.5 Tracking Performance Robustness Comparisons

Two tracking algorithms for reference model tracking are compared here. An output feedback compensator, and a time varying LQR solution are compared for tracking performance in the presence of parametric uncertainties. Linearized about nominal points along the trajectory, the approaches are identical when viewed in the frequency domain. In actual nonlinear simulations, the LQR solution breaks down. The reliance of the LQR solution on the accuracy of the linearized model and the inability to account for uncertainty in the output and feedforward matrices makes the LQR solution nonrobust. With no parametric uncertainties, the output feedback and time varying LQR solutions provide excellent performance. In the presence of uncertainty, the output feedback approach is superior.

6.5.1 Linearized Comparison

The tracking algorithms can be compared in the frequency domain at different nominal linearized points. The output feedback algorithm is approximated as a full state feedback algorithm for ease of comparison to the LQR solution. The time varying LQR solution computes new gains based on the current nominal point. The weights for the time varying solution are constant. Frequency domain characteristics are compared for three different nominal points along a sample trajectory. The sample trajectory requires a constant bank command of 50 degrees. The state is linearized at 5500 ft/sec, 4500 ft/sec, and 3500 ft/sec and the frequency domain properties are compared.

Figure 6.12 compares the loop gain, sensitivity, and complementary sensitivity for both controllers at the three different nominal points. The frequency domain properties are nearly identical at all points. In fact, the LQR solution indicates better performance for some characteristics. The steady state error of the altitude response and the altitude disturbance rejection properties are improved. These results indicate that the LQR solution provides excellent nominal convergence properties.

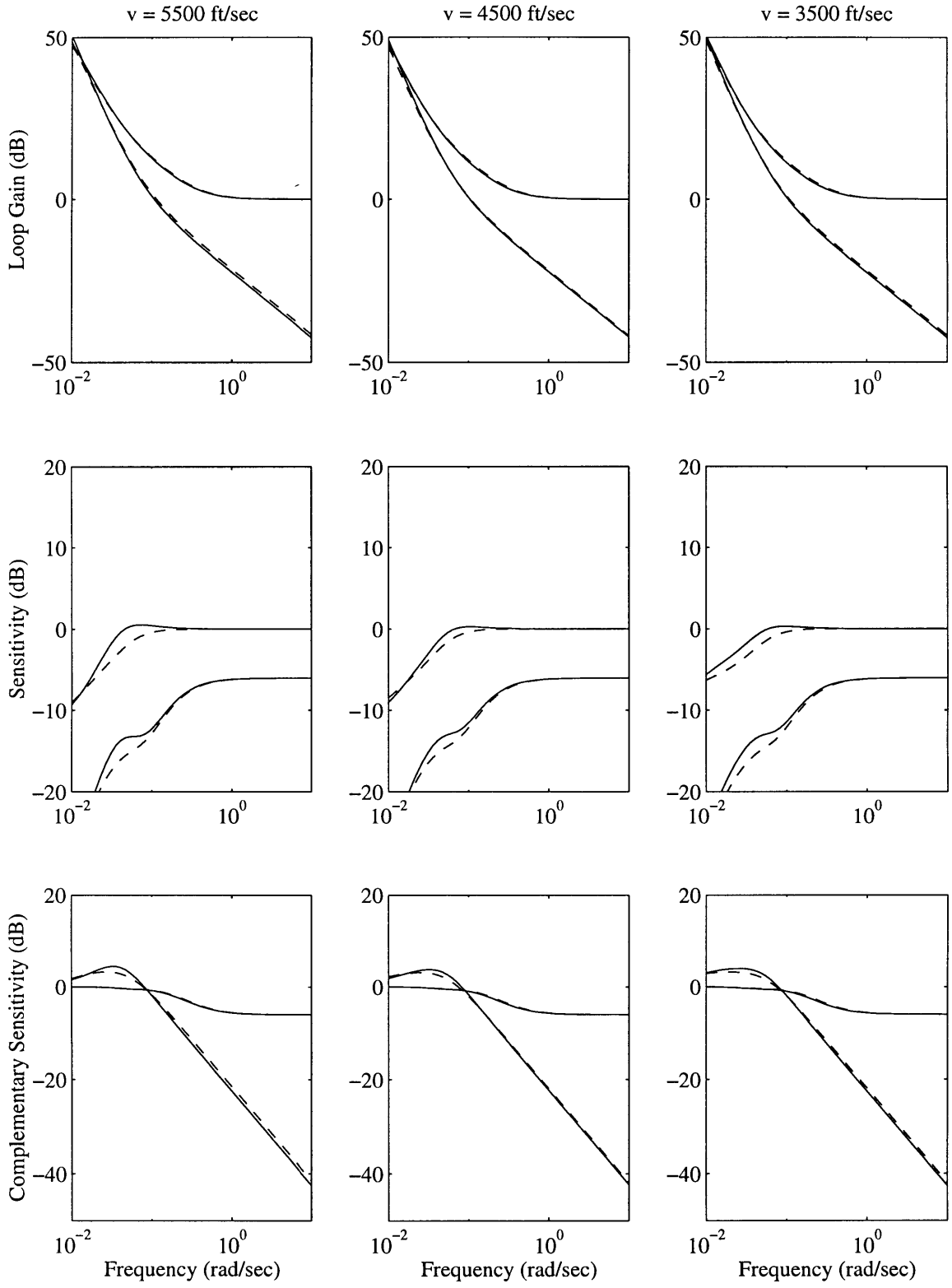

Figure 6.12 : Frequency Domain Comparison ('-' Output Feedback, '--' LQR)

Unfortunately, the compensator must be able to handle off nominal conditions. Although linearized analysis is useful, only conclusions about nominal performance can be drawn. To evaluate actual controller performance, simulations which integrate the nonlinear point mass equations of motion are used.

6.5.2 Nonlinear Simulation Results

To evaluate controller performance the equations of motion defined by 2.2-2.7 are integrated in the matlab simulation environment. The results presented here represent complete implementation of the guidance system, including reference model propagation and energy-range based redesign of the reference bank angle command. The overall performance results are not shown but the drag and altitude errors and bank angle and angle of attack error commands are included. The trajectory shown for all cases requires a $50°$ reference bank angle initially and this reference bank angle is redesigned throughout the trajectory to meet energy and range requirements. In addition there is a high cross range requirement. Test cases include the nominal case, lift and drag coefficient constant biases, and a constant density bias. The test cases shown only include positive biases but the effects of a negative bias are easily inferred as in all cases the control and state error effects are simply the negative of the errors shown.

Nominal Tracking

In the nominal case, both the output feedback compensator and the time varying LQR solution provide good tracking. This is expected because in this case the LQR solution has perfect knowledge of the plant dynamics and computes the optimal gains to minimize the state and control errors. Figure 6.13 below shows the state and control errors for a nominal trajectory. Drag error is driven to zero by both compensators and altitude error is effectively zero. Control application is minimal (as it should be because the plant dynamics are perfectly known). An initial transient is present due to small initialization errors at the start of closed loop tracking of the reference model. This transient is very short and not important as the controllers quickly converge to the correct steady state condition.

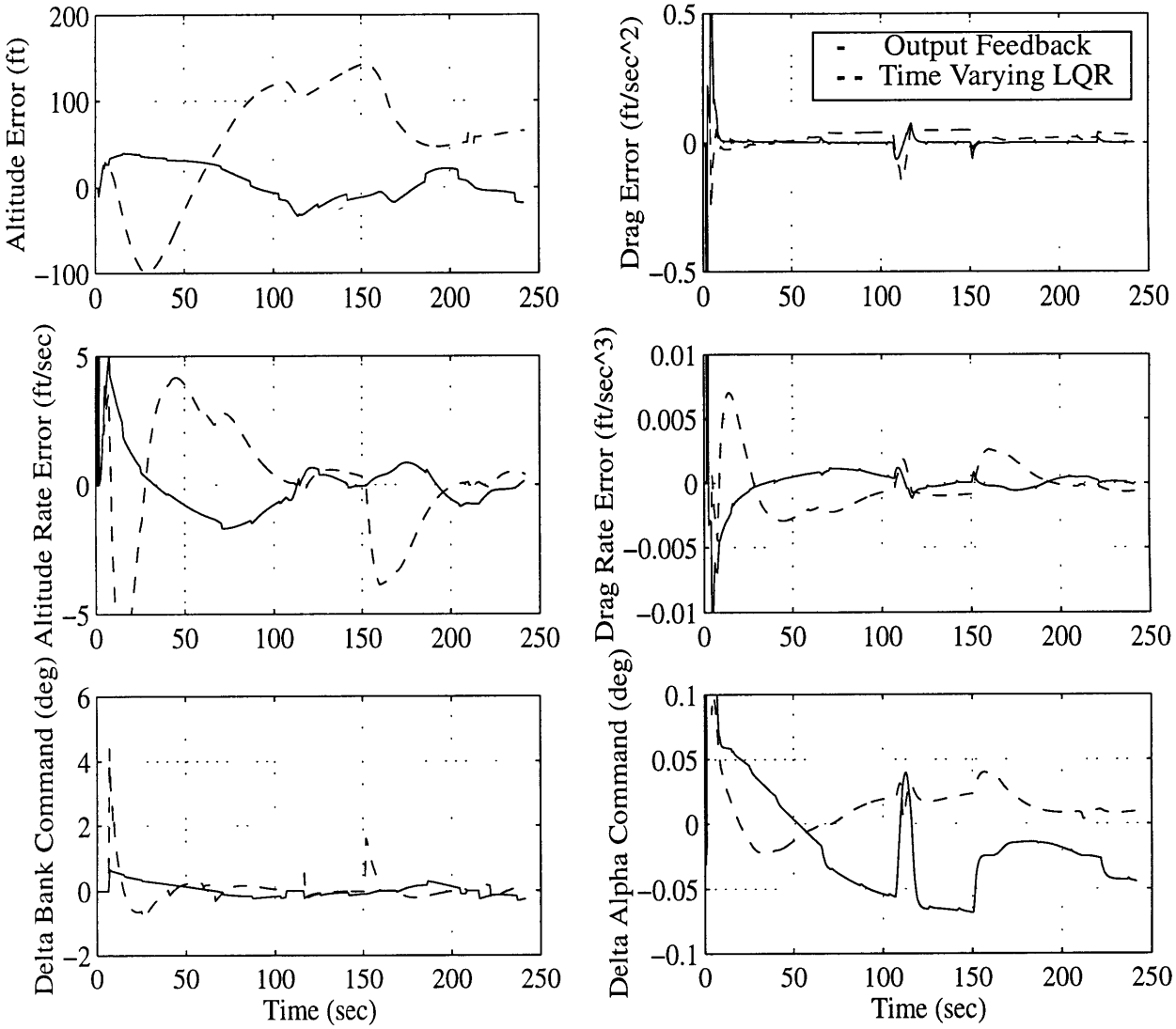

Figure 6.13 : State and control errors with no uncertainty

Drag Coefficient Bias

Now a constant +10% C_D bias is applied to the simulation. This corresponds to a reduction in vehicle *L/D*. A C_D bias is a feedforward uncertainty and it is expected that the LQR solution will have difficulty handling this uncertainty. The LQR solution has large steady state errors due to the feedforward uncertainty. The output feedback solution successfully drives the state errors to zero because the uncertainty is fed back directly. Figure 6.14 summarizes the state and control errors for this case.

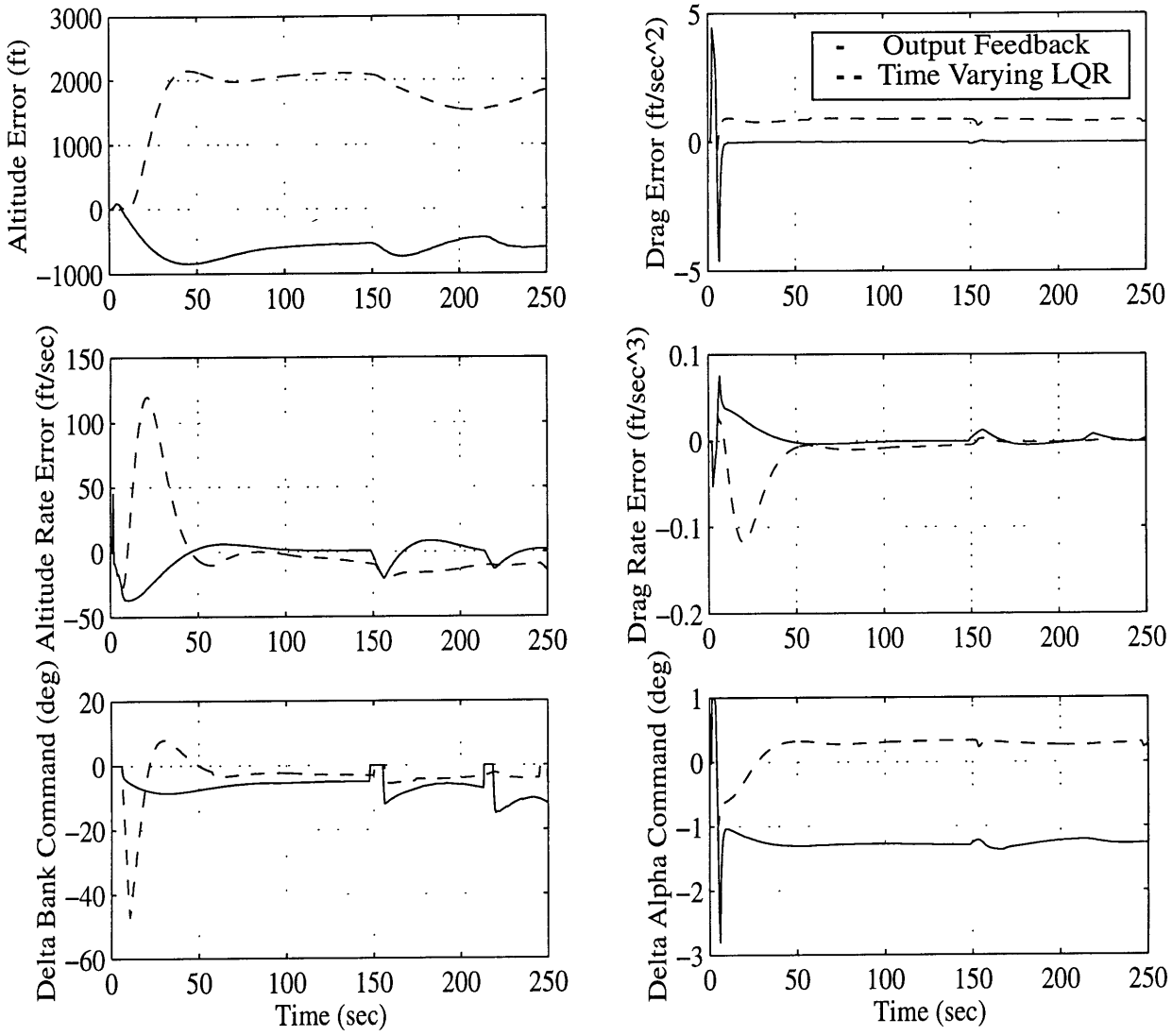

Figure 6.14 : State and control errors with +10% C_D bias

Note that the output feedback solution has steady state altitude error as predicted by the linearized frequency response. Because the drag error is driven to zero by the output feedback solution the altitude error is acceptable. However the LQR solution has both steady state altitude and drag errors. The steady state drag error of approximately 1.0 ft/sec^2 corresponds almost exactly to a 10% increase in the drag coefficient. This provides empirical evidence that the feedforward nature of the uncertainty makes the state feedback based LQR solution nonrobust.

Lift Coefficient Bias

A +10% C_L bias is applied to the simulation which causes an increase in vehicle *L/D*. In this case, both the LQR solution and the output feedback solution provide excellent tracking of the reference. Both compensators drive the drag error to zero and have acceptable levels of steady state altitude errors (as predicted by the frequency response). Figure 6.15 below summarizes the errors.

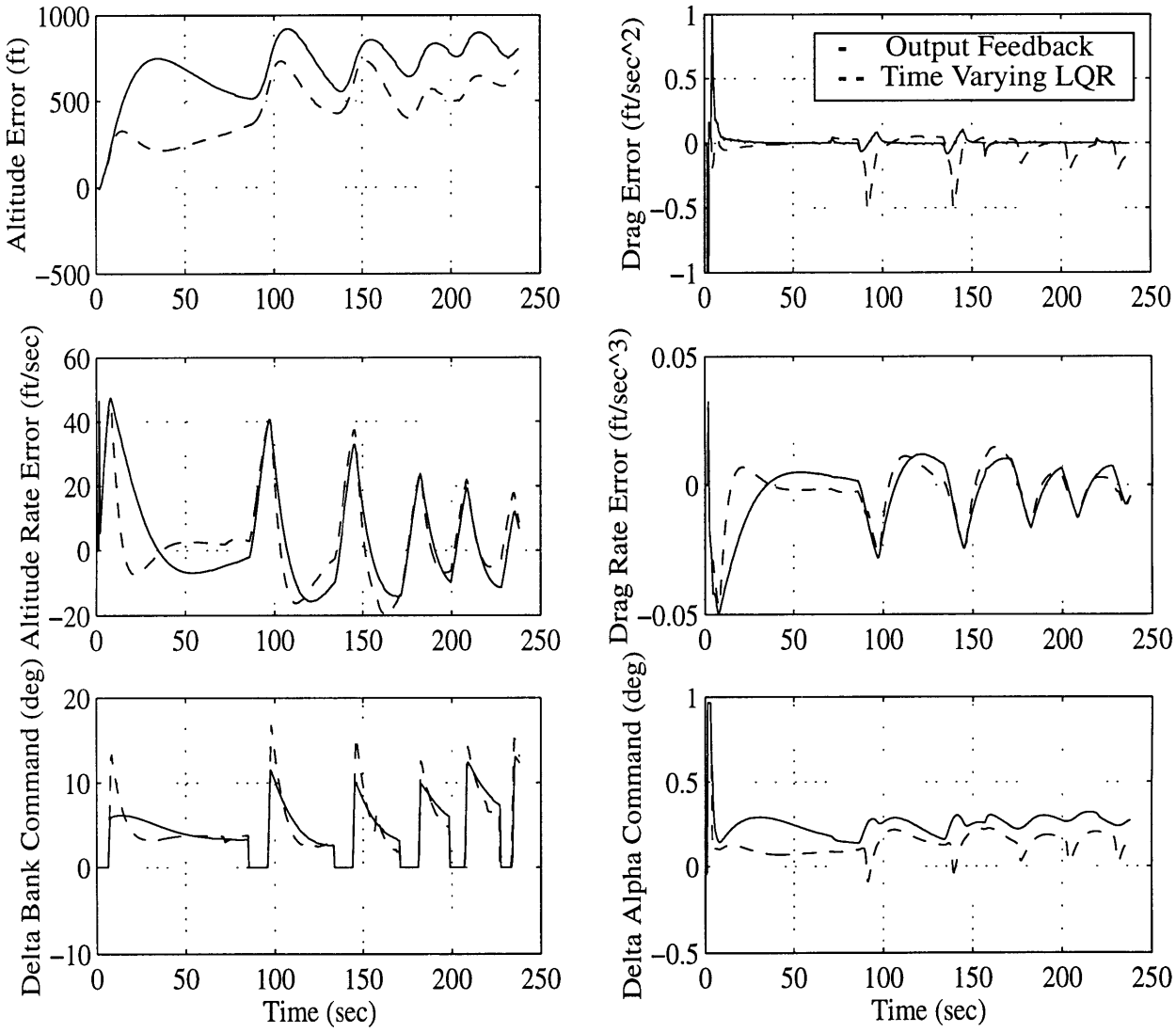

Figure 6.15 : State and control errors with +10% C_L bias

The "bumps" in the altitude and altitude rate tracking trajectory are due to roll reversals. This provides empirical evidence that the sensitivity of the flight path angle error state to parametric uncertainty is very high. Roll reversals also create a problem for drag tracking for the LQR

solution. The LQR solution attempts to null flight path angle errors using angle of attack control. This creates drag error transients during the roll reversals. The output feedback solution does not use any angle of attack to control flight path angle errors so these transients are not present. Again this provides evidence of the LQR solution's difficulty in dealing with feedforward control effects. Further evidence is found by noting that a lift coefficient bias is not a feedforward uncertainty in terms of drag tracking. Thus the LQR solution is expected to have good drag tracking properties and as evidenced above it does have this property.

An important fact concerning system robustness should be noted here. Primary rejection of a lift coefficient uncertainty is accomplished using bank angle to modulate the lift (*L/D*) and maintain good tracking. Rejection of drag coefficient uncertainties is accomplished by both angle of attack and bank angle control. This fact is important because the lift coefficient uncertainty can be viewed as a worst case scenario for performance robustness defined by bank angle saturation. The worst case *L/D* uncertainty can be defined explicitly in terms of bank angle difference from the reference to achieve saturation. This is useful for defining the robustness of a given target site.

Density Bias

The results for a +25% density bias are presented in figure 6.16. Density uncertainty is an output uncertainty in terms of drag tracking. The LQR solution results in large steady state drag and altitude errors. The output feedback solution successfully nulls both the drag and altitude errors. This test case provides further evidence of the LQR solution's difficulty in handling an output feedback problem where uncertainties in the output and feedforward terms are present.

In terms of performance robustness it should be noted that the output feedback solution uses primarily angle of attack control to null the density uncertainty. This allows density variation robustness to be defined in terms of angle of attack control saturation. Again this is a useful result for site selection.

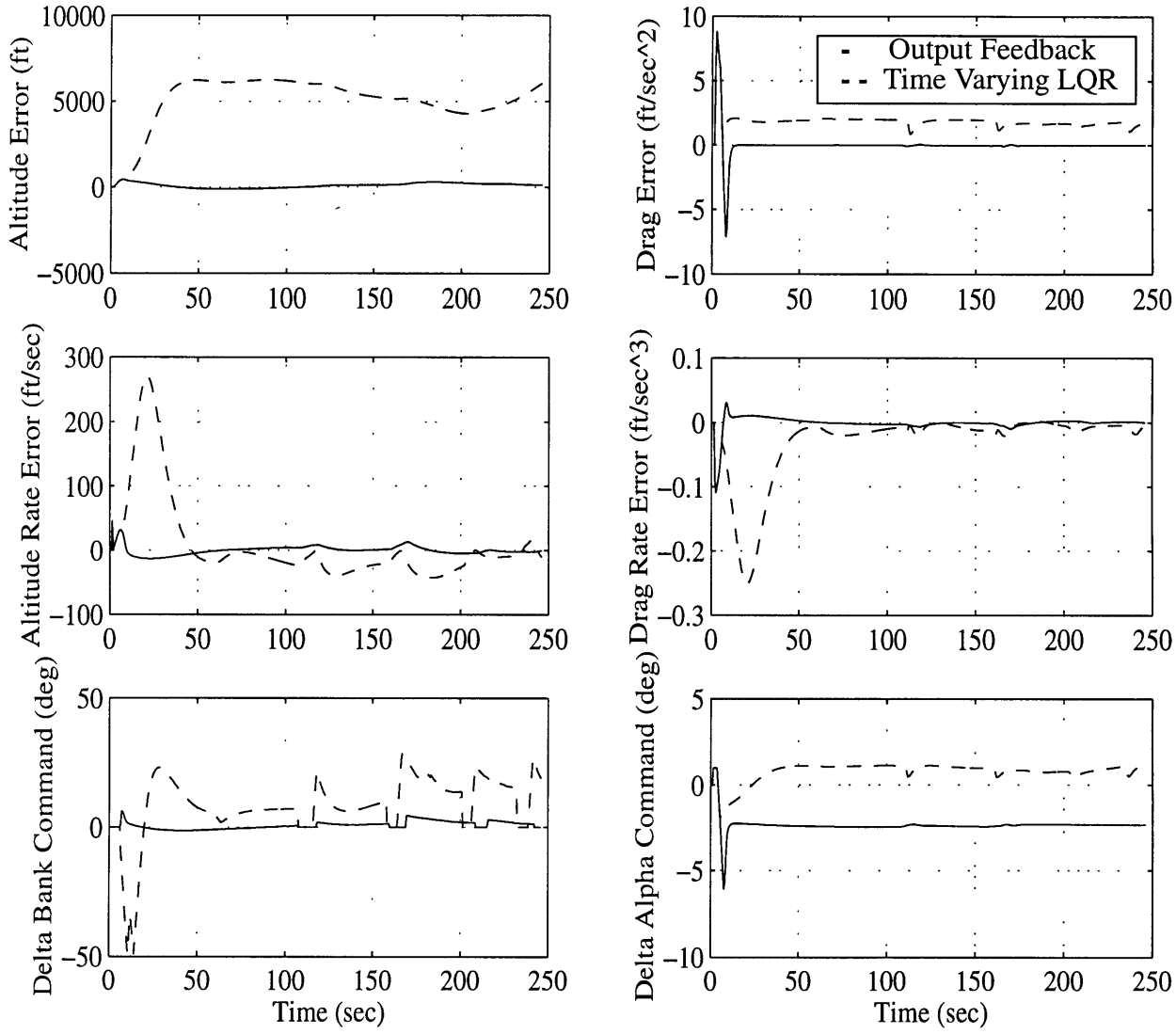

Figure 6.16 : State and control errors with +25% Density Bias

6.5.3 Tracking Algorithm Performance Summary

The output feedback and LQR solutions are both excellent in the nominal case. However the output feedback solution is far more robust. This is because the state feedback based LQR solution is not capable of effectively rejecting output and feedforward uncertainties. The output feedback compensator recognizes the nature of the drag and altitude tracking problem and is designed to effectively reject a wide class of uncertainties. Further, the output feedback compensator provides a simple and intuitive algorithm for reference model tracking.

Chapter 7

Performance Robustness Analysis

Algorithm performance robustness is verified through application of multiple uncertainties. Initial analysis focuses on two example cases. Both cases require a similar reference bank angle command but one has a high crossrange requirement and the other has no crossrange requirement. The effects of control saturation are analyzed and shown to be the driving force in limiting vehicle performance. Conservatism of vehicle footprint definition to provide robustness is addressed. A systematic method of defining target site robustness in the context of a reference dynamic model is presented. Results for multiple abort scenarios and parametric uncertainties verify system performance.

7.1 Nominal Performance Results

System performance with no uncertainty is relatively simple to verify. Because the dynamics are perfectly represented by the design algorithm, no tracking algorithm or redesign algorithm is actually necessary. Two example entry trajectories serve as a starting point for discussing performance robustness as a function of control saturation. Both cases are for a "full burn" (i.e. the engine does not fail and maximum velocity is achieved). Note that this is not representative of a true abort scenario. However, each example has a different landing site target: one with a high crossrange and the other with no crossrange. The comparison is presented because of the effects of target site crossrange on performance robustness and to introduce the general format used to define an abort scenario.

7.1.1 High Crossrange Example

The high crossrange example nominal performance is presented in figure 7.1. The landing site is at a downrange of 2.35 x 10^6 feet and a crossrange of 450000 feet. From now on, site targets are written as (2.35 x 10^6, 450000). Note that this point is not the actual TAEM interface target. The TAEM interface target is defined by a final range to go while heading towards the target.

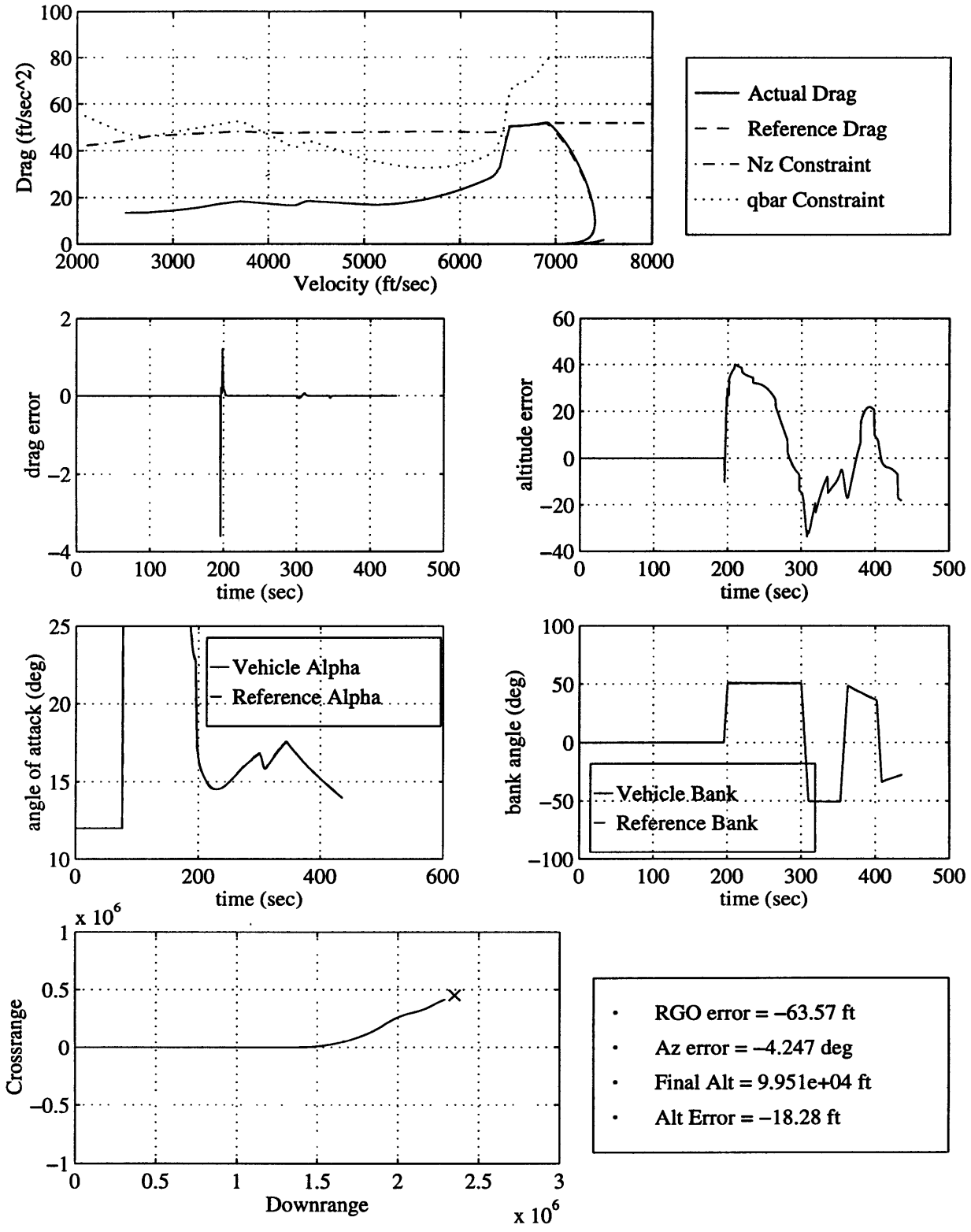

Figure 7.1 : High Cross Range Example

The TAEM interface range to go target is arbitrarily defined as 70000 feet. The actual value of the range to go target is irrelevant as the design and tracking algorithm can accommodate any range to go target within the bounds of control saturation.

The first plot in figure 7.1 shows the drag vs. velocity trajectories of the reference model and the actual vehicle. The drag-velocity trajectory and state space is useful in representing vehicle state constraints [8]. The drag-velocity representation above shows that no state constraint violations occur. The next plots present drag and altitude tracking errors and the actual and reference vehicle controls used to achieve tracking. The final plot illustrates the downrange and crossrange ground track. The trajectory above shows that the vehicle achieves the range to go target and that little control perturbation from the reference is necessary to track the model. Guidance nulls the crossrange error by executing roll reversals to keep the vehicle within the azimuth deadband.

7.1.2 Zero Crossrange Example

The second example uses a landing site target of (2.45×10^6, 0.0). Figure 7.2 illustrates nominal guidance system performance. Good tracking is again evident and the vehicle meets the final range and altitude targets. Again the tracking law applies only small control perturbations to null tracking errors because no uncertainties are present. There are no state constraint violations.

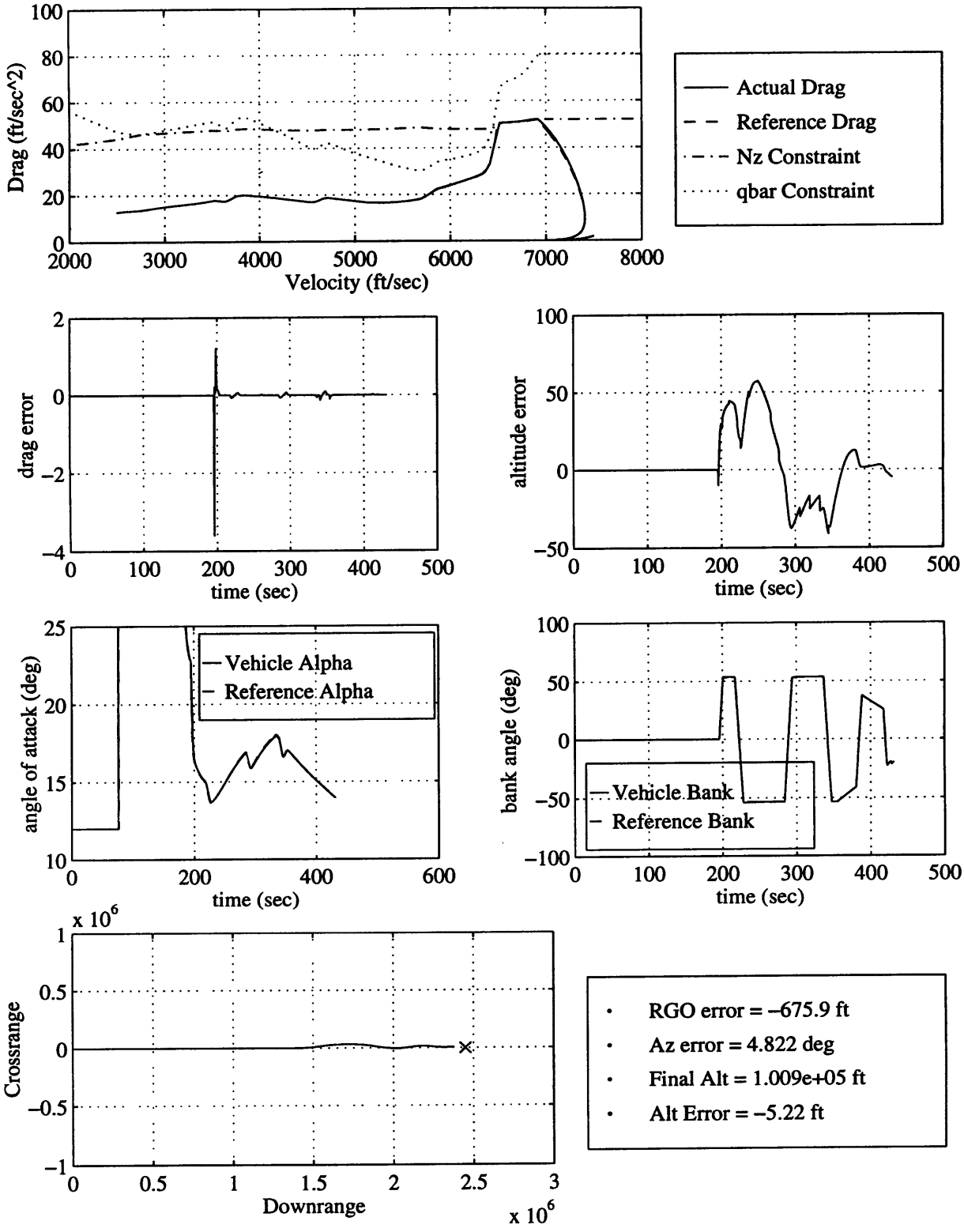

Figure 7.2 : Zero Cross Range Example

7.2 Control Saturation and Performance Robustness

Section 5.3.3 addresses the need to include an assessment of landing site robustness. No methods were identified, but the concept of site robustness as a function of constraint saturation was introduced. This section identifies methods to evaluate site robustness as a function of constraint violation and presents a motivating comparison to highlight the importance of including robustness in footprint definition and site selection.

7.2.1 Robust Footprint Definition: Analytic Approximations for Site Robustness as a Function of Control Saturation

Reference model tracking allows for simple definition of guidance robustness. The reference model represents the best knowledge of the vehicle dynamics. The only control perturbations required to ensure tracking are those necessary to reject plant uncertainties and disturbances. As convergence has been demonstrated for the tracking laws, the only limiting factor for tracking performance is control saturation.

A brief example motivates the discussion. Recall from chapter 6 that the tracking law rejects a lift coefficient bias primarily through application of bank angle control. Thus, rejecting a lift coefficient bias is a "worst-case" scenario for robustness as a function of bank angle saturation. Increasing the lift coefficient increases the in-plane *L/D*. This requires an increase in the bank angle to reduce the total overall *L/D* to maintain altitude tracking. The bank angle can be increased to reject any amount of lift coefficient uncertainty until the saturation limit (80 degrees for the simulations here) is reached. For some amount of lift coefficient bias the tracking law will no longer be capable of guaranteeing zero steady state error. If a site is chosen which requires nearly 80 degrees of reference bank angle, there is no longer any room to compensate for an increase in the lift coefficient. Thus the need to include robustness in footprint definition and site selection.

Two forms of control saturation can limit tracking performance: steady state control saturation and transient control saturation. If steady state saturation occurs then tracking is no longer achievable. An approximation of the amount of uncertainty leading to steady state saturation is

relatively simple to derive. Unfortunately, simply considering steady state saturation does not capture the entire problem. Transient control saturations can cause tracking errors which lead to the vehicle not reaching the target and in some cases the guidance algorithm is driven unstable by prolonged control saturations. Deriving an approximation to measure transient saturation is more difficult and requires linearization of the plant dynamics to use the l_1 transfer function norm. While the method presented here is only an approximation, in practice it serves very well and the examples shown support this.

Worst Case Uncertainty: Lift Coefficient Bias

Recall that density biases are primarily rejected by angle of attack control action. The tracking algorithm easily rejects the maximum expected density bias of +/- 25% without angle of attack saturation. Lift coefficient biases are rejected by bank angle control action. Drag coefficient biases are rejected by both bank angle and angle of attack control action. Because both C_D and C_L biases lead to *L/D* biases, the magnitude of the bank angle control is similar for both uncertainties. Because angle of attack control saturation is not a concern and because of the similarity in bank angle control for both lift and drag coefficient biases, a lift coefficient bias is examined as the worst case parametric uncertainty for control saturation. Only examining C_L biases simplifies the robustness analysis.

Steady State Control Saturation

A C_L bias is primarily rejected by bank angle control to adjust the total vehicle *L/D*. Recall that the vertical component of *L/D* is given by:

$$(L/D)_v = \frac{L\cos\sigma}{D} \qquad \textbf{7.1}$$

Now, insert a C_L bias and a steady state control perturbation to reject the bias:

$$(L/D)_v = \frac{L(1+\Delta_{C_L})\cos(\sigma+\Delta\sigma_{SS})}{D} \qquad \textbf{7.2}$$

Equating 7.1 and 7.2 yields the following expression for the parametric uncertainty rejected by a steady state bank angle perturbation:

$$\Delta_{C_L} = \frac{\cos(\sigma) - \cos(\sigma + \Delta\sigma_{SS})}{\cos(\sigma + \Delta\sigma_{SS})} \qquad 7.3$$

This is only an approximation and is slightly in error due to the small change in angle of attack commanded by the tracking algorithm. However, the approximation is valid in practice.

Transient Control Saturation

The steady state control perturbations to reject parametric uncertainties are found by the nonlinear solution above. However, analytic solution of the nonlinear equations of motion to estimate the peak transient control perturbation is difficult and impractical. Fortunately, linearized transfer function analysis proves useful here for estimating the peak transient control gain. A lift coefficient bias is a real parametric uncertainty. Lacking any tools to analyze this type of uncertainty, instead the lift coefficient bias is formulated as a disturbance. A C_L bias appears in the linearized plant dynamics or "A" matrix. It is impossible to write a transfer function directly from this uncertainty. For the purposes of this thesis' tracking algorithm, a different approach is possible and captures the desired information. The C_L bias is modeled as a constant disturbance signal acting on flight path angle as in figure 7.3. The "L_Δ" matrix is the input relationship from the C_L bias to the flight path angle dynamics. The transfer function from the input disturbance signal to the bank angle control signal describes the bank angle transient response characteristics after a roll reversal. This information provides a direct measurement of algorithm robustness. Modeling real parametric uncertainties as an input disturbance is a fairly standard approach [2].

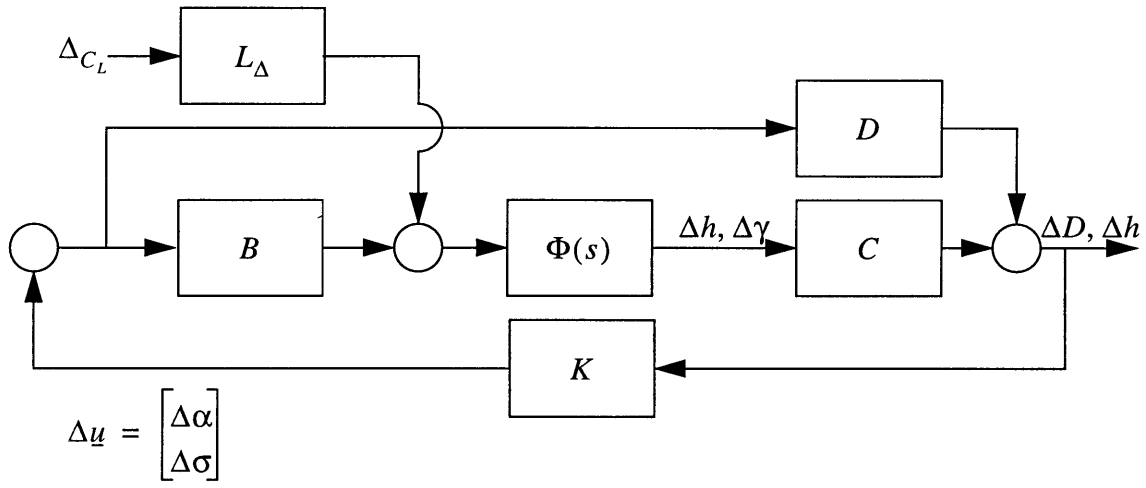

Figure 7.3 : Plant Uncertainty Representation

A short discussion of signal norms is necessary. Complete treatment of signal norms can be found in [2]. The signal norm of concern here is the l_1 norm. The l_1 norm is the l_∞-induced norm: the gain from the l_∞ norm of the input signal to the l_∞ norm of the output signal. The l_1 norm is useful because it quantifies the maximum peak to peak amplification of a signal. Note that all discussion of l_1 and l_∞ norms assume a discrete time linearization. This simplifies discussion and analysis. The input and output signals are l_∞, i.e. bounded in magnitude. The l_∞ norm defines the actual value of the peak magnitude of the signal. A signal is l_∞ if the l_∞-norm, given by equation 7.4, is bounded [2].

$$\|x\|_\infty = \sum_{k=-\infty}^{\infty} |x(k)|_\infty^\infty < \infty \qquad \textbf{7.4}$$

The l_1 transfer function (operator) norm is the l_∞-induced norm and is given by the l_1 norm (i.e. sum) of the impulse response of the transfer function matrix under consideration [2]. The l_1 operator norm is given by equation 7.5 [2]. Note that "R" represents the matrix operator associated with the impulse response of the transfer function matrix and "r_{ij}" are the elements of the matrix. "x" is the input signal. "Rx" is the output signal.

$$\|R\|_1 = \sup_{x \neq 0} \frac{\|Rx\|_\infty}{\|x\|_\infty} = \max_{1 \le i \le m} \sum_{j=1}^{n} \sum_{k=0}^{\infty} |r_{ij}(k)| \qquad \textbf{7.5}$$

The most important fact for the reader to note is that the l_1 norm simply gives the peak amplification of the peak value of the input signal and that the l_1 norm is computed by summing the absolute value of the elements of the discrete impulse response. This corresponds to the integral of the absolute value of the continuous impulse response.

Recall that a relationship between the peak magnitude of the transient control response and the parametric uncertainty magnitude is sought. The l_1 norm provides such a relationship. The l_1 norm of the transfer function from the input disturbance (uncertainty) signal to the control signal defines the peak control magnitude. The peak magnitude of the bank angle control is:

$$\Delta\sigma_{tr} = \|T_{u\Delta}\|_1 \Delta_{C_L} \qquad \textbf{7.6}$$

Recall equation 7.3,

$$\Delta_{C_L} = \frac{\cos(\sigma) - \cos(\sigma + \Delta\sigma_{SS})}{\cos(\sigma + \Delta\sigma_{SS})} \qquad \textbf{7.3}$$

Apply saturation limits to the bank angle:

$$\sigma_{min} < \sigma_{REF} + \Delta\sigma_{SS} + \Delta\sigma_{tr} < 80^\circ \qquad \textbf{7.7}$$

Now there are three equations and three unknowns (equations 7.3, 7.6 and 7.7). Equating the components of 7.7 and solving results in the following transcendental equations for the maximum positive and negative lift coefficient uncertainty with no control saturation:

$$\frac{\cos\sigma_{REF}}{\Delta^+_{C_L} + 1} - \cos(80^\circ - \|T_{u\Delta}\|_1 \Delta^+_{C_L}) = 0 \qquad \textbf{7.8}$$

$$\frac{\cos\sigma_{REF}}{\Delta^-_{C_L} + 1} - \cos(\sigma_{min} - \|T_{u\Delta}\|_1 \Delta^-_{C_L}) = 0 \qquad \textbf{7.9}$$

A first order gradient search solves equations 7.8 and 7.9. Then equations 7.3 and 7.6 can be used to generate approximations for the steady state and peak transient bank angle perturbations. The quantity Δ_{C_L} characterizes site robustness. Site robustness can be integrated into the footprint definition and site selection algorithms. Robustness is exactly characterized for any candidate target site using the above procedure. Computation of the l_1 norm is addressed in [2]. The procedure assumes that in the limit the impulse response converges to zero (finite impulse

response). Computing the l_1 norm requires using a linearized model. The majority of the linearized model is generated pre-flight but several parameters are modified depending on the abort initial conditions and the bank angle command for the candidate site. The l_1 norm and the linearized model are relatively stationary for the abort trajectories so this serves as a valid approximation. Although the above method is approximate, the comparison below demonstrates the method's utility in predicting robust performance.

7.2.2 Comparison between High and Zero Crossrange Examples

Section 7.1 presents two abort trajectories. Intuitively, the zero crossrange trajectory should be more robust than the high crossrange trajectory. The analytic tools presented above capture the robustness difference numerically for use by a site selection algorithm. Applying the analytic approximations and examining the actual trajectory results demonstrates the utility of the above method for landing site robustness assessment.

Applying the procedure outlined in section 7.2.1 results in the following maximum expected lift coefficient biases to prevent control saturation, steady state bank angle differences and maximum expected bank angle transient magnitudes for the two trajectories:

Table 7.1 : Site Robustness Assessment

	Zero Crossrange	High Crossrange
σ_{REF}	53.7°	50.5°
σ_{min}	0.0°	26.2°
$\Delta^{+}_{C_L}$	**0.1755**	**0.1850**
$\Delta\sigma^{+}_{SS}$	6.1°	7.2°
$\Delta\sigma^{+}_{tr}$	20.2°	22.8°
$\Delta^{-}_{C_L}$	**–0.2904**	**–0.1306**
$\Delta\sigma^{-}_{SS}$	–20.2°	–7.7°
$\Delta\sigma^{-}_{tr}$	–33.5°	–16.1°

These results indicate that the zero crossrange site should accept much larger reduction in *L/D* (-0.2904 vs. -0.1306) without constraint saturation. Figures 7.4 through 7.7 confirm this result. Figure 7.4 shows the zero crossrange trajectory with a -10% C_L bias. Figure 7.5 presents the high crossrange trajectory for the same bias. As expected, for both cases the vehicle successfully reaches the target. Steady state drag errors are zero while altitude errors are small. Final range errors for both cases are less than a mile.

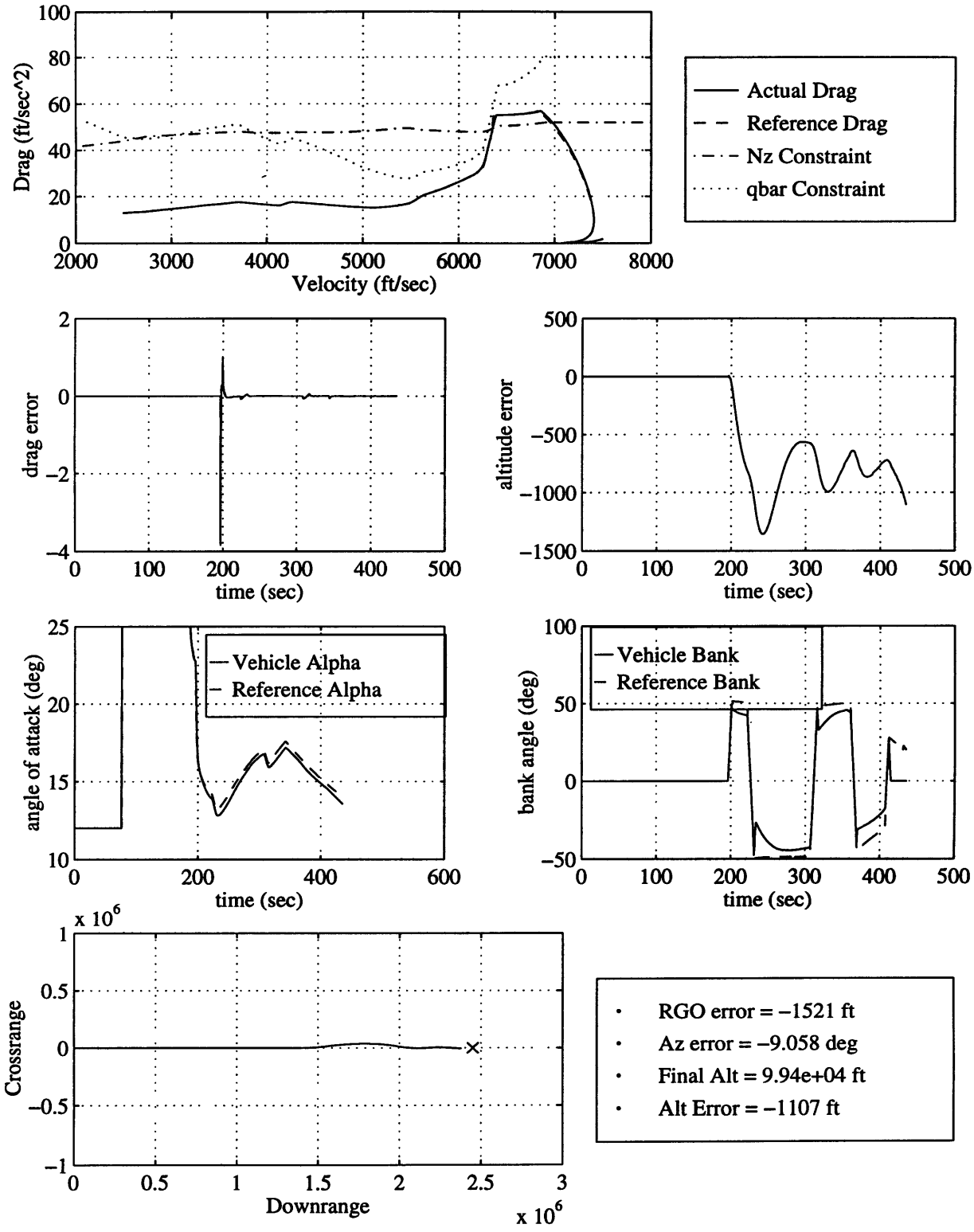

Figure 7.4 : Zero Crossrange Trajectory with -10% C_L bias

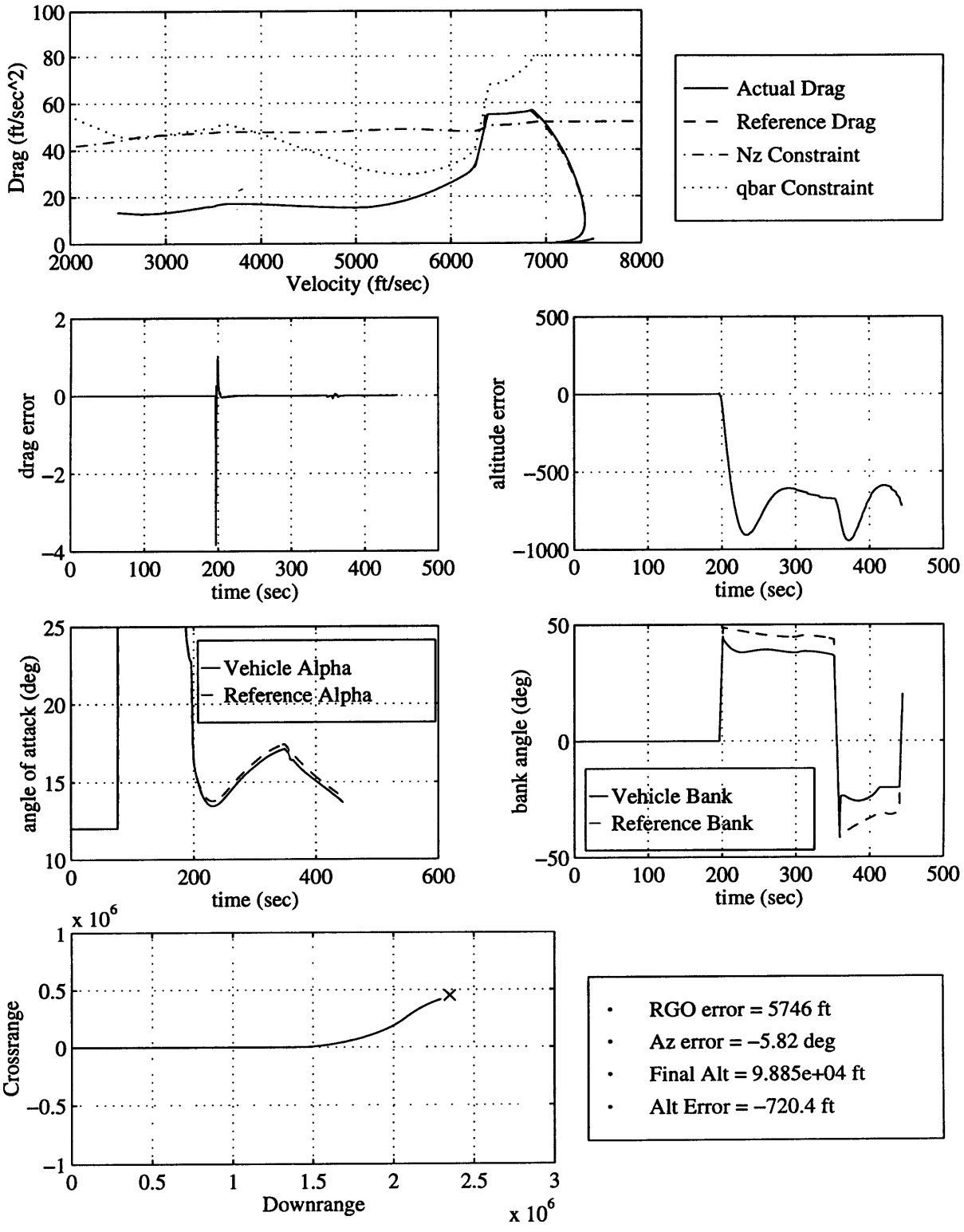

Figure 7.5 : High Crossrange Trajectory with -10% C_L bias

The accuracy of the predicted response can also be assessed. Table 7.2 compares the predicted and actual bank angle response characteristics. The actual transient peak magnitude is measured after a roll reversal. For the high crossrange case the measurement is after the first roll reversal. For the low crossrange case the measurement is after the second roll reversal because steady state was not achieved by the tracking algorithm prior to the first roll reversal. Uncertainty during the roll reversal appears as a worst case flight path angle disturbance. This is exactly what the l_1 norm predicts.

Table 7.2 : Predicted Bank Angle Response for -10% C_L bias

	Zero Crossrange			High Crossrange		
	Predicted	Actual	% Error	Predicted	Actual	% Error
$\Delta\bar{\sigma}_{SS}$	-4.83	-5.19	6.94	-5.58	-6.69	16.59
$\Delta\bar{\sigma}_{tr}$	-11.53	-11.05	-4.34	-12.35	-10.72	-15.21
$\Delta\bar{\sigma}_{tot}$	16.36	16.24	0.74	17.93	17.41	2.99

The prediction is reasonably accurate for both cases. Transient prediction in both cases is conservative. This is expected because the l_1 norm captures the potential worst case peak to peak gain. Steady state prediction for the high crossrange case is inaccurate because of the redesign of the reference model. The redesign function changes the reference bank angle from 50.5 degrees down to approximately 45 degrees. Recomputing the predicted steady state bank angle perturbation for a nominal bank angle of 45 degrees results in a predicted $\Delta\bar{\sigma}_{SS}$ of -6.78 degrees (only a 1.3% error). The prediction does not account for reference bank angle modifications due to the redesign. However, for robustness assessment the bank angle response prediction procedure outlined above is sufficiently accurate.

Now, to illustrate the effects of control saturation, apply a bias which exceeds the expected robustness limits. Figure 7.6 shows the zero crossrange trajectory for a -20% C_L bias while figure 7.7 presents the high crossrange trajectory for the same bias. The vehicle successfully reaches the

zero crossrange site but not the high crossrange site. The robustness assessment predicts that the high crossrange site can only be reached with a -13% C_L bias. In the actual simulation with the -20% C_L bias, bank angle control saturates, large steady state errors build up, and the site is not achievable. The robustness assessment predicts that the zero crossrange site is reachable for up to -29% C_L uncertainty. Guidance successfully compensates for the -20% C_L bias trajectory and reaches the target site.

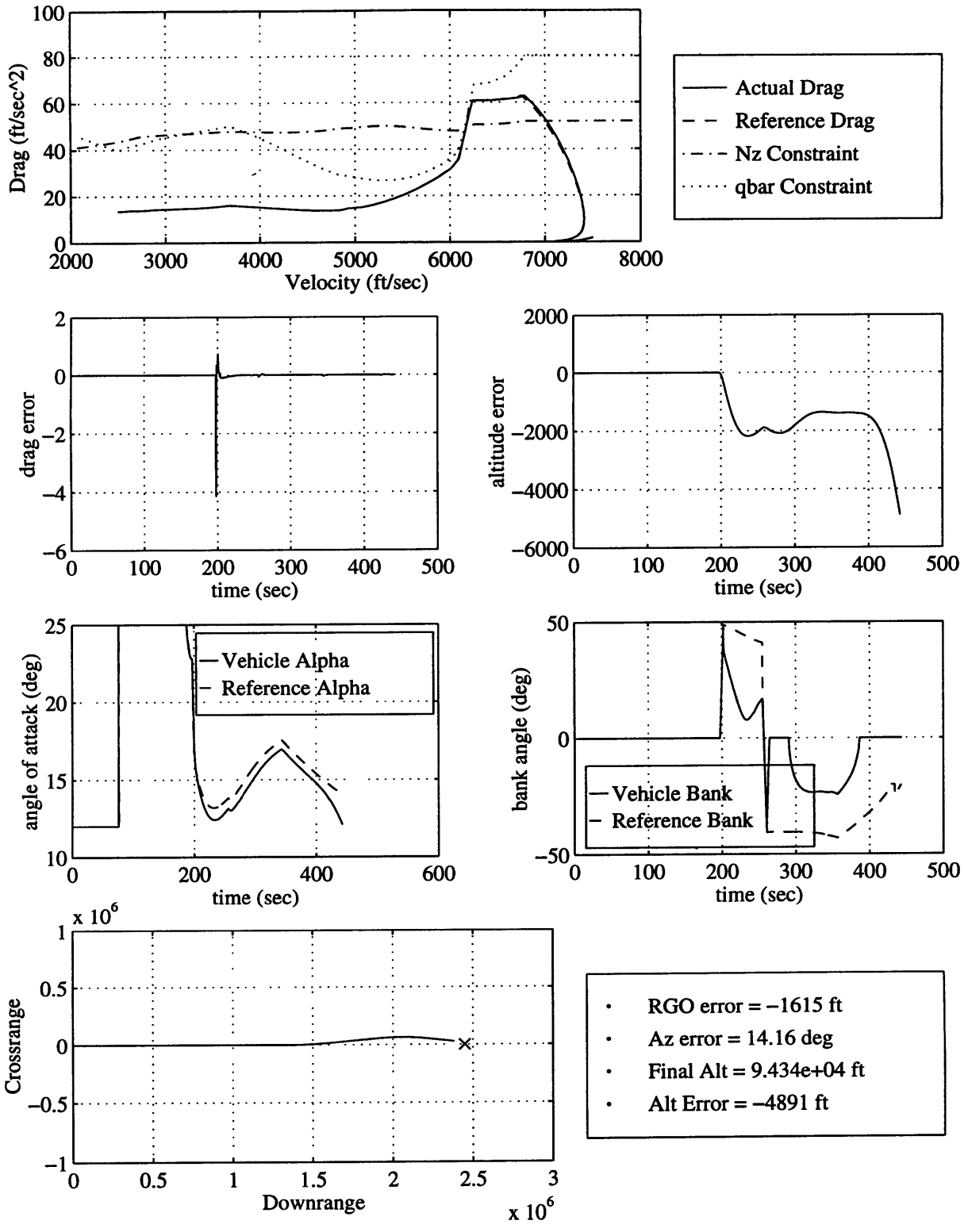

Figure 7.6 : Zero Crossrange Trajectory with -20% C_L bias. Little saturation occurs.

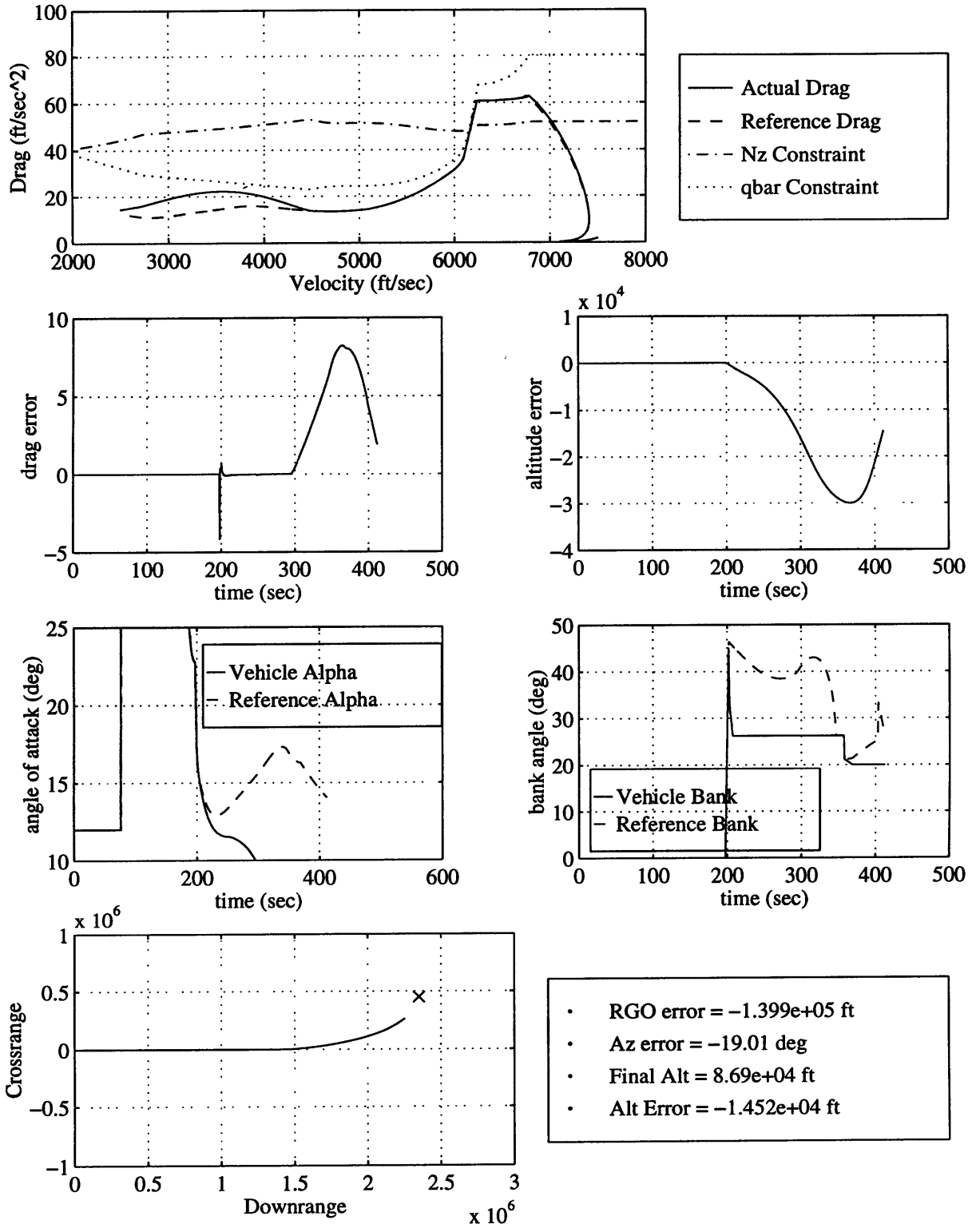

Figure 7.7 : High Crossrange Trajectory with -20% C_L bias. Large control saturations.

The zero crossrange trajectory experiences control saturation in the latter portion of the trajectory. This is because a lower nominal bank angle requires a greater reduction in the bank angle to increase lift ($\cos\sigma \sim 1$ for small bank angles). The saturation results in altitude tracking errors in the final phase of the trajectory. In chapter 5, a linear reduction in the reference bank angle to zero was identified as a method to meet final altitude requirements. The above example only reduces the bank angle to 20 degrees. For the nominal case the final altitude is not significantly sacrificed (again because $\cos\sigma \sim 1$ for small bank angles, a reduction to 20 degrees is similar to a reduction to 0 degrees for the final altitude). By using a reduction to only 20 degrees, rather than to zero, the robustness of the latter portion of the trajectory improves. The example above has a final altitude error of 4891 feet. If the final bank angle is zero, control saturation occurs much earlier in the trajectory and the final altitude error is nearly 15,000 feet. Furthermore, for the high crossrange example, if the final bank angle is zero, the crossrange requirements can not be met. These results lead to a modification of the linear reduction in the bank angle. Rather than reducing the bank angle to a target of zero, now the final bank angle is the minimum bank angle to meet crossrange requirements or 20 degrees, whichever is greater. This modification adds significant performance robustness to the terminal phase of the trajectory by giving the vehicle more control authority.

The comparison above highlights the importance of including a robustness prediction as part of the site selection algorithm. The robustness assessment tools are reasonably accurate and capture the important factors of site selection including crossrange requirements. Although this thesis does not implement a site selection algorithm, the robustness assessment tools are useful for reference model based guidance systems.

7.3 Robust Performance Results

The robust abort guidance algorithm can handle a wide variety of abort scenarios and parametric uncertainties. Analysis covers four abort scenarios: the zero crossrange and high crossrange mach 8 trajectories, a mach 7 trajectory and a mach 6 trajectory. Thirteen test cases were run for each scenario. These include nominal results, +/-10% C_L and C_D biases, and +/-25% density biases. Another test case starts with a positive uncertainty and then switches in mid-trajectory to a negative uncertainty. These are run for each type of uncertainty. Finally, stochastic uncertainties

are applied. The uncertainty is described by white noise passed through a low pass filter to simulate slowly varying correlated uncertainty. Although these test cases do not include every type of possible uncertainty, they capture the vast majority and verify algorithm robustness.

Figures 7.8 and 7.9 present the nominal mach 6 and mach 7 abort trajectories. The mach 6 target is at (1.35×10^6, 50000). The mach 7 target is (1.8×10^6, 100000). Both trajectories show good tracking properties and meet range and altitude targets at TAEM interface.

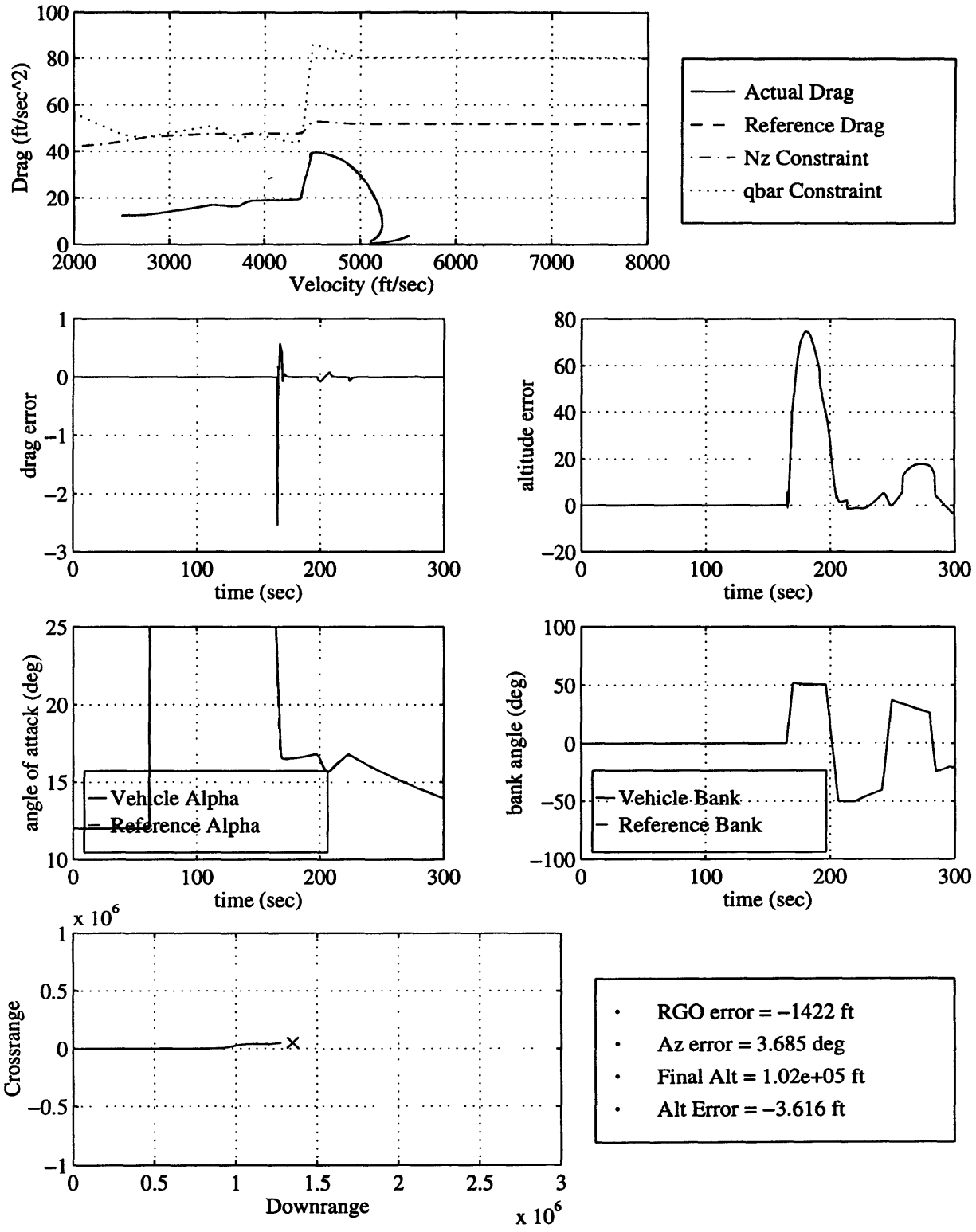

Figure 7.8 : Mach 6 Abort Trajectory

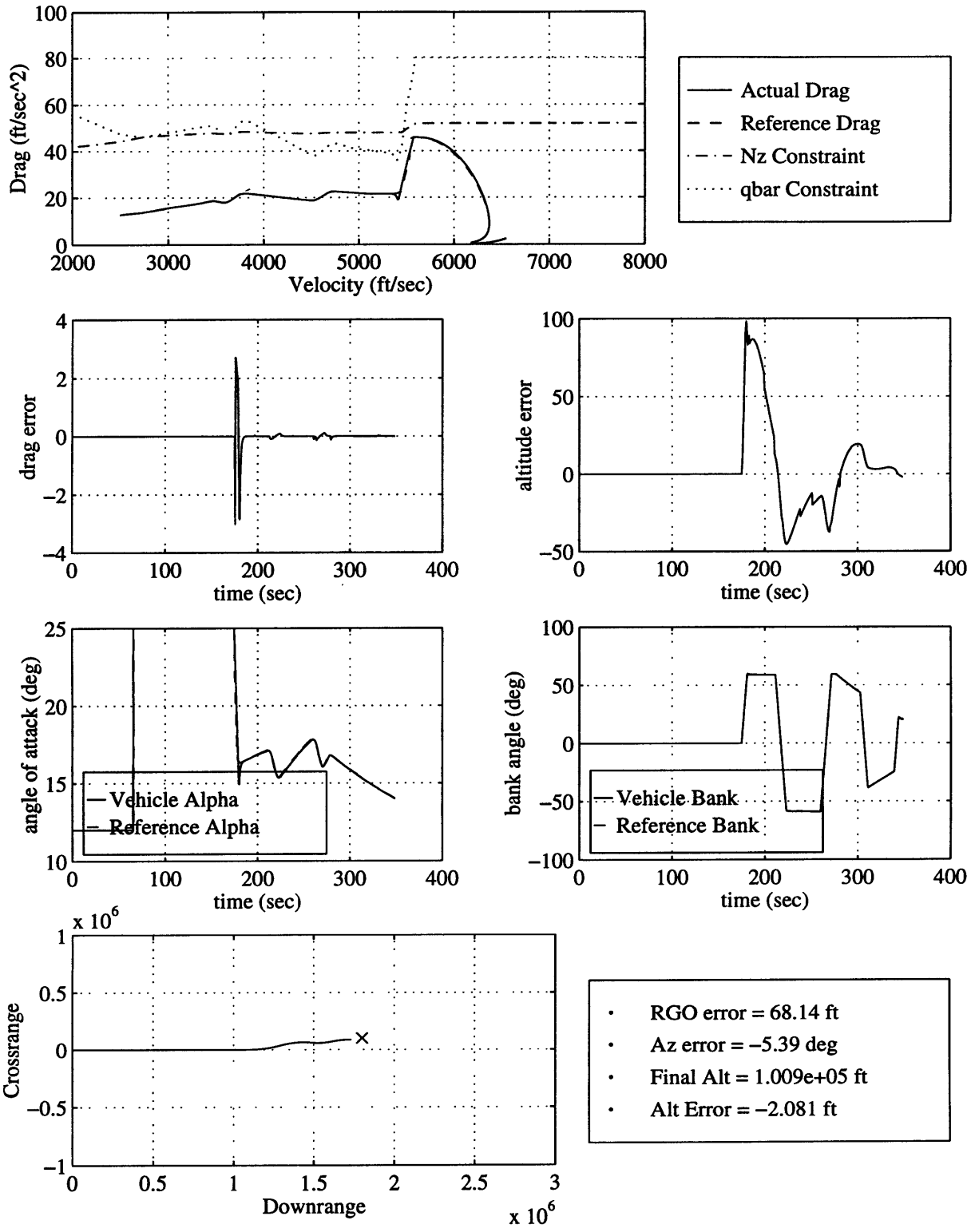

Figure 7.9 : Mach 7 Abort Trajectory

Performance goals are shown in table 7.3.

Table 7.3 : Guidance Performance Goals

$R_{GO_{ERR}}$	+/- 1 nm (6076 ft)
$h(t_f)$	100000 +/- 3000 ft
$\Delta h(t_f)$	+/- 1000 ft
Ψ_{ERR}	+/- 10°

Meeting the above goals allows TAEM to reach the landing site safely. Range to go error and final altitude are useful indicators for evaluating the performance of the redesign algorithm. Final altitude tracking error is useful for evaluating the performance of the tracking algorithm - especially because control saturation is much more likely in the latter portion of the trajectory. Azimuth error indicates that the site is sufficiently robust to meet both crossrange and tracking requirements. Throughout the presentation of results, when the above bounds are exceeded, the parameter is noted in bold and an explanation of the results is included.

Nominal results for each abort are in table 7.4. Range and altitude errors are in feet while azimuth error is in degrees. Nominal performance is excellent. Range, altitude, and azimuth errors are all small. Nominal performance should be very good. Without uncertainty, tracking and redesign are unnecessary.

Table 7.4 : Nominal Performance Results

	Parameter	Value
Mach 8 Zero Crossrange	$R_{GO_{ERR}}$	-675.9
	$h(t_f)$	100854.8
	$\Delta h(t_f)$	-5.2
	Ψ_{ERR}	4.82
Mach 8 High Crossrange	$R_{GO_{ERR}}$	-63.6
	$h(t_f)$	99506.6
	$\Delta h(t_f)$	-18.3
	Ψ_{ERR}	-4.25
Mach 7	$R_{GO_{ERR}}$	68.1
	$h(t_f)$	100914.4
	$\Delta h(t_f)$	-2.1
	Ψ_{ERR}	-5.39
Mach 6	$R_{GO_{ERR}}$	-1421.7
	$h(t_f)$	102029.8
	$\Delta h(t_f)$	-3.6
	Ψ_{ERR}	3.68

Next, table 7.5 includes results for drag uncertainties. Algorithm performance is good for all cases except for a few situations. The +10% C_D bias reduces the vehicle *L/D*. This type of uncertainty is difficult to reject because of the difficulty in meeting crossrange requirements while maintaining good tracking. The errors are not far outside of the bounds. In addition the shift scenario causes difficulty. The shift in parameter uncertainty creates problems for the redesign

algorithm. Predictor-corrector approaches experience similar difficulty [4]. Finally the mach 6 abort in general has more violations of the bounds. This can be expected because the CLAT phase is shorter and thus the vehicle has less range control authority.

Table 7.5 : Performance Results: C_D Uncertainty

		+10%	-10%	Shift +/- 10%	Stochastic
Mach 8 Zero Crossrange	$R_{GO_{ERR}}$	916.1	1668.5	3815.0	3422.7
	$h(t_f)$	100570.3	101705.9	101618.6	100841.5
	$\Delta h(t_f)$	-615.4	704.0	652.2	-37.5
	Ψ_{ERR}	7.00	-4.52	3.50	-3.09
Mach 8 High Crossrange	$R_{GO_{ERR}}$	**6572.8**	-1611.3	**9676.1**	3581.7
	$h(t_f)$	98920.9	99152.1	100039.5	98368.0
	$\Delta h(t_f)$	-615.0	711.2	625.1	-112.3
	Ψ_{ERR}	-0.76	5.91	-4.81	2.64
Mach 7	$R_{GO_{ERR}}$	-4186.7	5809.7	-2814.1	573.2
	$h(t_f)$	101285.3	100629.1	**103356.7**	101322.1
	$\Delta h(t_f)$	**-1021.7**	727.1	571.6	-699.1
	Ψ_{ERR}	5.68	5.17	-5.61	-4.17
Mach 6	$R_{GO_{ERR}}$	-2945.3	4696.6	-5225.2	**-7159.7**
	$h(t_f)$	101079.2	102019.6	**103901.8**	**103949.2**
	$\Delta h(t_f)$	**-1704.0**	631.7	552.8	105.1
	Ψ_{ERR}	-4.77	-6.27	0.36	5.08

The lift coefficient uncertainty has similar results. A reduction in *L/D* and the shift in *L/D* again have small violations of the performance bounds.

Table 7.6 : Performance Results C_L Uncertainty

		+10%	-10%	Shift +/- 10%	Stochastic
Mach 8 Zero Crossrange	$R_{GO_{ERR}}$	2819.4	-1520.6	**-6327.7**	1784.7
	$h(t_f)$	102179.5	99400.19	99240.9	101520.0
	$\Delta h(t_f)$	778.9	**-1107.4**	-818.1	-2.5
	Ψ_{ERR}	-4.22	-9.06	4.27	5.14
Mach 8 High Crossrange	$R_{GO_{ERR}}$	-462.2	5746.3	**-7156.9**	-883.8
	$h(t_f)$	99830.2	98845.3	97413.2	100229.9
	$\Delta h(t_f)$	802.4	-720.4	**-1131.2**	22.0
	Ψ_{ERR}	5.08	-5.82	-5.45	-3.90
Mach 7	$R_{GO_{ERR}}$	3896.7	-412.1	590.9	5147.2
	$h(t_f)$	100843.4	100451.8	96728.3	99878.2
	$\Delta h(t_f)$	829.1	**-1394.0**	-998.5	**-1030.3**
	Ψ_{ERR}	5.52	5.53	-5.84	-5.60
Mach 6	$R_{GO_{ERR}}$	3948.5	-1603.9	578.3	984.6
	$h(t_f)$	100912.1	100360.7	97369.9	101848.0
	$\Delta h(t_f)$	783.9	**-3769.0**	**-1024.6**	-208.6
	Ψ_{ERR}	-6.03	-0.28	4.96	4.72

Performance in the presence of density uncertainties is generally excellent. The few cases which do not meet specifications are only minor violations. Again the mach 6 abort has the greatest problems.

Table 7.7 : Performance Results: Density Uncertainty

		+25%	-25%	Shift +/- 25%	Stochastic
Mach 8 Zero Crossrange	$R_{GO_{ERR}}$	-667.6	**-6316.9**	-1471.0	3609.1
	$h(t_f)$	102000.0	99329.1	101022.8	98843.8
	$\Delta h(t_f)$	162.1	-495.1	-311.4	-103.1
	Ψ_{ERR}	3.05	-3.63	2.68	1.09
Mach 8 High Crossrange	$R_{GO_{ERR}}$	5395.0	-1862.3	-8.1	5265.1
	$h(t_f)$	100592.9	98102.1	100135.7	95205.5
	$\Delta h(t_f)$	121.2	-446.9	-350.0	-126.8
	Ψ_{ERR}	-6.49	-5.59	3.30	3.36
Mach 7	$R_{GO_{ERR}}$	-4519.8	**6316.7**	-3419.1	4814.3
	$h(t_f)$	101720.1	99439.5	100217.2	102303.3
	$\Delta h(t_f)$	182.2	-483.0	-373.9	-51.1
	Ψ_{ERR}	-4.01	-1.10	-5.69	-2.54
Mach 6	$R_{GO_{ERR}}$	-2312.1	-4343.2	2758.8	-1583.4
	$h(t_f)$	99763.8	**103576.8**	98843.1	102096.2
	$\Delta h(t_f)$	166.4	**-1433.5**	-426.1	17.7
	Ψ_{ERR}	-1.26	2.46	4.51	3.39

In general, algorithm performance is excellent. Altitude and range targets are met for virtually all of the cases. The mach 6 abort results are the only cause for concern. The mach 6 abort trajectory

is difficult because of the lack of range control authority due to the short CLAT phase. This provides yet another argument for extension of closed loop guidance to the alpha recovery phase for improved algorithm robustness.

Chapter 8

Conclusion

A model based approach for robust abort guidance is a logical extension and combination of the strengths of other entry guidance approaches. Reference profile based approaches rely on closed loop tracking of the profile to reject uncertainty but it is difficult to capture all of the available vehicle capability and guarantee profile feasibility using a profile based approach. The numerical predictor-corrector approach guarantees feasible trajectories and captures a large class of vehicle capability but rejection of environment uncertainties is completely dependent on estimates of those uncertainties. The reference model based approach takes the strengths of each method. Closed loop reference model tracking rejects environment uncertainties. Initializing the model at the start of closed loop tracking guarantees feasibility and captures the same large class of vehicle capability as the predictor-corrector approach.

The model based algorithm successfully handles any abort initial conditions and a wide range of parametric uncertainties. The major advantages associated with the model based approach include:

1. Preflight trajectory design is only concerned with nominal vehicle and environment conditions. This is because the nominal guidance algorithm only operates on the reference model (defined by the nominal vehicle dynamics). Any nominal guidance algorithm which the designer deems necessary can be applied to the reference model.
2. Initial in-flight trajectory design is simplified by reducing the problem to a single parameter search on bank angle to control final range. Initial trajectory design defines the vehicle footprint and builds up the framework for the redesign algorithm.
3. In-flight trajectory redesign is simplified because only the nominal vehicle dynamics are considered. Final vehicle range is defined simply by the current vehicle energy and the reference model bank angle.
4. Reference model initialization at start of closed loop tracking ensures trajectory feasibility.

5. Closed loop tracking of the reference model rejects parametric uncertainties. Design of the tracking algorithm lends itself well to linearized approaches because the reference model provides the nominal states and controls of the entire vehicle. For this application a simple output feedback algorithm has excellent performance. The redesign algorithm matches the energy and range states for a nominal vehicle. The redesign algorithm does not have to consider parametric uncertainties in the range prediction. This is because closed loop tracking of the reference model through control perturbations forces the vehicle to exhibit nominal behavior in terms of range control.
6. By using the model based formulation, trajectory robustness is accurately predicted strictly as a function of control saturation. The robustness of a given target site can be included in the site selection algorithm.

The advantages highlighted above stem directly from the model based formulation. The results presented in this thesis emphasize these advantages and verify performance under a variety of conditions. An optimization algorithm could accomplish many of the same goals but only through far more computation.

The focus of this thesis is not on developing an improved tracking algorithm or on design of optimal nominal trajectories. Rather, a simple and efficient methodology which fits a wide class of entry guidance problems is presented. The model based approach treats the guidance problem as a nonlinear control problem. The choice of approach for a guidance system is completely dependent on the application. Reference profiles generated pre-mission, numerical predictor-corrector approaches, model based guidance, and even trajectory optimization approaches all have strengths and weaknesses. Trading off the relative merits is the key to successful guidance system design.

Suggestions for future work

In terms of implementation, a great deal of analysis is necessary. The algorithm must be verified in a 6DOF environment with updated aerodynamic and mass properties. The reference model should be updated to include the contributions of the aerosurfaces. The tools developed for vehicle capability analysis, trajectory design and tracking, and robustness evaluation will help

significantly to streamline the process.

In addition to updating the analysis for a 6DOF environment, the algorithm could be extended to include the alpha recovery phase. The analysis presented throughout the thesis indicates that this extension is possible and would increase vehicle capability. This is especially true for low mach number aborts.

The tracking algorithm could possibly be significantly improved by an extensive evaluation of modern output feedback methodologies. Chapter 7 emphasized the effects of control saturation on vehicle performance and identified transient control saturation as the limiting factor for robustness. Transient control saturation was successfully predicted using the l_1 norm. This result naturally points to a need to explore l_1 optimization to minimize the transient control action [2]. The main advantage of l_1 optimization is the ability to include time domain constraints. The cost function would simply be to minimize the l_1 norm of the transfer function from the real uncertainty (modeled as a disturbance) to the control signal. Time domain constraints could be applied to help minimize control saturation.

Another even more interesting approach is the constrained optimization approach [13]. Constrained optimization takes advantage of the Youla parameterization to find controllers which are designed to satisfy some set of convex constraints. This methodology also can include time domain constraints and has numerous other potential advantages [13].

The key problem with either of these methodologies is that generally the solutions result in high order controllers. This is especially the case when integrators are required to drive steady state tracking error to zero. The need to include integrators can cause controller order to grow quickly to satisfy feasibility constraints. It is likely that a reduced order model could provide near optimal performance. It is even possible (if not likely) that the gains of the output feedback controller presented in chapter 6 could be modified to imitate an l_1 optimal solution. By performing l_1 analysis or using H_2 or H_∞ methodologies the "ideal" controller could be defined and this would provide a standard for comparison.

In addition to improving the tracking algorithm, an integration of the numerical predictor-corrector approach and the model based approach could provide a highly robust guidance algorithm. Recall that the numerical predictor-corrector approach relies on estimation of environment uncertainties to reject these uncertainties [4]. The author recommends an integrated system which combines the strengths of both approaches. Estimation of environment uncertainties could be applied to footprint definition and site selection while reference model tracking is used to guarantee that the vehicle reaches the target site. This allows the guidance algorithm to use the estimation of environment uncertainties to select a site which, in the perturbed environment, is more robust. Then the tracking algorithm, with its improved robustness, will be much more successful in achieving steady state tracking. By using closed loop reference model tracking the algorithm does not have to put full faith into the uncertainty estimates.

At this point, the model based abort guidance system has reached a starting point. The main concepts have been verified. The model based approach provides many advantages, especially in streamlining the design of a guidance algorithm and providing specific robustness measures. Future investigation should attempt to exploit these advantages and exploit the strengths of other approaches. Guidance systems will see constant improvement from combining and adapting the strong points of all possible approaches.

Appendix A

Range Prediction and Drag-Velocity State Space Relationships

Entry guidance systems can take advantage of drag-velocity relationships for range prediction. Here, two methods for range prediction are summarized. The most simple method is a "shooting method." Integrating the equations of motion for some control history yields an exact nominal predicted range. Optimizing to meet range requirements is computationally expensive so analytic approximations are sought. Recall that chapter 5 derives analytic range approximations as a function of drag-velocity profiles. The analytic approximations are dependent on the assumption that the flight path angle is small throughout the trajectory. The second method this appendix presents is a range prediction method which eliminates this assumption and predicts range exactly as a function of a drag-velocity profile.

Nominal Range Prediction by Integrating the Guidance Frame Equations of Motion

In the guidance frame, the radial position, velocity, and flight path angle are the states which govern vehicle motion. The equations of motion are:

$$\frac{dr}{dt} = v\sin\gamma \qquad \textbf{2.5}$$

$$\frac{dv}{dt} = -D - g\sin\gamma \qquad \textbf{2.6}$$

$$\frac{d\gamma}{dt} = \left(\frac{1}{v}\right)\left(L\cos\sigma - \left(g - \frac{v^2}{r}\right)\cos\gamma\right) \qquad \textbf{2.7}$$

The vehicle heading angle, downrange, and crossrange are outputs of the above dynamics and their equations of motion are:

$$\frac{d\psi}{dt} = \left(\frac{1}{v}\right)\left(L\frac{\sin\sigma}{\cos\gamma} - \frac{v^2}{r}\cos\gamma\sin\psi\right) \qquad \textbf{2.8}$$

$$\frac{dR_x}{dt} = v\cos\gamma\cos\psi \qquad \textbf{2.3}$$

$$\frac{dR_y}{dt} = v\cos\gamma\sin\psi \qquad \textbf{2.4}$$

A profile of bank angle and angle of attack commands can be specified and the system of equations given by equations 2.3-2.8 can be integrated over time to predict the vehicle's final altitude, downrange, and crossrange. An optimization program can then be used to define a command history which would achieve the range and altitude targets without constraint violation. However, time integrations are slow and require small stepsizes. Also, optimization in the presence of nonlinear state constraints tends to be slow to converge and complicated to implement. A representation of the vehicle dynamics which allows for analytic or faster range prediction without constraint violation is desirable.

Accurate Range Prediction by Including Flight Path Angle Prediction

Chapter 5 derives analytic range prediction approximations as a function of drag-velocity profiles. These approximations are heavily dependent on the small flight path angle assumption. This assumption is generally not valid for X-34 trajectories. An alternative approach is available which removes the small flight path angle assumption. Point solutions of the equations of motion can be used to determine the vehicle flight path angle and bank angle for any point on the trajectory. By including flight path angle prediction, the accuracy of the drag-velocity prediction improves. The flight path angle prediction can also be used to provide an accurate heading angle prediction and thus exact crossrange and downrange prediction is possible. By using point solutions of the equations of motion and integrating trajectories in drag-velocity space, highly accurate predictions can be made with very large velocity stepsizes. The large velocity step sizes decrease computation time. Owen Deutsch recognized the utility of exact solution of the drag-velocity profile for range prediction for an abort planner [3]. For trajectory design, Deutsch specifies a basis of drag-velocity profiles and determines the profile which meets range requirements by exact solution of the drag-velocity space dynamics. A slightly modified derivation is presented here based on Kremer and Mease presentation of a feedback linearized tracking law for entry guidance [14].

The first step in understanding how the trajectory is uniquely specified by a drag-velocity profile

is to examine the dynamic system of equations governing drag. Drag is an output of equations 2.5-2.7 and is given by:

$$D = \frac{1}{2}\rho v^2 C_D \frac{S_a}{m} \qquad \textbf{2.2}$$

Assuming the angle of attack command sequence is defined with respect to velocity then the drag dynamics are found by time differentiating the drag equation until the bank angle is found explicitly in the equations of motion. The resulting third order dynamic system is described by equations A.8-A.11. For simplicity, equation A.10 assumes that C_D is constant so that $\dot{C}_D$ is zero.

$$(z_1, z_2, z_3) = (D, \dot{D}, v) \qquad \textbf{A.8}$$

$$\dot{z}_1 = z_2 = \dot{D} = -\frac{Dv}{H}\sin\gamma - \frac{2D^2}{v} - \frac{2Dg\sin\gamma}{v} - \frac{D^2}{C_D}\frac{\partial C_D}{\partial v} - \frac{gD\sin\gamma}{C_D}\frac{\partial C_D}{\partial v} \qquad \textbf{A.9}$$

$$\dot{z}_2 = \ddot{D} = a + bu \qquad \textbf{A.10}$$

$$a = \left(\frac{D}{H} + \frac{2gD}{vH}\right)\left(g - \frac{v^2}{r}\right) + \dot{D}\left(\frac{\dot{D}}{D} - \frac{3D}{v}\right) - \frac{4D^3}{v^2} + \left(\left(-\frac{8D^2}{v^2} - \frac{\dot{D}}{v}\right)g\sin\gamma\right) - \frac{4Dg^2(\sin\gamma)^2}{v^2}$$

$$b = -\left(\frac{D^2}{H} + \frac{2gD^2}{vH}\right) \qquad u = \frac{L\cos\sigma}{D}$$

$$\dot{z}_3 = \dot{v} = -D + gH\left(\frac{\dot{D}v + 2D^2}{Dv^2 + 2DgH}\right) \qquad \textbf{A.11}$$

An important observation is that the dynamic system $(D, \dot{D}, v)$ is just a state transformation of the (r, v, γ) space. This is why it is possible, given a drag vs. velocity profile, to also define the flight path angle and bank angle profiles.

Flight path angle is solved by combining equations 2.6 and A.9. Note that C_D is specified with respect to velocity because the angle of attack has been specified with respect to velocity.

$$\dot{D} = \left[\frac{\partial D}{\partial v}\right]_{Ref}\frac{\partial v}{\partial t} = \left[\frac{\partial D}{\partial v}\right]_{Ref}(-D - g\sin\gamma)$$

$$= -\frac{Dv}{H}\sin\gamma - \frac{2D^2}{v} - \frac{2Dg\sin\gamma}{v} - \frac{D^2}{C_D}\frac{\partial C_D}{\partial v} - \frac{gD\sin\gamma}{C_D}\frac{\partial C_D}{\partial v} \qquad \textbf{A.12}$$

$$\sin\gamma = H\left(\frac{Dv\left[\frac{\partial D}{\partial v}\right]_{Ref} - 2D^2 - \frac{D^2 v}{C_D}\frac{\partial C_D}{\partial v}}{D(v^2) + 2DgH - \left[\frac{\partial D}{\partial v}\right]_{Ref} Hvg}\right) \qquad \textbf{A.13}$$

Radial position (altitude) is determined by assuming an exponential atmosphere and by solving equation 2.2 for altitude.

$$r = r_S - H\ln\left(\frac{2Dm}{\rho_S S_a v^2 C_D}\right) \qquad \textbf{A.14}$$

Finally, the nominal bank angle profile can be determined by solving equation A.10 for u and then solving for the bank angle:

$$u = \left(\frac{1}{b}\right)(\ddot{D}_{Ref} - a) \qquad \textbf{A.15}$$

$$\sigma = \text{acos}\left(\frac{u}{L/D}\right) \qquad \textbf{A.16}$$

Now, because the flight path angle, altitude, and bank angle have been specified with respect to velocity the following equations can be integrated with respect to velocity for exact range prediction:

$$\Delta R_x = -\int_{v_0}^{v_f} \frac{v\cos\gamma\cos\psi}{D + g\sin\gamma} dv \qquad \textbf{5.1}$$

$$\Delta R_y = -\int_{v_0}^{v_f} \frac{v\cos\gamma\sin\psi}{D + g\sin\gamma} dv \qquad \textbf{5.2}$$

$$\Delta\psi = -\int_{v_0}^{v_f} \left(\frac{1}{D + g\sin\gamma}\right)\left(\frac{1}{v}\right)\left(L\frac{\sin\sigma}{\cos\gamma} - \frac{v^2}{r}\cos\gamma\sin\psi\right) dv \qquad \textbf{A.17}$$

This is an important result. The drag-velocity profile uniquely specifies the vehicle behavior. All parameters for the entire trajectory can be derived from the drag-velocity profile. Crossrange correction is included and even roll reversals. The most useful aspect is that by integrating with respect to velocity with all parameters fixed by point solutions of the drag-velocity trajectory, much larger stepsizes can be used to integrate the system defined by 5.1, 5.2 and A.17. The end result is faster range prediction via integration of drag-velocity trajectories.

The author does not recommend the use of drag-velocity based range prediction for an X-34

trajectory redesign algorithm. The highly uncertain nature of the alpha recovery phase makes it difficult to capture the entire vehicle capability by specifying a family a drag-velocity profiles. Chapter 5 provides more details as well as a far more robust energy-range method for trajectory redesign.

Constraint Representation

In addition to facilitating accurate range prediction, the drag-velocity space is also extremely useful for representing vehicle constraints. Normal load and dynamic pressure are the most important constraints for X-34 trajectories. With a fixed angle of attack vs. velocity profile, the vehicle constraints are represented directly in the drag-velocity space as upper limits on the vehicle drag.

Normal load is given by equation 2.9:

$$n = \frac{L\cos\alpha + D\sin\alpha}{g} \qquad \textbf{2.9}$$

The normal load constraint is given as n_{max} = 4.0 g's. With a fixed angle of attack vs. velocity profile, the drag level corresponding to a load factor of 4.0 g's is solved for each velocity by equation A.18 (derived from equation 2.9):

$$D_n(v) = \frac{n_{max}g}{\left(\frac{C_L(v)}{C_D(v)}\cos\alpha(v) + \sin\alpha(v)\right)} \qquad \textbf{A.18}$$

Dynamic pressure is given by equation 2.10:

$$q = \frac{1}{2}\rho v^2 \qquad \textbf{2.10}$$

The drag level corresponding to a q_{max} of 700 lbf/ft^2 is given for each velocity by:

$$D_q(v) = q_{max}C_D(v)\frac{S_a}{m} \qquad \textbf{A.19}$$

References

[1] Athans, M. and L. Lublin, "Linear Quadratic Regulator Control," 6.245 Multivariable Control Systems Lecture Notes, Spring 1996.

[2] Dahleh, M. A. and I. J. Diaz-Bobillo, *Control of Uncertain System*, Prentice Hall, Inc., Englewood Cliffs, NJ, 1995.

[3] Deutsch, O. "Mission Planner Requirements and Design," C. S. Draper Laboratory Memo #E44-96-002, May 24, 1996.

[4] Dierlam, T. A., *Entry Vehicle Performance Analysis and Atmospheric Guidance Algorithm for Precision Landing on Mars*, S.M. Thesis, Department of Aeronautics and Astronautics, MIT, Jun. 1990.

[5] Engel, A. G., *Aeroassist Flight Experiment AFESIM All-Digital Functional Simulation Vol. 3 Environment Models*, C. S. Draper Laboratory Report #CSDL-R-1951, Oct. 15, 1987.

[6] Findlay, J. T., G. M. Kelly, and P. A. Troutman, *Final Report - Shuttle Derived Atmospheric Density Model Part 2: STS Atmospheric Implications for AOTV Trajectory Analysis - a Proposed GRAM Perturbation Density Model*, NASA Contractor Report #NAS9-17158, Analytical Mechanics Associates, Inc., Dec. 1984.

[7] Fuhry, D. P., *A Design Study of Onboard Navigation and Guidance During Aerocapture at Mars*, S.M. Thesis, Department of Aeronautics and Astronautics, MIT, May 1988.

[8] Harpold, J. C. and C. A. Graves, Jr., "Shuttle Entry Guidance," *Journal of the Astronautical Sciences*, Vol. 27, No. 3, Jul.-Sep., 1979, pp. 239-268.

[9] Ishimoto, S., "Guidance Algorithm for Suborbital Flight Experiment of Unmanned Lifting Entry Vehicle," Proceedings of the AIAA Guidance, Navigation, and Control Conference, Baltimore, MD, Aug. 7-10, 1995.

[10] Lu, P., "Entry Guidance and Trajectory Control for Reusable Launch Vehicle," *Journal of Guidance, Control, and Dynamics*, Vol. 20, No. 1, Jan.-Feb. 1997, pp. 143-149.

[11] Lu, P., "Nonlinear Predictive Controllers for Continuous Systems," *Journal of Guidance, Control, and Dynamics*, Vol. 17, No. 3, May-Jun. 1994, pp. 553-560.

[12] Maciejowski, J. M., *Multivariable Feedback Design*, Addison-Wesley Publishing Company, Inc. Wokingham, England, 1989.

[13] McGovern, L. K., *A Constrained Optimization Approach to Control with Application to Flexible Structures*, S.M. Thesis, MIT, Jun. 1996.

[14] Mease, K. D. and J.-P. Kremer, "Shuttle Entry Guidance Revisited Using Nonlinear Geometric Methods," *Journal of Guidance, Control, and Dynamics*, Vol. 17, No. 6, Nov.-Dec. 1994.

[15] Moore, T. E., *Space Shuttle Entry Terminal Area Energy Management*, NASA Technical Memorandum 104744, Nov. 1991.

[16] NASA X-34 Web Page, http://rlv.msfc.nasa.gov/RLV_HTMLs/RLVX34.html.

[17] Powers, W., *RTLS Abort Training Manual*, NASA Mission Operations Directorate, Training Division, Flight Training Branch, Apr. 1987.